PHYSICAL REVIEW D **92,** 123527 (2015)

Models of dark matter halos based on statistical mechanics: The fermionic King model

Pierre-Henri Chavanis,[1] Mohammed Lemou,[2] and Florian Méhats[2]

[1]*Laboratoire de Physique Théorique, Université Paul Sabatier, 118 route de Narbonne 31062 Toulouse, France*

[2]*CNRS and IRMAR, Université de Rennes 1 and INRIA-Rennes Bretagne Atlantique, France*

(Received 10 March 2015; published 22 December 2015)

We discuss the nature of phase transitions in the fermionic King model which describes tidally truncated quantum self-gravitating systems. This distribution function takes into account the escape of high-energy particles and has a finite mass. On the other hand, the Pauli exclusion principle puts an upper bound on the phase-space density of the system and stabilizes it against gravitational collapse. As a result, there exists a statistical equilibrium state for all accessible values of energy and temperature. We plot the caloric curves and investigate the nature of phase transitions as a function of the degeneracy parameter in both microcanonical and canonical ensembles, extending the work of Chavanis [Int. J. Mod. Phys. B 20, 3113 (2006)] for box-confined configurations. We consider stable and metastable states and emphasize the importance of the latter for systems with long-range interactions. Phase transitions can take place between a "gaseous" phase unaffected by quantum mechanics and a "condensed" phase dominated by quantum mechanics. The phase diagram exhibits two critical points, one in each ensemble, beyond which the phase transitions disappear. There also exists a region of negative specific heats and a situation of ensemble inequivalence for sufficiently large systems. In the microcanonical ensemble, gravitational collapse (gravothermal catastrophe) results in the formation of a small degenerate object containing a small mass. This is accompanied by the expulsion of a hot envelope containing a large mass. In the canonical ensemble, gravitational collapse (isothermal collapse) leads to a small degenerate object containing almost all the mass. It is surrounded by a tenuous envelope. We apply the fermionic King model to the case of dark matter halos made of massive neutrinos following the work of de Vega, Salucci, and Sanchez [Mon. Not. R. Astron. Soc. 442, 2717 (2014)]. The gaseous phase describes large halos and the condensed phase describes dwarf halos. Partially degenerate configurations describe intermediate-size halos. We argue that large dark matter halos cannot harbor a fermion ball because these nucleus-halo configurations are thermodynamically unstable (saddle points of entropy). Large dark matter halos may rather contain a central black hole resulting from a dynamical instability of relativistic origin occurring during the gravothermal catastrophe. We relate the existence of black holes to the microcanonical critical point and determine the minimum halo mass above which black holes can form. We also compare fermionic and bosonic models of dark matter and discuss the value of the mass of the dark matter particle in each case.

DOI: 10.1103/PhysRevD.92.123527 PACS numbers: 95.35.+d, 98.35.Gi, 98.62.Gq

I. INTRODUCTION

Self-gravitating systems have a very particular thermodynamics first investigated by Antonov [1] and Lynden-Bell and Wood [2] in relation to stellar systems such as globular clusters made of classical point-mass stars. A first curiosity is the existence of negative specific heats [2]. It is well known in astrophysics that self-gravitating systems have negative specific heats [3]. However, when considered from the viewpoint of statistical mechanics, this property leads to an apparent paradox since the specific heat must be positive in the canonical ensemble as it measures the variance of the fluctuations of energy. As first understood by Thirring [4], and further discussed by Lynden-Bell and Lynden-Bell [5], this paradox is solved by realizing that the statistical ensembles are inequivalent. Negative specific heats are allowed in the microcanonical ensemble (MCE) while they are forbidden in the canonical ensemble (CE).[1] The inequivalence of statistical ensembles is not restricted to self-gravitating systems. It may arise in other systems with long-range interactions due to the nonadditivity of the energy [6]. However, the statistical mechanics of self-gravitating systems presents specific difficulties [7–9] that are absent in other systems with long-range interactions.

[1]MCE describes an isolated system evolving at fixed energy while CE describes a dissipative system coupled to a thermal bath fixing its temperature. For the sake of completeness, we shall consider the two ensembles in this paper even if MCE is usually the most relevant to describe astrophysical systems.

First, there is no statistical equilibrium state in a strict sense because a self-gravitating system in an infinite domain has no maximum of entropy or free energy.[2] There are not even critical points of entropy or free energy because the isothermal self-gravitating sphere, corresponding to the Boltzmann distribution coupled to the Poisson equation, has infinite mass [11]. Therefore, the statistical mechanics of self-gravitating systems is essentially an out-of-equilibrium problem [12]. The absence of a statistical equilibrium state in an unbounded domain is related to the fact that self-gravitating systems like globular clusters have the tendency to evaporate [13]. However, evaporation is a slow process so that, on an intermediate time scale, self-gravitating systems appear to be self-confined. Furthermore, stellar systems like globular clusters are never totally isolated from the surroundings. In practice, they feel the tides of a nearby galaxy. As a result, the stars escape when they reach sufficiently high energies. This implies that the density profile of the cluster vanishes at a finite radius R interpreted as a tidal radius.

There are two possibilities to solve the infinite mass problem of the self-gravitating isothermal sphere. A first possibility, introduced by Antonov [1], is to enclose the system within a "box" so as to artificially prevent its evaporation. The box radius mimics the tidal radius of more realistic systems. This procedure is appreciated by theorists first because it is simple, and second because it allows one to develop a rigorous statistical mechanics of self-gravitating systems based on the ordinary Boltzmann distribution. However, for astrophysical applications, this model is too idealized because self-gravitating systems in nature are not enclosed in boxes! Another possibility is to take the evaporation of high-energy stars into account and use the King model [14]. This is a truncated Boltzmann distribution obtained from the usual Boltzmann distribution by subtracting a constant term so that the distribution vanishes at the escape energy. This distribution has a finite mass. It can be derived from a kinetic theory based on the classical Landau equation [14].

Even when self-gravitating systems are confined in boxes, or when evaporation is properly taken into account by using the King model, a second difficulty arises which is now related to the fact that self-gravitating systems have the tendency to collapse [13]. In the box model, it is found that statistical equilibrium states exist only above a critical energy $E_c = -0.335GM^2/R$ in MCE and above a critical temperature $T_c = GMm/(2.52Rk_B)$ in CE, both

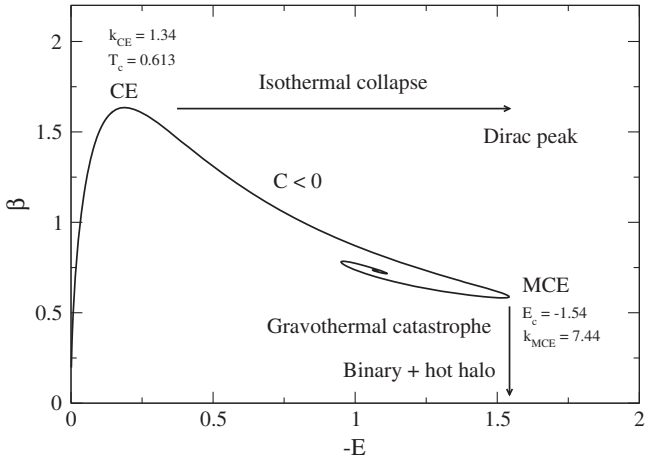

FIG. 1. Series of equilibria of the classical King model. It has a snail-like (spiral) structure but only the part of the curve up to CE in the canonical ensemble and up to MCE in the microcanonical ensemble is stable (the region between CE and MCE where the specific heat is negative corresponds to a region of ensemble inequivalence).

discovered by Emden [15]. The series of equilibria of classical isothermal spheres has the form of a spiral and these critical points correspond to turning points of energy and temperature. Stable configurations have a density contrast $\rho(0)/\rho(R) < 709$ in MCE and $\rho(0)/\rho(R) < 32.1$ in CE [1,2,7,16–19]. There are more stable states in MCE than in CE due to ensemble inequivalence (a stable equilibrium state in CE is always a stable equilibrium state in MCE but not the converse [6]). These configurations are metastable (local entropy maxima in MCE and local free energy maxima in CE)[3] but their lifetime is considerable since it scales as e^N (except close to the critical point) [19]. For globular clusters with $N \sim 10^6$ this lifetime is so great that metastable states can be considered as stable states.[4]

[2]We can always increase the entropy at fixed mass and energy in MCE and we can always increase the free energy at fixed mass in CE by spreading the system to infinity (see Appendixes A and B of Ref. [10]). The absence of a statistical equilibrium state in an unbounded domain can also be directly inferred from the fact that the integrals defining the density of states in MCE and the partition function in CE diverge at large distances [7].

[3]There is no global maximum of entropy or free energy. In MCE, one can always increase the entropy at fixed mass and energy by forming a binary star surrounded by a hot halo. The entropy diverges when the binary is made tighter and tighter, and the halo hotter and hotter (see Appendix A of Ref. [10]). In CE, one can always increase the free energy by approaching the particles at the same point. The free energy diverges when a Dirac peak containing all the particles is formed (see Appendix B of Ref. [10]). The absence of a strict statistical equilibrium state in a box can also be directly inferred from the divergence of the density of states in MCE and from the divergence of the partition function in CE at small distances [7,20].

[4]When the system is in a metastable state, the spontaneous formation of a binary star surrounded by a hot halo in MCE ($S \to +\infty$) or the spontaneous formation of a Dirac peak in CE ($J \to +\infty$) is a very rare event since its probability scales as e^{-N}. Indeed, in order to leave a metastable state, the system has to overcome a huge barrier of entropy or free energy whose height scales as N. This requires very particular correlations and takes too much time to be physically relevant.

Similar results are obtained with the classical King model (see Fig. 1) as shown by Katz [21] and further analyzed in Ref. [22] (Paper I). Therefore, a self-gravitating system can reach a statistical equilibrium state described by the King model (truncated Boltzmann distribution) at sufficiently high energies and at sufficiently high temperatures, even if there is no statistical equilibrium state in a strict sense [7–9]. However, for $E < E_c$ or $T < T_c$, there is no statistical equilibrium state anymore and the system undergoes gravitational collapse.[5] This is called gravothermal catastrophe [2] in MCE and isothermal collapse [17] in CE. In MCE, the gravothermal catastrophe leads to a binary star surrounded by a hot halo [23]. In CE, the isothermal collapse leads to a Dirac peak containing all the particles [24]. Therefore, the result of the gravitational collapse is to form a singularity: a "binary star + hot halo" in MCE and a "Dirac peak" in CE [9].

These results have been obtained from a *thermodynamical approach*, pioneered by Antonov [1] and Lynden-Bell and Wood [2] (see also Refs. [7–10,16–19]), where the maximization of the Boltzmann entropy at fixed mass and energy in MCE or the minimization of the Boltzmann free energy in CE are considered in order to get the "most probable" state. These results have been confirmed by a more rigorous *statistical mechanics* approach, developed by Horwitz and Katz [25,26] and de Vega and Sanchez [27,28], starting directly from the density of states in MCE or from the partition function in CE and using field-theoretical methods. By using the theory of large deviations, one can show on general grounds that these two approaches are physically equivalent [6].

The previous results are valid for classical particles such as stars in globular clusters. If we now consider a gas of self-gravitating fermions, gravitational collapse stops when the system becomes degenerate as a consequence of the Pauli exclusion principle. In that case, the singularity (tight binary or Dirac peak) is smoothed out and replaced by a compact object which is a completely degenerate "fermion ball" similar to a white dwarf star. At finite temperature, this compact object is surrounded by a dilute atmosphere (vapor) so that the whole configuration has a "core-halo" structure. Therefore, when quantum mechanics is properly accounted for, the system is stabilized against gravitational collapse. In that case, there exists an equilibrium state for any accessible value of energy and temperature. We can therefore study phase transitions between a "gaseous phase" unaffected by quantum mechanics and a "condensed phase" dominated by quantum mechanics.[6] The nature of these phase transitions has been discussed in detail by Chavanis [29–34] (see a review in Ref. [9]) in the case where the fermions are confined within a box. Similar phase transitions are obtained if, instead of quantum particles, we consider classical particles and regularize the gravitational potential at short distances [31,35–38] or take into account the finite size of the particles by considering a hard-spheres gas [7,29,34,39–41]. For completeness, we should also mention the seminal paper of Lynden-Bell and Lynden-Bell [5] and the series of papers by Miller and collaborators [42–48] who studied phase transitions in the system of concentric spherical gravitating shells introduced by Hénon [49]. Even if the details of the phase transitions depend on the specific form of the small-scale regularization, the phenomenology of these phase transitions is relatively universal, as described in Ref. [9]. In the present paper, we extend the study of Ref. [9] to the fermionic King model. This extension is important because the fermionic King model is more realistic than box models. Furthermore, the fermionic King model may have applications in astrophysics and cosmology. Indeed, it may provide a realistic model of dark matter halos made of massive neutrinos.

The observation of the rotation curves of galaxies has revealed that the galaxies are surrounded by a halo of dark matter [50]. The nature of dark matter remains unknown and constitutes one of the greatest challenge of modern cosmology. The cold dark matter (CDM) model is successful at describing the large-scale structures of the Universe but it encounters many problems at the scale of galactic or subgalactic structures. In particular, CDM simulations [51] lead to r^{-1} cuspy density profiles at galactic centers (at the scales of the order of 1 kpc and smaller) while most rotation curves indicate a smooth core density [52]. On the other hand, the predicted number of satellite galaxies around each galactic halo is far beyond what we see around the Milky Way [53]. It is therefore

[5]In practice, the energy and the temperature slowly decrease with time due to collisions and evaporation until a point at which there is no equilibrium state anymore (see Appendix A). In that case, the system collapses. This corresponds to a saddle-node bifurcation. Therefore, the lifetime of stellar systems is controlled by evaporation and gravitational collapse.

[6]For self-gravitating fermions, there exists a strict statistical equilibrium state (global maximum of entropy or global maximum of free energy) for all accessible values of energy and temperature. There may also exist metastable states (local maxima of entropy or local maxima of free energy) that are as much, or even more, relevant than fully stable states. Indeed, the choice of the equilibrium state depends on a notion of "basin of attraction" and the metastable states may be reached more easily from generic initial conditions than the fully stable states that require very particular correlations. For example, in order to pass from the gaseous phase to the condensed phase, the system must cross a huge barrier of entropy or free energy and evolve through an intermediate phase in which some particles must approach very close to each other. Inversely, to pass from the condensed phase to the gaseous phase, the system must cross a huge barrier of entropy or free energy and evolve through an intermediate phase in which some particles must escape from the condensate. The probability of such events is extremely low so that, in practice, the system remains in the metastable phase [9,19].

necessary to develop new models of dark matter in order to solve these problems (cusp problem and missing satellite problem).

Several authors [9,29,30,54–74] have proposed to describe dark matter halos as a gas of fermions.[7] The Pauli exclusion principle avoids density cusps at the halo center and solves the problems of the CDM model. The necessity of taking quantum mechanics into account in the physics of galactic halos was demonstrated by Destri, de Vega, Salucci and Sanchez [70–74] (denoted DdVSS below). Quantum mechanics is particularly relevant for compact dwarf halos. Indeed, DdVSS [70–74] have shown that compact (small) dark matter halos are quantum (degenerate) objects stabilized against gravitational collapse by the Pauli exclusion principle while large (gaseous) halos are classical (nondegenerate) objects stabilized by thermal motion (intermediate size halos are stabilized by both). Using the fact that the smallest known dark matter halo is completely degenerate, DdVSS [70–74] obtained a lower bound of about 2 keV/c^2 on the mass of the fermions (other authors [75] obtained a smaller lower bound of about $m = 200\ \mathrm{eV}/c^2$ based on the analysis of the velocity dispersion of dwarf spheroidal galaxies). The dark matter particle may be a sterile neutrino [76,77].[8] In these studies, the usual Fermi-Dirac distribution is used. However, at finite temperature, this distribution coupled to the Poisson equation leads to models of dark matter halos with an infinite mass (because the density decreases as r^{-2} at large distances). This prevents one from determining the caloric curves of dark matter halos and studying the thermodynamical stability of the configurations (the problem is mathematically ill posed). If we want to obtain the caloric curves of dark matter halos (which is the main objective of this paper), it is indispensable to go beyond the usual Fermi-Dirac distribution and use a model that has a finite mass.

We propose to describe dark matter halos by the fermionic King model. This model takes into account the evaporation of high-energy particles and has a finite mass. This model was introduced by Ruffini and Stella [55] as a heuristic extension of the classical King model to the case of fermions. It was introduced independently by Chavanis [63,80] who derived it from a kinetic theory based on the fermionic Landau equation. As explained in Paper I, the fermionic King model can describe either a gas of fermions (e.g. massive neutrinos) at statistical equilibrium or a collisionless system of particles (classical or quantum) experiencing a process of violent relaxation of Lynden-Bell's type [62,63,80–82]. In Paper I, we have considered large dark matter halos for which quantum mechanics is negligible. We have shown that such halos are relatively well described by the classical King model at, or close to, the limit of microcanonical stability (see Fig. 2).[9] At that point, the King profile can be approximated by the modified Hubble profile [13]. It has an isothermal core, an isothermal halo, and a polytropic envelope of index $n = 5/2$. The density profile is flat in the core and decreases as r^{-3} in the halo. The marginal King profile and the modified Hubble profile are relatively similar to the Burkert profile [52] that gives a good fit of many dark matter halos.[10]

For large dark matter halos, the problems of the CDM model (density cusps and missing satellites) are solved by thermal effects, not by quantum mechanics. This corresponds to warm dark matter (WDM). However, quantum mechanics becomes important for dwarf and intermediate size halos. In this paper, in order to describe all types of dark matter halos, we consider the fermionic King model with an arbitrary level of quantum degeneracy.

The density profiles and rotation curves of self-gravitating fermions describing dark matter halos have

[7]There are also several studies describing dark matter halos as a gas of bosons (see Paper I for a detailed list of references).

[8]A sterile neutrino with a mass in the keV/c^2 range may have been detected recently as a dark matter constituent [78,79].

[9]The classical King model defines a one-parameter family of distribution functions parametrized by the concentration parameter k. This family of distribution functions is plotted in Fig. 18 of Paper I for different values of k. The Boltzmann distribution corresponds to $k \to +\infty$. However, we have shown in Paper I that the King model becomes unstable when $k > k_{\mathrm{MCE}} = 7.44$. We have also given arguments according to which dark matter halos should be described by the King model at, or close to, the point of marginal stability $k = k_{\mathrm{MCE}}$. Therefore, the curve called King in Fig. 2 corresponds to the marginal King model with $k = k_{\mathrm{MCE}}$. It physically differs from the isothermal (Boltzmann) distribution, corresponding to $k \to +\infty$.

[10]The Burkert profile [52] fitting observations has a flat core and a density profile that decreases as r^{-3} at large distances. The NFW profile [51] fitting N-body simulations also decreases as r^{-3} at large distances but presents a cusp $\rho \propto r^{-1}$ for $r \to 0$ (instead of a core) in contradiction with the observations [52]. The modified Hubble profile [13] has a flat core and a density profile that decreases as r^{-3} at large distances, similarly to the Burkert profile. The modified Hubble profile is a particular case of the family of density profiles introduced empirically by Moore *et al.* [83] and de Vega and Sanchez [73,74] [it corresponds to the indices $(\alpha, \beta, \gamma) = (2, 3, 0)$ in Ref. [83] and to the index $\alpha = 3/2$ in Refs. [73,74]]. These authors mention that this profile gives a good fit of the observations of dark matter halos (it may even fit dark matter halos better than the Burkert profile). However, no rigorous justification is given for such profiles and for the value of the selected indices, except for the fact that they provide a good fit of dark matter halos. Our approach, that is based on the physically motivated King model, provides a *justification* of their empirical results by showing that the asymptotic behavior r^{-3} of the density profile that is common to the NFW, Burkert and modified Hubble profiles (and that determines the indices in the profiles of Refs. [73,74,83]) corresponds to the marginal King model that has an asymptotic logarithmic slope $\alpha_{\mathrm{MCE}} = -d\ln\rho/d\ln r \simeq 3$ (see Fig. 20 of Paper I). This justifies why the observed density profile of dark matter halos decreases as r^{-3} (marginal King) instead of r^{-2} (isothermal). We refer to Sec. VII.H of Paper I for a detailed discussion of this issue.

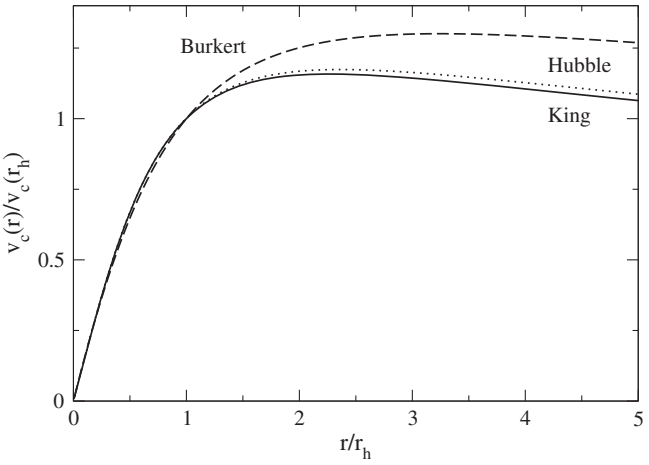

FIG. 2. Normalized rotation curve of the classical King model at the point of marginal stability (full line) compared with the modified Hubble profile (dotted line) and Burkert profile (dashed line). All these profiles coincide up to the halo radius. The similarities and the differences between the marginal King profile ($k = k_{\rm MCE} = 7.44$) considered in Ref. [22] and the isothermal (Boltzmann) profile ($k \to +\infty$) considered by DdVSS [70–74] are discussed in detail in Sec. VII.H. of Ref. [22].

been obtained by several authors in the past [9,29,30,54–74] with an emphasis recently given by DdVSS [70–74]. However, these curves are often based on the usual Fermi-Dirac distribution, which has the undesirable feature of having an infinite mass (because it decreases as r^{-2} for $r \to +\infty$). In our paper, we provide density profiles and rotation curves based on the fermionic King model, which has a finite mass. This distinction is important. In Paper I (see in particular Sec. VII H), we showed that close to the point of marginal stability, the density profile of the King model decreases at large distances as r^{-3} [in agreement with the observational Burkert profile [52] and with the numerical Navarro-Frenk-White (NFW) profile [51]] instead of r^{-2} (corresponding to the isothermal sphere). These remarks concern the tail of the density profile. On the other hand, we recall that the density profiles of self-gravitating fermions based on the Fermi-Dirac distribution or on the fermionic King model present, like the Burkert profile (and unlike the NFW profile), a central core (instead of a cusp) due to quantum pressure and/or thermal pressure, as emphasized by DdVSS [70–74].

The paper is organized as follows. In Sec. II, we introduce the fermionic King model. This distribution function is appropriate to describe dark matter halos if they are made of massive neutrinos at statistical equilibrium or if they have experienced a violent relaxation of Lynden-Bell's type. In Sec. III, we discuss general properties of the fermionic King model. We show that it generically has a polytropic core of index $n = 3/2$, a classical isothermal halo, and a polytropic envelope of index $n = 5/2$. In Sec. IV, we study the nature of phase transitions in the fermionic King model depending on the value of the degeneracy parameter (i.e. the size of the system). We emphasize the importance of metastable states in systems with long-range interactions. In Sec. V, we plot the density profiles and the rotation curves of the fermionic King model. We discuss their ability to describe dark matter halos. We follow the series of equilibria for increasing concentration parameter. We argue in connection with DdVSS [70–74] that large dark matter halos are non-degenerate, intermediate size halos are partially degenerate, and dwarf halos are completely degenerate. We show that gravitational collapse in MCE results in the formation of a small degenerate object containing a small mass accompanied by the expulsion of a hot envelope containing a large mass. By contrast, gravitational collapse in CE leads to a small degenerate object containing almost all the mass surrounded by a tenuous envelope. In Secs. VI–IX, we argue that large dark matter halos cannot contain a fermion ball because this nucleus-halo structure is thermodynamically unstable (saddle point of entropy). This may explain why black holes are observationally favored over fermion balls at the center of galaxies. In Appendix A, we discuss subtle issues concerning the dynamical and thermodynamical stability of the fermionic King model. In Appendix B, we give arguments according to which MCE is more appropriate than CE to describe dark matter halos. In Appendix C, we introduce dimensionless quantities that can be related to observations. In Appendix D, we compare fermionic and bosonic models of dark matter and discuss the value of the mass of the dark matter particle in each case. In Appendix E, we determine whether dark matter halos are classical or quantum objects depending on their mass. In Appendix F, we determine the temperature of dark matter halos. In Appendix G, we determine the maximum mass of relativistic compact objects that dark matter halos may contain at their center. In Appendix H, we argue that large dark matter halos may harbor a central black hole and we determine the minimum halo mass above which black holes can form. In Appendix I, we discuss general scenarios of formation of dark matter halos depending on the nature of the dark matter particle.

II. MODELS OF DARK MATTER HALOS BASED ON STATISTICAL MECHANICS

We consider the possibility that dark matter halos can be described by the fermionic King model defined by [55,63,80]

$$f = \eta_0 \frac{1 - e^{\beta(\epsilon-\epsilon_m)}}{1 + e^{\beta\epsilon+\alpha}} \quad \text{if } \epsilon \leq \epsilon_m, \tag{1}$$

and $f = 0$ if $\epsilon \geq \epsilon_m$. Here, $f(\mathbf{r}, \mathbf{v})$ gives the mass density of particles with position $\mathbf{r}$ and velocity $\mathbf{v}$, $\rho(\mathbf{r}) = \int f(\mathbf{r}, \mathbf{v}) d\mathbf{v}$ gives the mass density of particles with position $\mathbf{r}$, $\eta_0 = gm^4/h^3$ is the maximum accessible value of the distribution

function fixed by the Pauli exclusion principle (m is the mass of the particles, h is the Planck constant, and $g = 2s+1$ is the spin multiplicity of the quantum states[11]), $\epsilon = v^2/2 + \Phi(\mathbf{r})$ is the individual energy of the particles by unit of mass, $\Phi(\mathbf{r})$ is the gravitational potential determined by the Poisson equation $\Delta\Phi = 4\pi G\rho$, ϵ_m is the escape energy, $\beta = m/k_B T$ is the inverse temperature, and $\epsilon_F = -\alpha/\beta$ is the chemical potential (Fermi energy).[12]

For $\epsilon_m \to +\infty$, we recover the Fermi-Dirac distribution $f = \eta_0/(1+e^{\beta\epsilon+\alpha})$.

In the nondegenerate limit $\alpha \to +\infty$, we recover the classical King model $f = \eta_0 e^{-\beta\epsilon_m-\alpha}[e^{-\beta(\epsilon-\epsilon_m)} - 1]$ which reduces to the Boltzmann distribution $f = \eta_0 e^{-(\beta\epsilon+\alpha)}$ for $\epsilon_m \to +\infty$.

The fermionic King model (1) can be derived from a kinetic theory based on the fermionic Landau equation by looking for a quasistationary state of this equation such that $f = 0$ at $\epsilon = \epsilon_m$ [63,80].

The fermionic King model (1) will be of the form of Eq. (I-17)[13] provided that $\beta\epsilon_m + \alpha$ can be treated as a constant along the series of equilibria. We write this constant as

$$A \equiv \eta_0 e^{-\beta\epsilon_m-\alpha}. \tag{2}$$

Using Eq. (2), the fermionic King model can be rewritten as

$$f = A\frac{\frac{\eta_0}{A} - e^{\beta\epsilon+\alpha}}{1+e^{\beta\epsilon+\alpha}}. \tag{3}$$

It is of the form of Eq. (I-17) with $\mathcal{F}(x) = (\mu - e^x)/(1+e^x)$ where we have introduced the degeneracy parameter $\mu = \eta_0/A$. The function $\mathcal{F}(x)$ vanishes at $x_0 = \ln\mu$ and we check that Eq. (2) satisfies the general relation $\beta\epsilon_m + \alpha = x_0$ of Paper I. Using Eq. (2), the fermionic King model can also be rewritten as

$$f = A\frac{e^{-\beta(\epsilon-\epsilon_m)} - 1}{1+\frac{A}{\eta_0}e^{-\beta(\epsilon-\epsilon_m)}}. \tag{4}$$

It is of the form of Eq. (I-19) with $\mathcal{F}_s(x) = (e^{-x}-1)/(1+e^{-x}/\mu)$. By construction $\mathcal{F}_s(0) = 0$.

In the nondegenerate limit $\alpha \to +\infty$, we recover the classical King model. Using Eq. (3) it can be written as

$$f = A\left[\frac{\eta_0}{A}e^{-(\beta\epsilon+\alpha)} - 1\right], \tag{5}$$

corresponding to $\mathcal{F}(x) = \mu e^{-x} - 1$. Alternatively, using Eq. (4), it can be written as

$$f = A[e^{-\beta(\epsilon-\epsilon_m)} - 1], \tag{6}$$

corresponding to $\mathcal{F}_s(x) = e^{-x} - 1$.

Finally, following the method of Paper I, we can determine the generalized entropy (I-9) associated with the King model. For the fermionic King model we get

$$C(f) = A\left[\left(1+\frac{f}{A}\right)\ln\left(1+\frac{f}{A}\right) - \frac{f}{A}\right] + \eta_0\left[\left(1-\frac{f}{\eta_0}\right)\ln\left(1-\frac{f}{\eta_0}\right) + \frac{f}{\eta_0}\right] - \ln\left(\frac{\eta_0}{A}\right)f \tag{7}$$

and for the classical King model we obtain

$$C(f) = A\left[\left(1+\frac{f}{A}\right)\ln\left(1+\frac{f}{A}\right) - \frac{f}{A}\right] - \ln\left(\frac{\eta_0}{A}\right)f. \tag{8}$$

We note that our description of the self-gravitating Fermi gas is based on a mean-field approximation where the correlations between particles are neglected (except for the exclusion principle) and on the Thomas-Fermi (TF) approximation where the quantum potential (accounting for the Heisenberg uncertainly principle) is also neglected. These approximations are commonly made to describe self-gravitating fermions such as electrons in white dwarf stars, neutrons in neutron stars, and massive neutrinos in dark matter halos. Hertel and Thirring [84,85] have established that these approximations are rigorously valid in a proper thermodynamic limit where $N \to +\infty$.

III. THE FERMIONIC KING MODEL

In this section, we apply the general formalism developed in Paper I to the case of the fermionic King model.

A. The distribution function

The fermionic King model is defined by

$$f = A\frac{e^{-\beta(\epsilon-\epsilon_m)} - 1}{1+\frac{1}{\mu}e^{-\beta(\epsilon-\epsilon_m)}} \quad \text{if } \epsilon \le \epsilon_m, \tag{9}$$

$$f = 0 \quad \text{if } \epsilon \ge \epsilon_m, \tag{10}$$

where ϵ_m is the escape energy at which the particles leave the system ($f = 0$) and $\mu = \eta_0/A$ is the degeneracy parameter. For $\epsilon \to -\infty$, the fermionic King distribution tends to a constant value $f \to \mu A = \eta_0$ so it is equivalent to a polytropic distribution of index $n = 3/2$ [13]. For intermediate energies, it can be approximated by the

[11] In the numerical applications, we shall take $s = 1/2$ and $g = 2$.

[12] The preceding relations are written in the case where dark matter is a quantum gas made of fermions (e.g. massive neutrinos) at statistical equilibrium. They remain valid if dark matter is a collisionless gas undergoing a process of violent relaxation of Lynden-Bell's type [62,63,80–82]. In that case, the physical meaning of η_0 and β is different as explained in Paper I.

[13] Here and in the following (I-x) refers to Eq. (x) of Paper I.

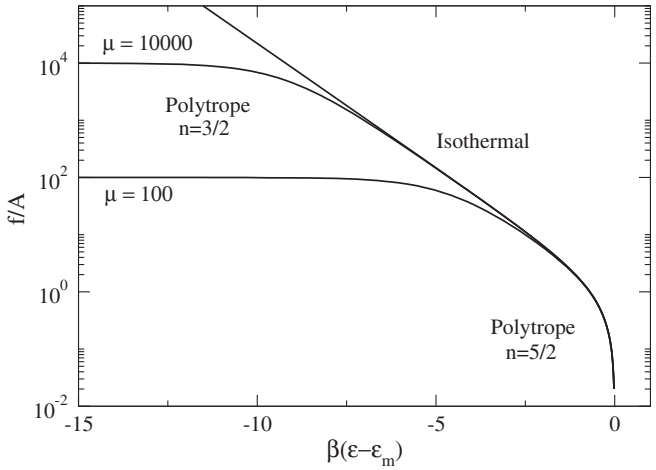

FIG. 3. The distribution function $f(\epsilon)$ in scaled variables showing the polytropic core, the isothermal halo, and the polytropic envelope.

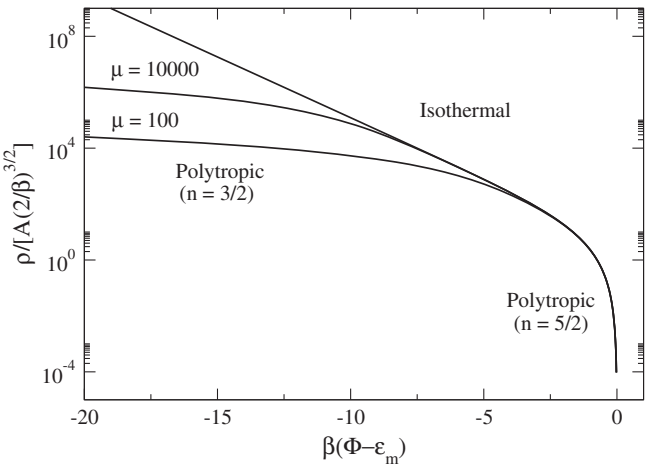

FIG. 4. The density $\rho(\Phi)$ in scaled variables showing the polytropic core, the isothermal halo, and the polytropic envelope.

Boltzmann distribution $f \sim Ae^{-\beta(\epsilon-\epsilon_m)}$. For $\epsilon \to \epsilon_m^-$, it reduces to $f \sim A\beta(\epsilon_m - \epsilon)/(1+1/\mu)$ so it is equivalent to a polytropic distribution of index $n = 5/2$ [13]. Therefore, the fermionic King model generically describes a cluster with a polytropic core of index $n = 3/2$, a classical isothermal halo, and a polytropic envelope of index $n = 5/2$. The proportion of these different regions depends on the concentration parameter $k = \beta(\epsilon_m - \Phi_0)$ as shown in the sequel. The distribution function $f(\epsilon)$ is represented in Fig. 3.

The fermionic King distribution is of the form of Eq. (I-19) with

$$\mathcal{F}_s(x) = \frac{e^{-x}-1}{1+\frac{1}{\mu}e^{-x}}. \tag{11}$$

The asymptotic behaviors of the functions $I_n(z)$ defined in Paper I with Eq. (11) for small and large values of z are easily obtained. For $z \to 0$, using the fact that $\mathcal{F}_s(x) \sim -x/(1+1/\mu)$ for $x \to 0$, we get

$$I_n(z) \sim \frac{1}{1+\frac{1}{\mu}} \frac{8\pi}{(2n+1)(2n+3)} z^{(2n+3)/2}. \tag{12}$$

For $z \to +\infty$, using the fact that $\mathcal{F}_s(x) \to \mu$ for $x \to -\infty$, we get

$$I_n(z) \sim \frac{4\pi\mu}{2n+1} z^{(2n+1)/2}. \tag{13}$$

B. The equation of state

The normalized gravitational potential is defined by $\chi(r) = \beta[\epsilon_m - \Phi(r)]$. For $\chi \to +\infty$, using Eqs. (I-27), (I-37) and (13), we find that

$$\rho \sim A\left(\frac{2}{\beta}\right)^{3/2} \frac{4\pi}{3}\mu\chi^{3/2}, \qquad p \sim \frac{1}{3}A\left(\frac{2}{\beta}\right)^{5/2} \frac{4\pi}{5}\mu\chi^{5/2}, \tag{14}$$

leading to the equation of state

$$p \sim \frac{1}{5}\left(\frac{3}{4\pi\eta_0}\right)^{2/3}\rho^{5/3}. \tag{15}$$

This polytropic equation of state of index $n = 3/2$ is valid at high densities.

For $\chi \to 0$, using Eqs. (I-27), (I-37) and (12), we find that

$$\rho \sim A\left(\frac{2}{\beta}\right)^{3/2} \frac{8\pi}{15} \frac{1}{1+\frac{1}{\mu}}\chi^{5/2},$$
$$p \sim \frac{1}{3}A\left(\frac{2}{\beta}\right)^{5/2} \frac{8\pi}{35} \frac{1}{1+\frac{1}{\mu}}\chi^{7/2}, \tag{16}$$

leading to the equation of state

$$p \sim \frac{1}{7}\left(\frac{15}{4\pi A\beta}\right)^{2/5}\left(1+\frac{1}{\mu}\right)^{2/5}\rho^{7/5}. \tag{17}$$

This polytropic equation of state of index $n = 5/2$ is valid at low densities.

For intermediate densities, we obtain an isothermal equation of state $p \sim \rho/\beta$.

For $\Phi \to -\infty$, the density is related to the gravitational potential by $\rho(\Phi) \propto (-\Phi)^{3/2}$ which corresponds to a polytropic distribution of index $n = 3/2$. For intermediate values of Φ, we get the Boltzmann distribution $\rho(\Phi) \propto e^{-\beta\Phi}$. For $\Phi \to \epsilon_m^-$, the density is related to the gravitational potential by $\rho(\Phi) \propto (\epsilon_m - \Phi)^{5/2}$ which corresponds to a polytropic distribution of index $n = 5/2$. The relation $\rho(\Phi)$ is represented in Fig. 4.

C. The polytropic limit $k \to 0$

In the limit $k \to 0$, the function χ is always small, so we can use the approximation (12) everywhere. As a result, the King model is equivalent to a pure polytrope ($p = K\rho^{1+1/n}$) of index $n = 5/2$ and polytropic constant $K = (1/7)(15/4\pi A\beta)^{2/5}(1 + 1/\mu)^{2/5}$. The degeneracy parameter μ affects the value of the polytropic constant but its effect is weak when $\mu \gg 1$. The differential equation (I-33) reduces to the Lane-Emden equation (I-77). The results of Paper I can be easily generalized to account for the μ dependence of the different quantities when $k \to 0$. We get $\tilde{R} \sim 20.0(1 + 1/\mu)^2/\tilde{\beta}^2$, $\tilde{\beta} \sim 5.77(-\tilde{E})^{1/2}(1 + 1/\mu)$, $\tilde{R} \sim -3/(5\tilde{E})$, $\tilde{\beta} = 2.02k^{1/3}(1 + 1/\mu)^{2/3}$, $\tilde{R} \sim 4.90k^{-2/3}(1 + 1/\mu)^{2/3}$, and $\tilde{E} \sim -0.123k^{2/3}(1 + 1/\mu)^{-2/3}$. We also note that $\epsilon \to -3/5$, $\eta \sim -\xi_1\theta_1' k \sim 0.409k$, $\mathcal{K} \to 4.93$, $\tilde{\rho}_0 \sim 0.584k^2(1 + 1/\mu)^{-2}$, $\tilde{\sigma}_0^2 \sim 0.141k^{2/3}(1 + 1/\mu)^{-2/3}$, and $\beta\sigma_0^2 \sim (2/7)k$.

D. The completely degenerate limit $k \to +\infty$

In the limit $k \to +\infty$, we can use the approximation (13) everywhere. As a result, the fermionic King model is equivalent to a pure polytrope ($p = K\rho^{1+1/n}$) of index $n = 3/2$ and polytropic constant $K = (1/5)(3/4\pi\eta_0)^{2/3}$. This corresponds to the completely degenerate limit, valid at $T = 0$, in which the distribution function is $f = \eta_0 H(\epsilon - \epsilon_F)$ where $H(x)$ is the Heaviside function and $\epsilon_F = -\alpha/\beta$ is the Fermi energy. We note that, in this limit, the Fermi energy coincides with the escape energy since Eq. (2), which can be rewritten as $\epsilon_m - \epsilon_F = (1/\beta)\ln\mu$, reduces to $\epsilon_F = \epsilon_m$ for $\beta \to +\infty$. Defining $\theta = \chi/k$ and $\xi = \zeta/\sqrt{k}$, we find that the differential equation (I-33) reduces to the Lane-Emden equation

$$\frac{1}{\xi^2}\frac{d}{d\xi}\left(\xi^2\frac{d\theta}{d\xi}\right) = -\theta^{3/2}, \tag{18}$$

$$\theta(0) = 1, \qquad \theta'(0) = 0, \tag{19}$$

corresponding to a polytrope $n = 3/2$ [11]. Solving this equation numerically, we obtain $\xi_1 = 3.65$ and $\theta_1' = -0.203$. Using the theory of polytropes, we can analytically obtain the radius $R_{\rm min}$ and the energy $E_{\rm min}$ of the completely degenerate cluster at $T = 0$. This corresponds to the ground state of the self-gravitating Fermi gas. Proceeding as in Paper I, we get

$$MR^3 = \frac{\chi}{\eta_0^2 G^3} \tag{20}$$

and

$$E = -\frac{3G^2M^{7/3}\eta_0^{2/3}}{7\chi^{1/3}}, \tag{21}$$

where $\chi = 9\omega_{3/2}/2048\pi^4 = 5.97 \times 10^{-3}$. Introducing the dimensionless variables defined in Paper I, we obtain

$$\tilde{E}_{\rm min} = -\frac{3}{7\chi^{1/3}}\frac{1}{(8\sqrt{2}\pi)^{2/3}}\mu^{2/3} = -0.219\mu^{2/3}, \tag{22}$$

$$\tilde{R}_{\rm min} = \chi^{1/3}(8\sqrt{2}\pi)^{2/3}\mu^{-2/3} = 1.96\mu^{-2/3}. \tag{23}$$

These two quantities are related to each other by $\tilde{E}_{\rm min} = -3/7\tilde{R}_{\rm min}$. From Eqs. (I-42), (18) and (19), we also find that

$$\tilde{\beta} \sim \left(\frac{3}{4\pi\mu}\right)^{2/3}(-\xi_1^2\theta_1')^{4/3}k \sim 1.45\mu^{-2/3}k \to +\infty. \tag{24}$$

Finally, we note that $\epsilon \to -3/7$, $\eta \sim -\xi_1\theta_1' k \sim 0.741k \to +\infty$, $\mathcal{K} \to (5/2)(1 - \xi_1\theta_1') = 4.35$, $\tilde{\rho}_0 \to (4\pi\mu/3)^2/(-\xi_1^2\theta_1')^2 = 2.40\mu^2$, $\tilde{\sigma}_0^2 \to 0.276\mu^{2/3}$, and $\beta\sigma_0^2 \sim (2/5)k$.

E. The degeneracy parameter μ

An important quantity in the theory is the degeneracy parameter $\mu = \eta_0/A$. Since A has the dimension of a typical distribution function $\langle f\rangle$, the degeneracy parameter can be rewritten as $\mu = \eta_0/\langle f\rangle$. It represents the ratio between the maximum distribution function η_0 fixed by the Pauli exclusion principle and the typical distribution function of the system $\langle f\rangle$. If we write $\langle f\rangle \sim MR^{-3}V^{-3}$ where M is the typical mass of the system, R its typical radius and V its typical velocity, and use a virial-type relation $V \sim (GM/R)^{1/2}$, we obtain $\langle f\rangle \sim G^{-3/2}M^{-1/2}R^{-3/2}$. As a result, the degeneracy parameter $\mu \sim \eta_0 G^{3/2}M^{1/2}R^{3/2}$ coincides, up to a multiplicative constant, with the degeneracy parameter $\mu_{\rm box}$ introduced in the study of box-confined self-gravitating fermions (see Sec. 5.5 of Ref. [9]). As discussed in more detail in Ref. [9], μ is a measure of the size of the system. Large values of μ correspond to large dark matter halos and small values of μ correspond to small dark matter halos. We shall keep this interpretation in mind in our analysis.

We have argued in Paper I that A should be kept fixed along a series of equilibria. Since η_0 is given, μ can be regarded as a dimensionless measure of A. Fixing A is equivalent to fixing μ. Therefore, each series of equilibria is characterized by a given value of A or, equivalently, by a given value of μ.

IV. PHASE TRANSITIONS IN THE FRAMEWORK OF THE FERMIONIC KING MODEL

A detailed study of phase transitions in the self-gravitating Fermi gas has been performed by Chavanis

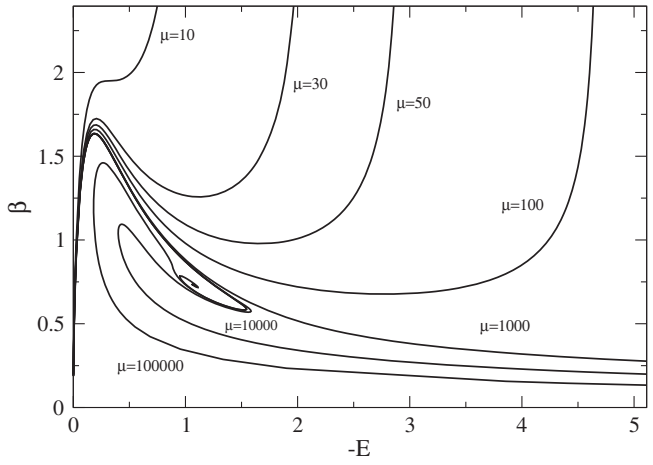

FIG. 5. Series of equilibria of the fermionic King model for different values of μ. The thick line corresponds to the classical King model ($\mu \to +\infty$). Note that for large values of μ, the minimum energy $E_{\rm min}(\mu)$ corresponding to $T = 0$ is outside the frame of the figure.

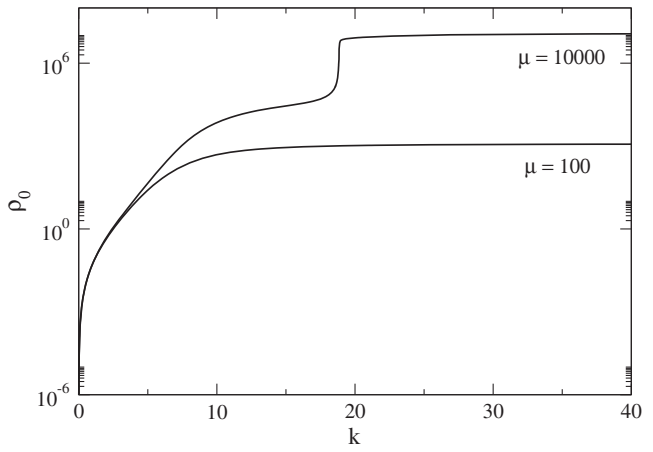

FIG. 6. Central density normalized by $(4\pi G)^3 A^2 M^2$ as a function of k in semilogarithmic scales.

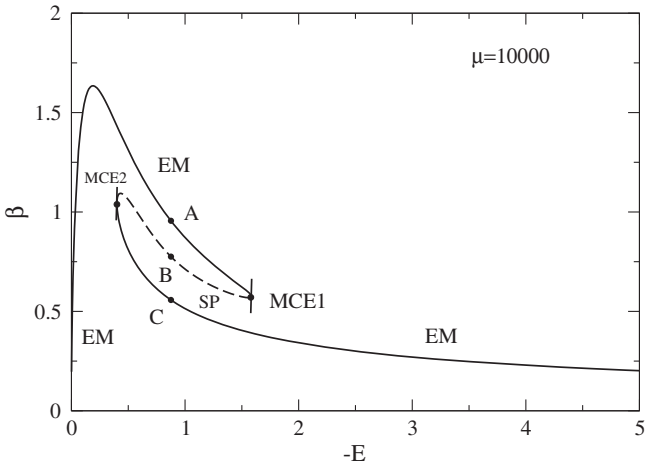

FIG. 7. Series of equilibria of the fermionic King model with $\mu = 10^4$.

[29–34] (see a review in Ref. [9]) in the case where the fermions are confined within a box. In this section, we extend this study to the case of the fermionic King model. This extension is important because this model has a finite mass so it does not require the introduction of an artificial box.

A. Series of equilibria

The series of equilibria $\beta(E)$ of the fermionic King model is represented in Fig. 5 for different values of μ. The method of construction of the series of equilibria is described in Paper I for a general distribution function of the form $f = f(\epsilon)$ with $f'(\epsilon) < 0$. We recall that A is fixed along a series of equilibria and that the thermodynamical parameters β and E correspond to the dimensionless parameters $\tilde{\beta}$ and $\tilde{E}$ of Paper I. On the other hand, S and J refer to S/M and J/M. We also recall that, for each value of μ, the series of equilibria is parametrized by the concentration parameter $k = \beta(\epsilon_m - \Phi_0)$ going from $k = 0$ at $(E, \beta) = (0, 0)$ to $k = +\infty$ at $(E, \beta) = (E_{\rm min}, +\infty)$ where $E_{\rm min}(\mu)$ is the minimum accessible energy (ground state) corresponding to $T = 0$ [see Eq. (22)]. The concentration parameter k is a monotonically increasing function of the normalized central density as shown in Fig. 6.

The shape of the series of equilibria $\beta(E)$ of the fermionic King model crucially depends on the value of the degeneracy parameter μ as shown in Fig. 5. In the nondegenerate limit $\mu \to +\infty$, we recover the spiral corresponding to the classical King model (see Fig. 1). However, for smaller values of μ, we see that the effect of quantum mechanics (Pauli exclusion principle) is to unwind the spiral. Depending on the value of μ, the series of equilibria can have different shapes. In the following, we consider two typical series of equilibria, one corresponding to a relatively large value of μ equal to 10^4 (Sec. IV B) and one corresponding to a relatively small value of μ equal to 100 (Secs. IV C and IV D).

B. Large halos in MCE: $\mu = 10^4$

For $\mu = 10^4$ (large halos), the series of equilibria of the fermionic King model is represented in Fig. 7. It has a Z-shape structure.

In this section, and in the next one, we assume that the system is isolated. In that case, the control parameter is the energy E and the relevant statistical ensemble is MCE. In MCE, we must determine maxima of entropy at fixed mass and energy. Since the curve $\beta(E)$ is multivalued, phase transitions occur in MCE. Using the Poincaré theorem (see Paper I), we deduce that all the states on the upper branch of the series of equilibria are entropy maxima (EM) until the first turning point of energy MCE1. For large values of μ, this critical energy is close to the energy $E_c = -1.54$

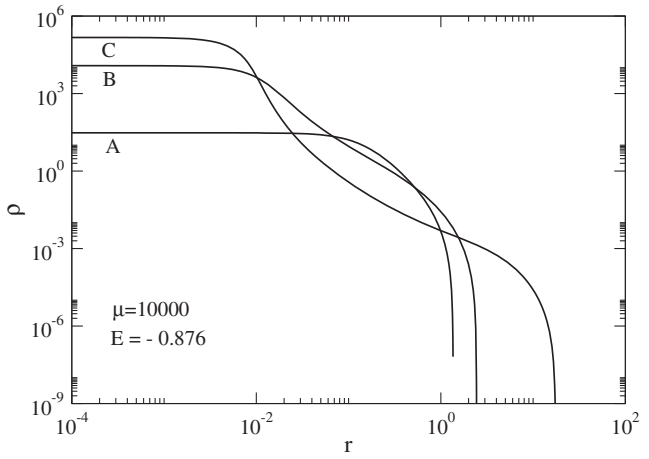

FIG. 8. Normalized density profiles corresponding to the different phases of the fermionic King model with $\mu = 10^4$ and $E = -0.876$. Here and in the following figures, the radial distance is scaled by $1/(4\pi GM^{1/3}A^{2/3})$ and the density by $(4\pi G)^3A^2M^2$. The "core-halo" structure of solutions B and C comprising a dense degenerate nucleus (fermion ball) surrounded by an atmosphere is clearly visible.

corresponding to the classical King model ($\mu \to +\infty$). At that point, the curve turns clockwise so that a mode of stability is lost. This mode of stability is regained at the second turning point of energy MCE2 at which the curve turns anticlockwise. The corresponding energy $E_*(\mu)$ depends on the value of μ and tends to $E_*(\mu) \to 0$ for $\mu \to +\infty$. The configurations on the branch between MCE1 and MCE2 are saddle points (SP) of entropy while the configurations on the lower branch after MCE2 are EM.

The solutions on the upper branch are stable (EM). They are nondegenerate and have a smooth density profile. They form the "gaseous phase" unaffected by quantum

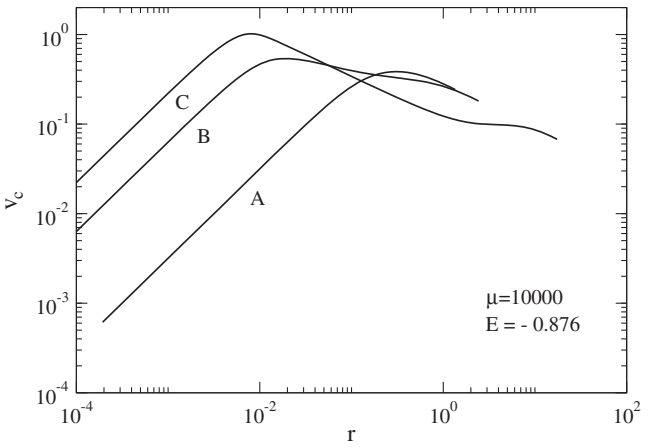

FIG. 9. Normalized rotation curves corresponding to the different phases of the fermionic King model with $\mu = 10^4$ and $E = -0.876$. Here and in the following figures, the radial distance is scaled by $1/(4\pi GM^{1/3}A^{2/3})$ and the circular velocity by $4\pi GA^{1/3}M^{2/3}$.

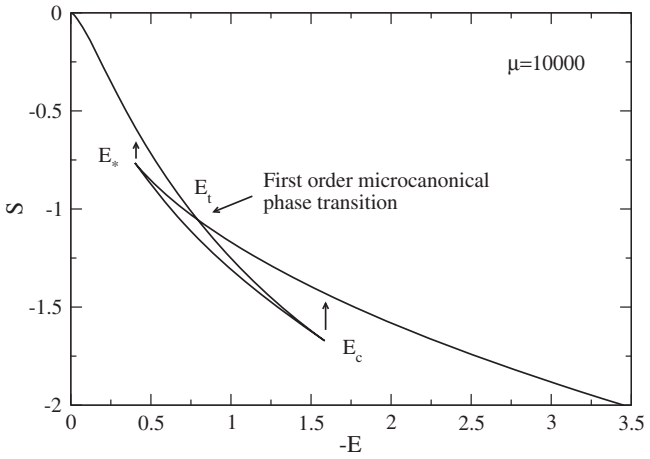

FIG. 10. Entropy of each phase versus energy for $\mu = 10^4$.

mechanics (see solution A in Figs. 8 and 9). The solutions on the lower branch are also stable (EM). They have a core-halo structure consisting of a degenerate nucleus (fermion ball) surrounded by a dilute atmosphere (vapor). They form the "condensed phase" dominated by quantum mechanics (see solution C in Figs. 8 and 9). The nucleus (condensate) is equivalent to a completely degenerate self-gravitating fermion ball at $T = 0$ with the maximum phase-space density η_0. It is stabilized against gravitational collapse by the Pauli exclusion principle. The solutions on the intermediate branch are unstable (SP). They are similar to the solutions of the gaseous phase but they contain a small embryonic degenerate nucleus, like in the condensed phase, playing the role of a "germ" in the language of phase transitions (see solution B in Figs. 8 and 9). These solutions form a barrier of entropy that the system has to cross in order to pass from the gaseous phase to the condensed phase, or inversely (see Ref. [9] for more details).

If we compare the entropy of the solutions (see Fig. 10), we expect a first-order microcanonical phase transition to take place at a transition energy $E_t(\mu)$ where the entropy of

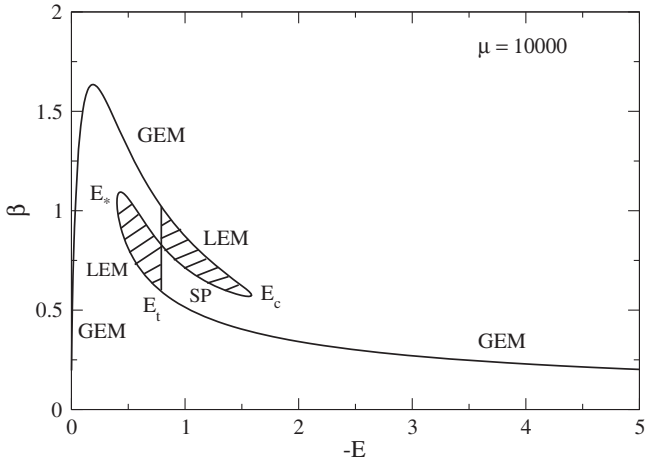

FIG. 11. Maxwell construction for $\mu = 10^4$ in MCE.

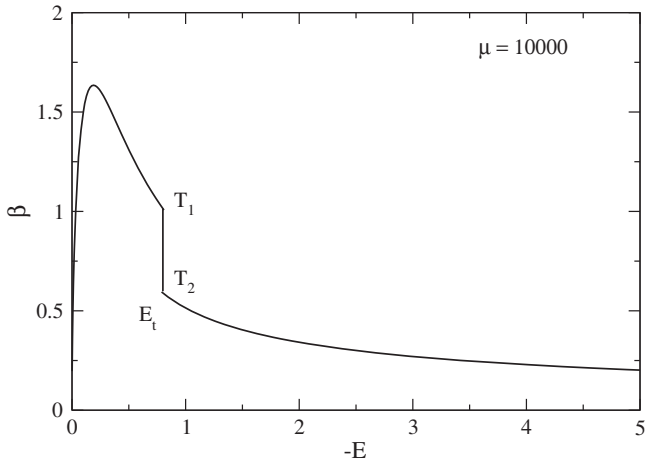

FIG. 12. Strict microcanonical caloric curve for $\mu = 10^4$.

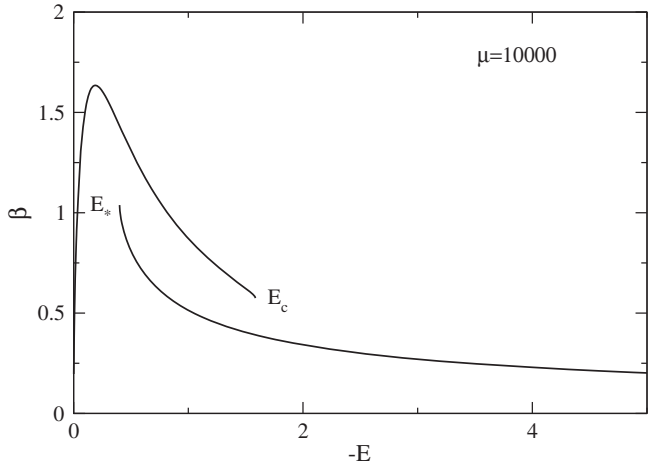

FIG. 13. Physical microcanonical caloric curve for $\mu = 10^4$.

the gaseous phase and the entropy of the condensed phase become equal. The transition energy $E_t(\mu)$ can also be obtained by performing a Maxwell construction (see the vertical plateau in Fig. 11) [9]. For $E > E_t$ the gaseous phase is fully stable [global entropy maximum (GEM) at fixed mass and energy] while the condensed phase is metastable [local entropy maximum (LEM) at fixed mass and energy]. For $E < E_t$ the gaseous phase is metastable (LEM) while the condensed phase is fully stable (GEM). The strict caloric curve is obtained by keeping only the fully stable states (see Fig. 12). It is marked by a discontinuity of the inverse temperature $\beta = \partial S/\partial E$ at $E = E_t(\mu)$. Equivalently, the first derivative of the entropy is discontinuous at the transition (see Fig. 10). This characterizes a microcanonical first-order phase transition. The specific heat $C = dE/dT$ is also discontinuous at the transition. If $E_t > E_{\rm gas}$ (where $E_{\rm gas}$ is the energy corresponding to the first turning point of temperature) the specific heat passes from a positive to a negative value. If $E_t < E_{\rm gas}$, the specific heat is always negative at the transition (the crossover occurs for $\mu \simeq 8.02 \times 10^5$ and $E_t = E_{\rm gas} = -0.189$; see the intersection between E_t and $E_{\rm gas}$ in Fig. 29).

However, for systems with long-range interactions, the metastable states are long-lived because the probability that a fluctuation triggers a phase transition and drives the system towards the fully stable state is extremely weak. Indeed, the system has to cross the entropic barrier played by the solution on the intermediate branch.[14] For systems with long-range interactions, the height of the entropic barrier scales linearly with the number N of particles and, consequently, the probability of transition scales like e^{-N}. For $N \gg 1$, the transition is a very rare event. Therefore, the metastable states are extremely robust. They have considerably large lifetimes scaling as e^N [9,19]. The microcanonical first-order phase transition at E_t does *not* take place in practice and, for sufficiently large values of N, the system remains frozen in the metastable phase past the transition energy E_t. Accordingly, the strict caloric curve of Fig. 12 is not physical. The physical microcanonical caloric curve is the one shown in Fig. 13 which takes the metastable states into account. It is obtained from the series of equilibria of Fig. 7 by discarding only the unstable saddle points of entropy that form the intermediate branch.

The phase transitions of the fermionic King model are summarized in Fig. 14. At $E = 0^-$, the system is in the gaseous phase where quantum mechanics is completely negligible. At some transition energy E_t, a first-order phase transition is expected to occur and drive the system towards the condensed phase dominated by quantum mechanics. However, gaseous states are still metastable, and long-lived, beyond this point so the first-order phase transition

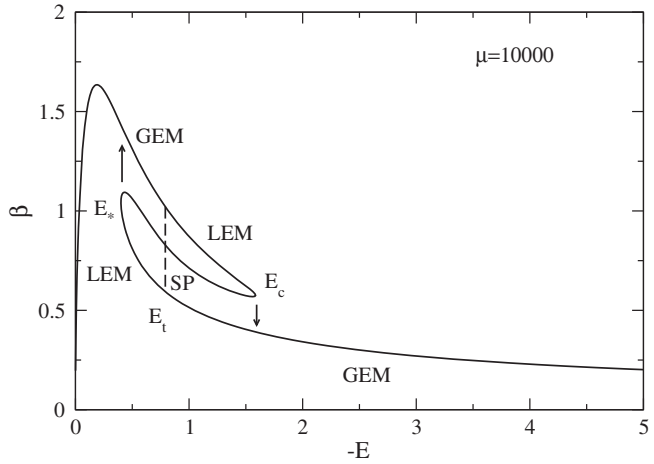

FIG. 14. Summary of the phase transitions of the fermionic King model with $\mu = 10^4$ in MCE.

[14]To pass from the gaseous phase to the condensed phase, the system must spontaneously form a small nucleus where the particles are closely packed together. To pass from the condensed phase to the gaseous phase, the system must spontaneously form a massive atmosphere.

does not take place in practice. If we decrease the energy, the system remains in the gaseous phase until the critical energy $E_c(\mu)$ at which the gaseous phase disappears. This is similar to a spinodal point in the language of phase transitions. For $E < E_c(\mu)$, the system undergoes a gravitational collapse (gravothermal catastrophe). This corresponds to a saddle-node bifurcation. However, the collapse stops when the core of the system becomes degenerate. In that case, it ends up in the condensed phase. The system has a "core-halo" structure with a degenerate nucleus surrounded by a nondegenerate atmosphere. The condensate results from the balance between the gravitational attraction and the pressure due to the Pauli exclusion principle. This is a very compact object equivalent to a completely degenerate fermion ball at $T = 0$. Since the collapse is accompanied by a discontinuous jump of entropy (see Fig. 10), this is sometimes called a microcanonical zeroth-order phase transition. If we now increase the energy, the system remains in the condensed phase until the critical energy $E_*(\mu)$ at which the condensed phase disappears. Indeed, the first-order phase transition expected at $E_t(\mu)$ does not take place in practice due to the long lifetime of the metastable states. For $E > E_*(\mu)$, the system undergoes an "explosion" reversed to the collapse and returns to the gaseous phase. In this sense, we can describe a hysteretic cycle in MCE (see the arrows in Figs. 10 and 14). These microcanonical phase transitions exist only above a microcanonical critical point $\mu_{\rm MCP} = 1980$ (see Sec. IV E).

C. Small halos in MCE: $\mu = 100$

For $\mu = 100$ (small halos), the series of equilibria is represented in Fig. 15. It has an N-shape structure. Since the curve $\beta(E)$ is univalued there is no phase transition in MCE. All the configurations are fully stable (GEM). However, there is a sort of condensation (clustering) as the energy is progressively decreased (see Figs. 16 and 17). At high energies, the equilibrium states are nondegenerate.

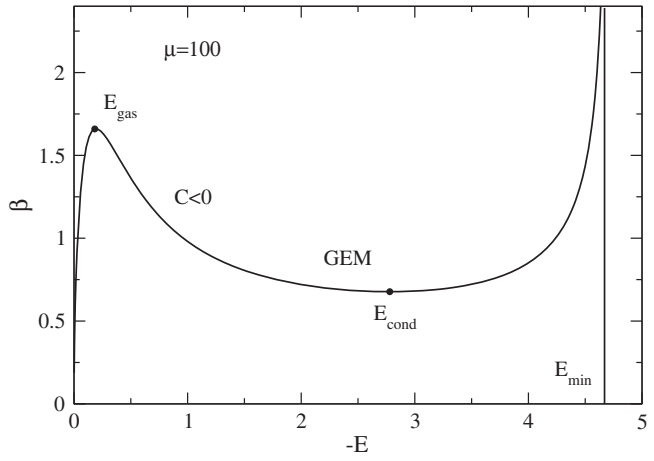

FIG. 15. Series of equilibria of the fermionic King model with $\mu = 100$.

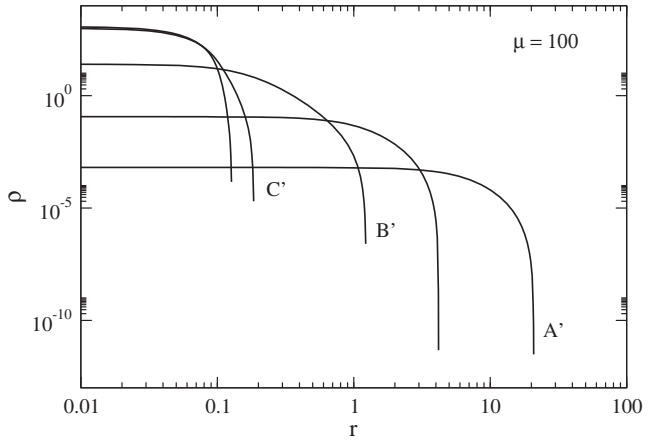

FIG. 16. Normalized density profiles along the series of equilibria with $\mu = 100$ in logarithmic scales. We have selected $k = 0.142$ ($E = -0.0329$, $\beta = 1.03$; solution A'), $k = 1.31$ ($E = -0.181$, $\beta = 1.66$), $k = 4.99$ ($E = -0.914$, $\beta = 1.03$; solution B'), $k = 18.0$ ($E = -4.27$, $\beta = 1.03$; solution C'), and $k = 41$ ($E = -4.65$, $\beta = 2.51$). The central density increases as the energy decreases.

At intermediate energies, between the energies $E_{\rm gas}$ and $E_{\rm cond}$ corresponding to the extrema of temperature, the caloric curve displays a region of negative specific heats ($C = dE/dT < 0$). In this region, the equilibrium states have a "core-halo" structure with a partially degenerate nucleus and a nondegenerate envelope (atmosphere). As energy is further decreased, the nucleus becomes more and more degenerate and contains more and more mass. At the minimum energy $E_{\rm min}$, corresponding to $T = 0$, all the mass is in the completely degenerate nucleus. In that case, the atmosphere has been swallowed and the system reduces to a pure fermion ball with a maximum phase-space density η_0 fixed by the Pauli exclusion principle.

The entropy versus energy curve $S(E)$ is represented in Fig. 18. Since $S''(E) = -1/(CT^2)$, the entropy displays a

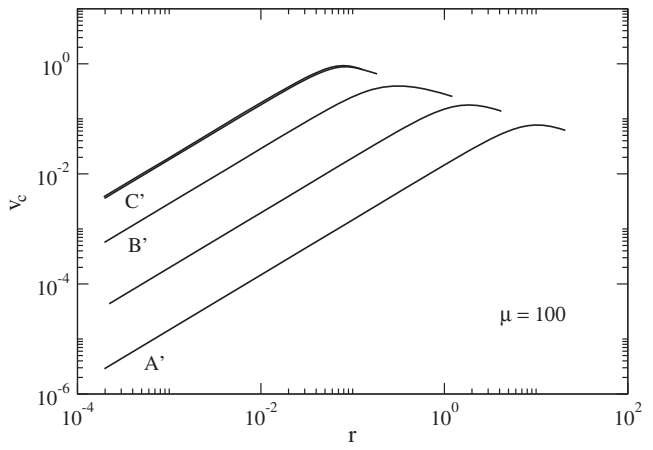

FIG. 17. Normalized rotation curves along the series of equilibria with $\mu = 100$ in logarithmic scales.

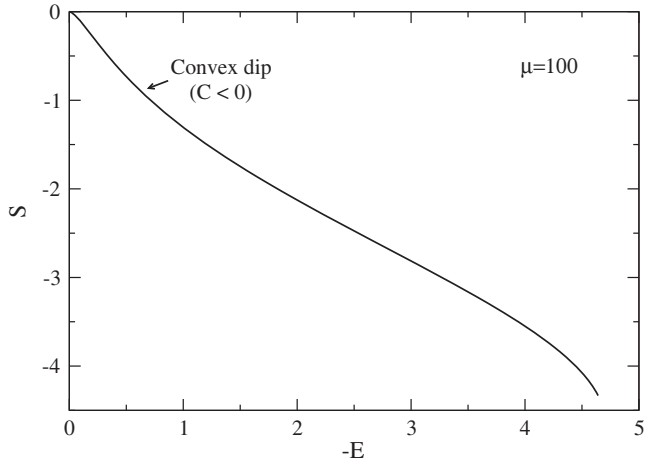

FIG. 18. Entropy versus energy for $\mu = 100$.

convex intruder ($S'' > 0$) in the region of negative specific heat ($C < 0$). For systems with long-range interactions, for which the energy is nonadditive, the region of negative specific heat in the caloric curve (see Fig. 15) and the convex intruder in the entropy versus energy curve (see Fig. 18) are allowed in MCE.

D. Small halos in CE: $\mu = 100$

In this section, we consider a dissipative system in contact with a thermal bath imposing its temperature T. In that case, the control parameter is the temperature T and the relevant statistical ensemble is CE. In CE, we must determine maxima of free energy at fixed mass. Considering again the case $\mu = 100$ (small halos), we note that the series of equilibria $E(\beta)$ represented in Fig. 19 is multivalued. This gives rise to canonical phase transitions. Using the Poincaré theorem, we deduce that all the states on the left branch of the series of equilibria are free energy maxima (FEM) until the first turning point of temperature

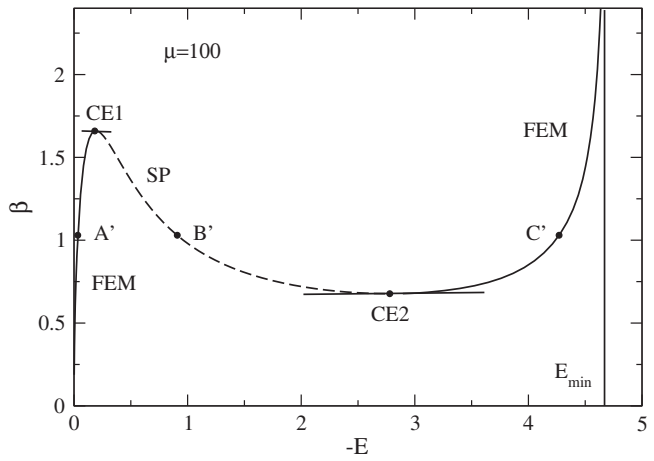

FIG. 19. Series of equilibria of the fermionic King model with $\mu = 100$.

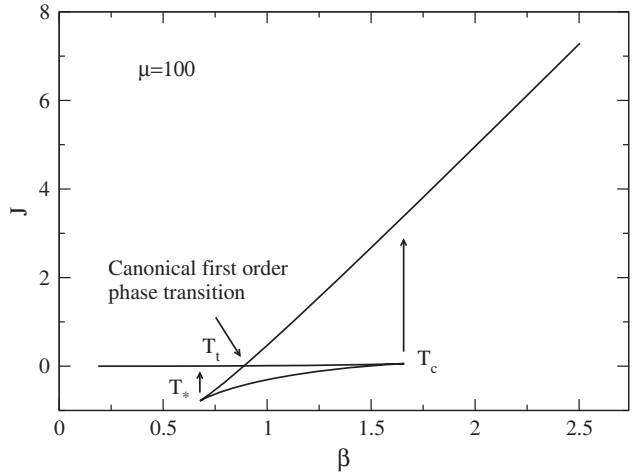

FIG. 20. Free energy of each phase versus temperature for $\mu = 100$.

CE1. For large values of μ, this critical temperature is close to the temperature $T_c = 0.613$ corresponding to the classical King model ($\mu \to +\infty$). At that point, the curve turns clockwise so that a mode of stability is lost. This mode of stability is regained at the second turning point of temperature CE2 at which the curve turns anticlockwise. The corresponding temperature $T_*(\mu)$ depends on the value of μ and tends to $T_*(\mu) \to +\infty$ for $\mu \to +\infty$. The configurations on the branch between CE1 and CE2 are SP of free energy while the configurations on the right branch after CE2 are FEM.

The configurations on the left branch are stable (FEM). They form the "gaseous phase" (see solution A' in Figs. 16 and 17). The solutions on the right branch are also stable (FEM). They form the "condensed phase" (see solution C' in Figs. 16 and 17). They have a very tenuous atmosphere. The solutions on the intermediate branch are unstable (SP). These solutions (see solution B' in Figs. 16 and 17) form a barrier of free energy that the system has to cross in order to pass from the gaseous phase to the condensed phase, or inversely [9].

If we compare the free energy of the configurations (see Fig. 20), we expect a canonical first-order phase transition to take place at a transition temperature $T_t(\mu)$ where the free energy of the gaseous phase and the free energy of the condensed phase become equal.[15] The transition temperature $T_t(\mu)$ can also be obtained by performing a Maxwell construction (see the horizontal plateau in Fig. 22) [9]. For $T > T_t$ the gaseous phase is fully stable [global free energy maximum (GFEM) at fixed mass] while the condensed

[15]We note that for large values of μ, secondary canonical first-order phase transitions appear, as shown in Fig. 21, due to the winding of the series of equilibria (see Fig. 5). However, this is essentially a mathematical curiosity because these phase transitions take place between unstable saddle points of free energy. As a result they may not be physical.

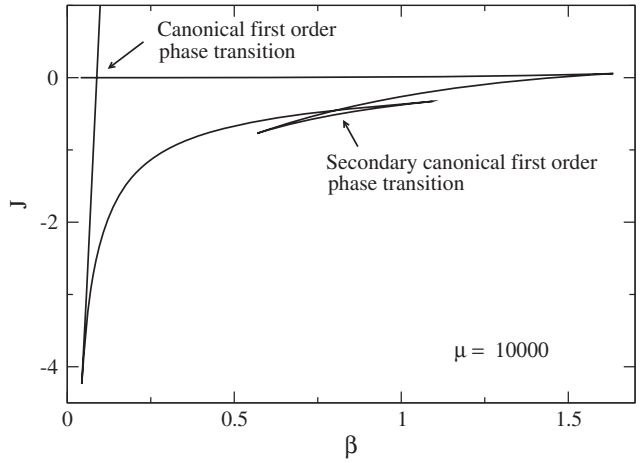

FIG. 21. Free energy versus temperature for $\mu = 10^4$.

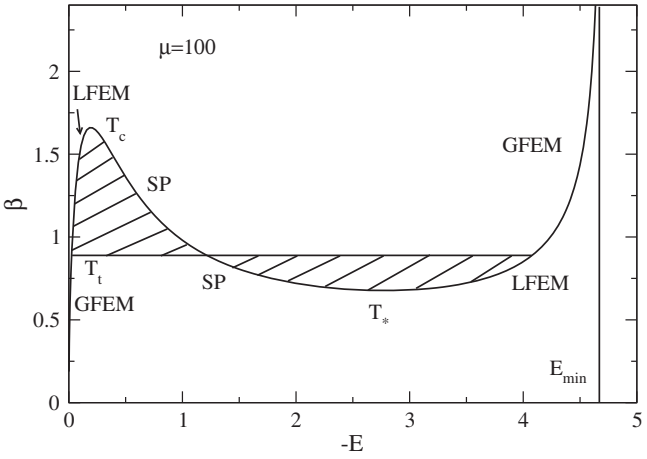

FIG. 22. Maxwell construction for $\mu = 100$ in CE.

phase is metastable [local free energy maximum (LFEM) at fixed mass]. For $T < T_t$ the gaseous phase is metastable (LFEM) while the condensed phase is fully stable (GFEM). The strict caloric curve in CE is obtained by keeping only the fully stable states (see Fig. 23). It is marked by a discontinuity of the energy $E = -\partial J/\partial\beta$ at $T = T_t(\mu)$. Equivalently, the first derivative of the free energy is discontinuous at the transition (see Fig. 20). This characterizes a canonical first-order phase transition. The specific heat $C = dE/dT$ is also discontinuous at the transition.

It is instructive to compare the strict canonical caloric curve of Fig. 23 with the microcanonical caloric curve of Fig. 15 for the same value of the degeneracy parameter $\mu = 100$. We see that the region of negative specific heats in MCE is replaced by an isothermal phase transition (plateau) in CE that connects the gaseous phase (left branch) to the condensed phase (right branch). This corresponds to a situation of strict ensemble inequivalence: the energies between E_1 and E_2 are accessible in MCE but not in CE.

However, for systems with long-range interactions, the metastable states must be considered as stable states as explained previously. The canonical first-order phase transition at T_t does *not* take place in practice because, for sufficiently large values of N, the system remains frozen in the metastable phase past the transition temperature T_t. Therefore, the strict caloric curve of Fig. 23 is not physical. The physical canonical caloric curve is the one shown in Fig. 24 which takes the metastable states into account. It is obtained from the series of equilibria of Fig. 19 by discarding only the unstable saddle points of free energy that form the intermediate branch. These configurations lie in the region of negative specific heats that is forbidden in CE. As a result, the region of physical ensemble inequivalence corresponds to the energies between $E_{\rm gas}$ and $E_{\rm cond}$. These energies are accessible in the microcanonical ensemble but not in the canonical ensemble (compare Figs. 15 and 24).

The phase transitions of the fermionic King model in CE are summarized in Fig. 25. For $T \to +\infty$, the system is in the gaseous phase where quantum mechanics is completely negligible. At some transition temperature T_t, a first-order phase transition is expected to occur and drive the system

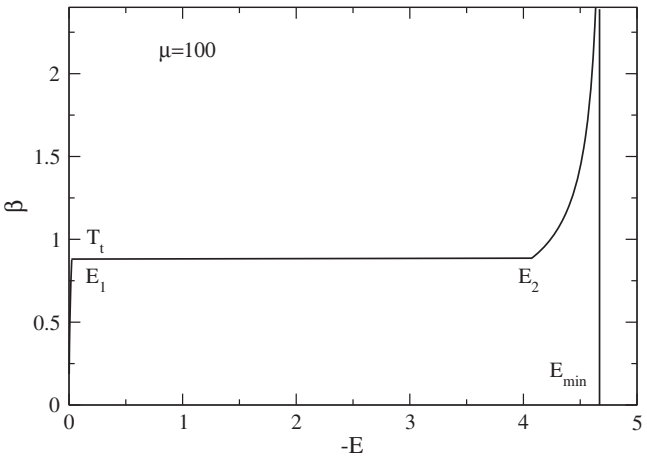

FIG. 23. Strict canonical caloric curve for $\mu = 100$.

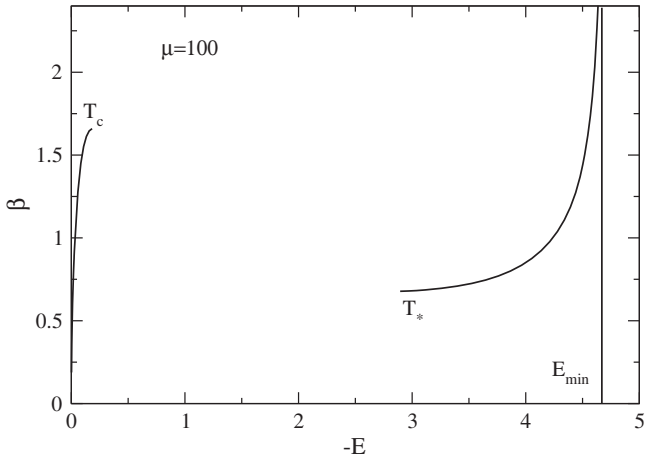

FIG. 24. Physical canonical caloric curve for $\mu = 100$.

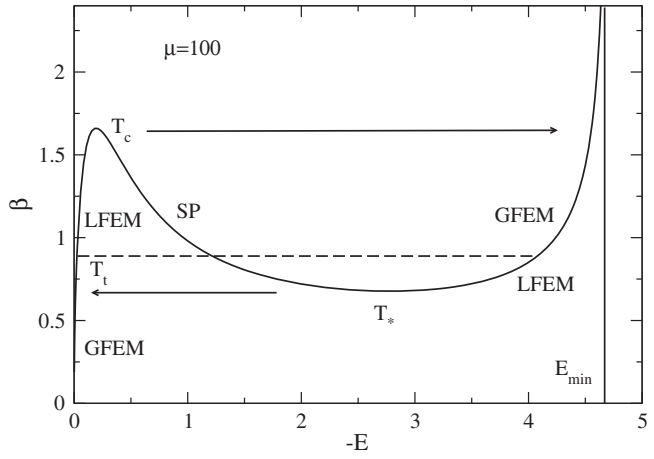

FIG. 25. Summary of the phase transitions of the fermionic King model with $\mu = 100$ in CE.

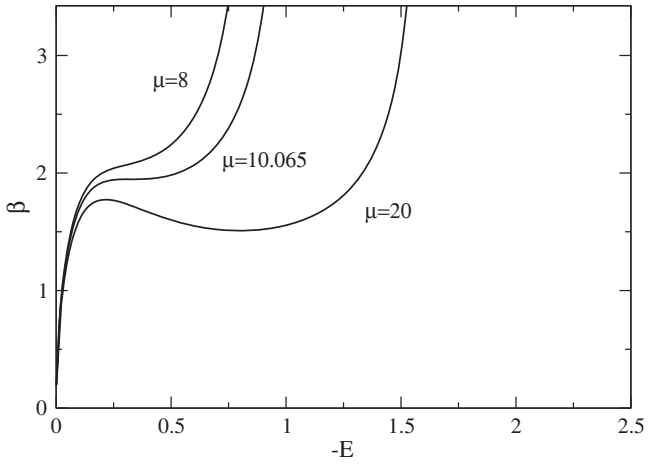

FIG. 26. Enlargement of the caloric curve near the canonical critical point ($\mu_{\rm CCP} = 10.1$, $E_{\rm CCP} = -0.325$, $\beta_{\rm CCP} = 1.95$).

towards the condensed phase. However, gaseous states are still metastable, and long-lived, beyond this point so the first-order phase transition does not take place in practice. Therefore, if we decrease the temperature, the system remains in the gaseous phase until the critical temperature $T_c(\mu)$ at which the gaseous phase disappears. This is similar to a spinodal point in the language of phase transitions. For $T < T_c(\mu)$, the system undergoes a gravitational collapse (isothermal collapse). This corresponds to a saddle-node bifurcation. However, the collapse stops when the core of the system becomes degenerate. In that case, it ends up in the condensed phase. The system has a "core-halo" structure with a degenerate nucleus surrounded by a nondegenerate atmosphere. The condensate results from the balance between the gravitational attraction and the pressure due to the Pauli exclusion principle. This is a very compact object equivalent to a completely degenerate fermion ball at $T = 0$. Since the collapse is accompanied by a discontinuous jump of free energy (see Fig. 20), this is sometimes called a canonical zeroth-order phase transition. If we now increase the temperature, the system remains in the condensed phase until the critical temperature $T_*(\mu)$ at which the condensed phase disappears. Indeed, the first-order phase transition expected at $T_t(\mu)$ does not take place in practice because of the long lifetime of the metastable states. For $T > T_*(\mu)$, the system undergoes an "explosion" reversed to the collapse and returns to the gaseous phase. In this sense, we can describe a hysteretic cycle in the canonical ensemble (see the arrows in Figs. 20 and 25). Preliminary numerical simulations illustrating this hysteretic cycle for self-gravitating fermions have been performed in Ref. [86]. These canonical phase transitions exist only above a canonical critical point $\mu_{\rm CCP} = 10.1$ (see Sec. IV E).

E. Microcanonical and canonical critical points

The deformation of the series of equilibria of the fermionic King model as a function of the degeneracy parameter μ ($\sim$ system's size) is represented in Fig. 5. There exist two critical points in the problem, one in each ensemble.

For $\mu < \mu_{\rm CCP} \simeq 10.1$, the curve $\beta(E)$ is monotonic, so there is no phase transition. For $\mu > \mu_{\rm CCP} \simeq 10.1$, the curve $E(\beta)$ is multivalued so that a canonical phase transition takes place. At the canonical critical point $\mu_{\rm CCP}$, the caloric curve $E(\beta)$ presents an inflection point and the canonical phase transition disappears (see Fig. 26). At that point the specific heat is infinite. For $\mu > \mu_{\rm MCP} \simeq 1980$, the curve $\beta(E)$ is multivalued so that a microcanonical phase transition takes place (in addition to the canonical phase transition that exists for any $\mu > \mu_{\rm CCP}$). At the microcanonical critical point $\mu = \mu_{\rm MCP}$, the caloric curve $\beta(E)$ presents an inflection point and the microcanonical phase transition disappears (see Fig. 27). At that point the specific heat vanishes.

Therefore, for $\mu > \mu_{\rm MCP}$, the system exhibits a microcanonical and a canonical phase transition, for

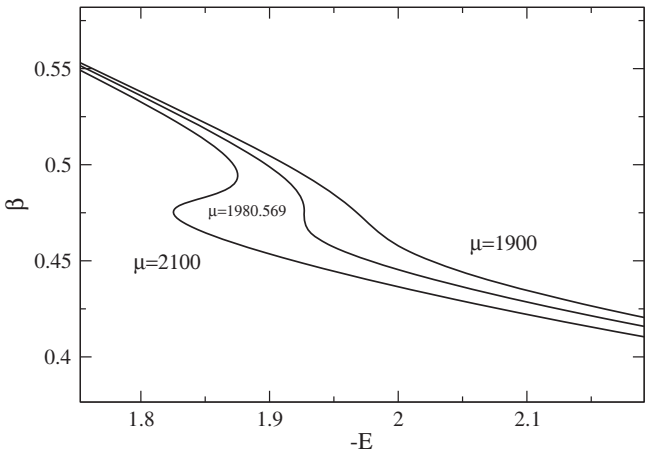

FIG. 27. Enlargement of the caloric curve near the microcanonical critical point ($\mu_{\rm MCP} = 1980$, $E_{\rm MCP} = -1.93$, $\beta_{\rm MCP} = 0.474$).

$\mu_{CCP} < \mu < \mu_{MCP}$ the system exhibits only a canonical phase transition, and for $\mu < \mu_{CCP}$ the system does not exhibit any phase transition. We recall, however, that because of the presence of long-lived metastable states, the first-order phase transitions are not physically relevant. Only the zeroth-order phase transitions that occur at E_c in MCE and at T_c in CE (spinodal points) are relevant. We also recall that the secondary turning points of energy and temperature that appear for large values of μ are not physically relevant because they concern unstable saddle points. Only the first and the last turning points of energy and temperature are physically relevant. Therefore, despite the mathematical complexity of the spiral that appears for large values of μ, the physical nature of the phase transitions remains relatively simple.

F. Phase diagrams

Typical caloric curves illustrating microcanonical and canonical phase transitions are shown in Figs. 11 and 22 respectively. The phase diagram of the fermionic King model can be directly deduced from these curves by identifying characteristic energies and characteristic temperatures.

In CE, we denote by T_t the temperature of transition (determined by the equality of the free energies of the two phases), T_c the end point of the metastable gaseous phase (first turning point of temperature), and T_* the end point of the metastable condensed phase (last turning point of temperature). The canonical phase diagram is represented in Fig. 28. It shows in particular the canonical critical point

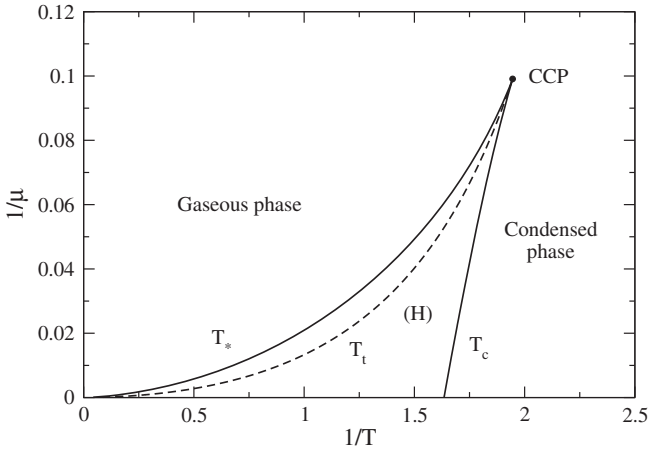

FIG. 28. Canonical phase diagram of the fermionic King model. The H zone between T_c and T_* corresponds to a hysteretic zone where the actual phase depends on the history of the system. If the system is initially prepared in a gaseous state, it remains gaseous until the minimum temperature T_c at which it collapses and becomes condensed. Inversely, if the system is initially prepared in a condensed state, it remains condensed until the maximum temperature T_* at which it explodes and becomes gaseous.

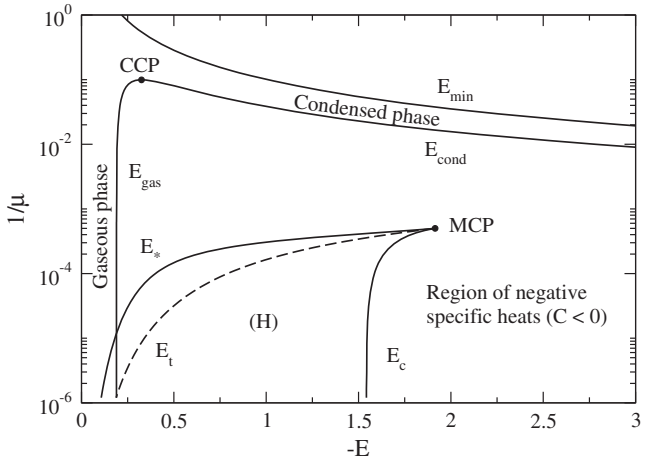

FIG. 29. Microcanonical phase diagram of the fermionic King model. The H zone between E_c and E_* corresponds to a hysteretic zone where the actual phase depends on the history of the system. The phase diagram in MCE is more complex than in CE due to the existence of the negative specific heat region that is forbidden in CE. This corresponds to a region of ensemble inequivalence.

$\mu_{CCP} = 10.1$ at which the canonical phase transition disappears.

In MCE, we denote by E_t the energy of transition (determined by the equality of the entropy of the two phases), E_c the end point of the metastable gaseous phase (first turning point of energy), and E_* the end point of the metastable condensed phase (last turning point of energy). We also denote by E_{gas} the energy at which we enter the zone of negative specific heat (first turning point of temperature) and E_{cond} the energy at which we leave the zone of negative specific heat (last turning point of temperature). Finally, we introduce the minimum energy E_{min} (ground state). The microcanonical phase diagram is represented in Fig. 29. It shows in particular the microcanonical critical point $\mu_{MCP} = 1980$ at which the microcanonical phase transition disappears.

V. DENSITY PROFILES AND ROTATION CURVES OF THE FERMIONIC KING MODEL

In this section, we study how the density profiles and the rotation curves of the fermionic King model depend on the values of μ, E, and T. We also discuss their ability at describing dark matter halos. In Secs. V A–V C we consider MCE and in Secs. V D–V F we consider CE.

A. The effect of increasing μ for fixed $E > E_c$

We consider the series of equilibria of Fig. 7 corresponding to $\mu = 10^4$. We take an energy $E = -0.876$ larger than the critical energy $E_c = -1.54$ of gravitational collapse (gravothermal catastrophe). At that energy, the system can be found in three different states: a gaseous phase (solution

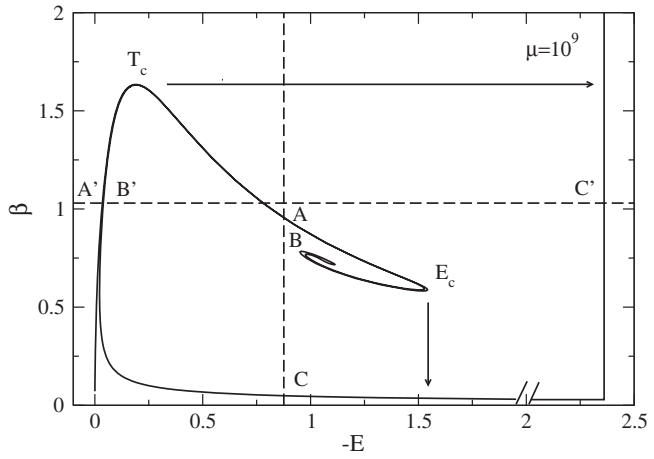

FIG. 30. Series of equilibria of the fermionic King model with $\mu = 10^9$. For large but finite values of μ, the series of equilibria winds up and makes several turns before finally unwinding. A mode of stability is lost each time the curve winds up (rotates clockwise) and a mode of stability is regained each time the curve unwinds (rotates anticlockwise). Therefore, only the part of the series of equilibria before the first turning point and after the last turning point is stable.

A), an embryonic phase (solution B), and a condensed phase (solution C). We study the evolution of the solutions A, B and C as μ increases.

For large values of μ, the series of equilibria rotates several times before unwinding (see Figs. 30 and 31 obtained for $\mu = 10^9 \gg 1$). The branches A and B approach each other while the branch C moves away. For $\mu \to +\infty$, the branches A and B superimpose while the branch C coincides with the $\beta = 0$ axis (see Fig. 30). In this limit, we recover the spiral corresponding to the classical King model (see Fig. 1).

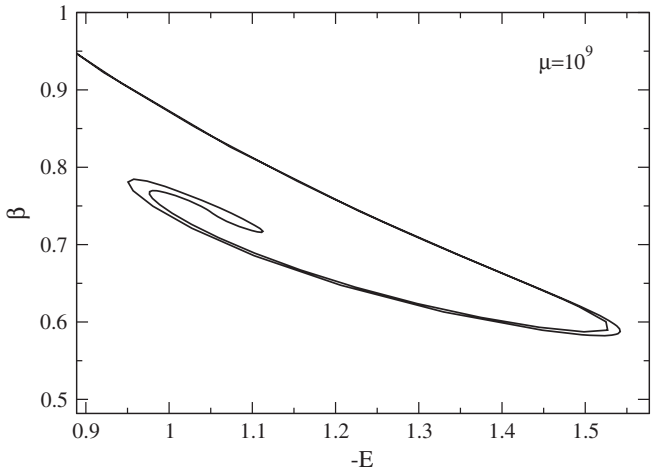

FIG. 31. Zoom on the spiral of Fig. 30. The spiral rotates several times before unwinding. However, this is essentially a mathematical curiosity since the states on the spiral are unstable, and hence unphysical.

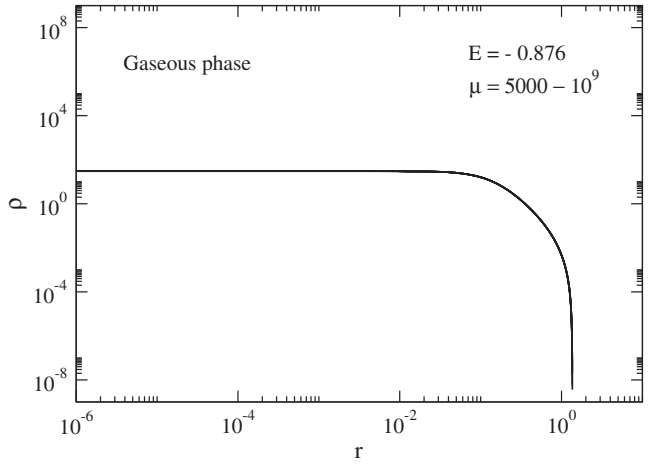

FIG. 32. Density profile of the gaseous phase (solution A) for different values of μ in logarithmic scales (here and in the following figures we have selected $\mu = 5000$, 10^4, 10^5, 10^6, 10^7, 10^8 and 10^9). For sufficiently large values of μ the density profile of the gaseous phase does not change. It reaches an asymptotic profile corresponding to the classical King model.

Solution A (gaseous phase) does not significantly change with μ and tends to the classical King distribution for $\mu \to +\infty$ (see Figs. 32–34). Since the classical King model close to the point of marginal microcanonical stability ($E_c = -1.54$) describes large dark matter halos relatively well (see Paper I), and since the chosen energy $E = -0.876$ is relatively close to E_c, we shall take the asymptotic profile of Figs. 32–34 as a reference in our discussion (see the dotted lines in Figs. 35–40).

Solution B (embryonic phase) is similar to solution A (gaseous phase) except that it contains a small embryonic nucleus of high density. This is a completely degenerate compact object equivalent to a fermion ball at $T = 0$. Therefore, solution B has a core-halo structure. The mass, the size and the absolute value of the potential energy of the

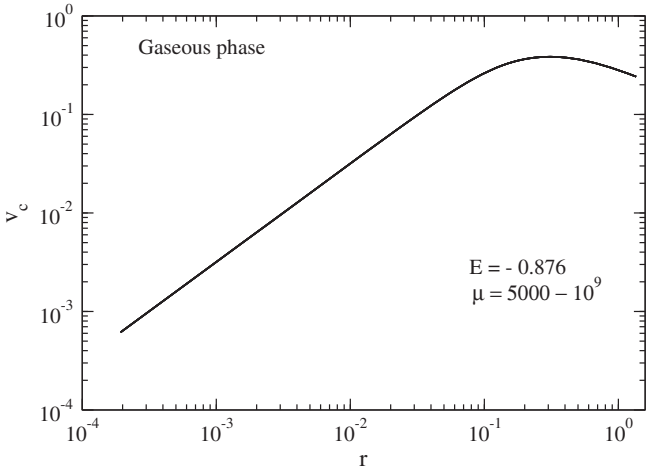

FIG. 33. Circular velocity profile of the gaseous phase for different values of μ in logarithmic scale.

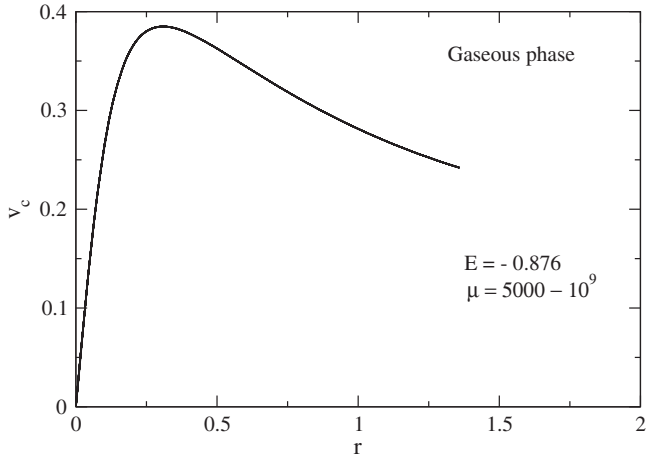

FIG. 34. Circular velocity profile of the gaseous phase for different values of μ in linear scale.

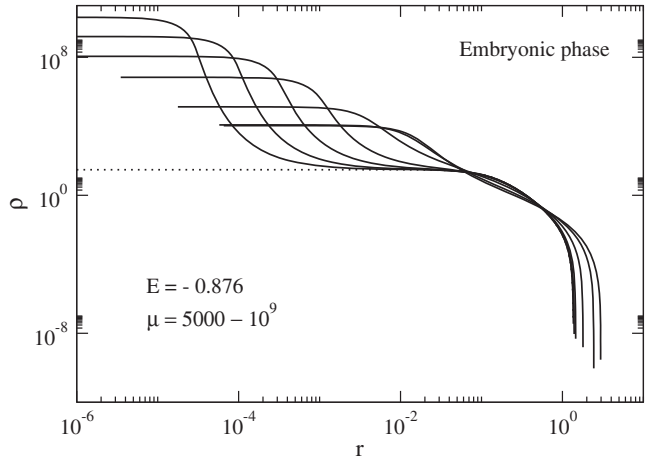

FIG. 35. Density profile of the embryonic phase (solution B) for different values of μ in logarithmic scales (the central density increases with μ). For increasing μ, solution B coincides with solution A (gaseous phase; dotted line) corresponding to the classical King model, except that it contains a small embryonic degenerate nucleus (fermion ball) with a small mass and a small absolute value of potential energy. This nucleus, equivalent to a polytrope of index $n = 3/2$, is followed by a plateau of constant density induced by the gravity of the central nucleus as detailed in Ref. [62].

nucleus decrease as μ increases. As a result, for $\mu \gg 1$, solutions A and B have almost the same temperature ($\beta_A \simeq \beta_B$) and the profiles A and B coincide outside of the nucleus (see Figs. 35–37). This is why the branches A and B in the series of equilibria superimpose for $\mu \to +\infty$ (see Fig. 30). Still, the two solutions A and B are physically distinct. In particular, solution B is unstable as further discussed in Sec. VI.

Solution C (condensed phase) is very different from solution A (gaseous phase) and from solution B (embryonic phase). Like solution B, it has a core-halo structure. It

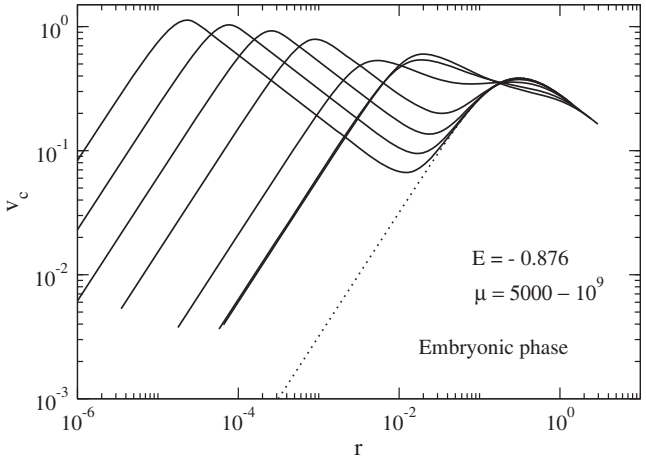

FIG. 36. Circular velocity profile of the embryonic phase for different values of μ in logarithmic scales. For increasing μ, solution B approaches solution A (gaseous phase; dotted line) corresponding to the classical King model, except at very small radii. The presence of a small nucleus (fermion ball) where $v_c \propto r$, followed by a plateau where $v_c \propto r^{-1/2}$, manifests itself by a secondary peak in the rotation curve at the very center of the system (see Fig. 37). However, these distances are probably not accessible to observations. Furthermore, these solutions are thermodynamically unstable (saddle points of entropy) so this secondary peak may not be physical.

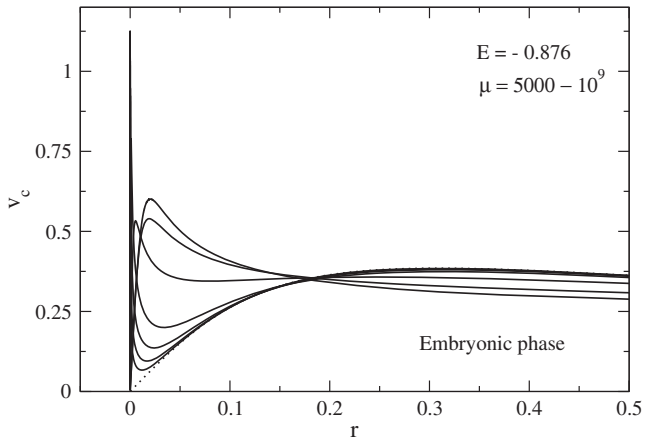

FIG. 37. Circular velocity profile of the embryonic phase for different values of μ in linear scales. For large values of μ, we recover the classical King model (dotted line) except at the very center. The secondary peak due to the degenerate nucleus (fermion ball) manifests itself by a spike near the origin.

contains a small degenerate nucleus with high density (condensate) that has a small mass and a small radius. However, unlike solution B, the nucleus has a very negative potential energy. Since energy is conserved in MCE, this implies that the halo must be very hot. This is why β_C is small (see Fig. 30). Since the halo is hot, it expands at very large distances (see Figs. 38–40). The mass and the size of the nucleus decrease as μ increases while the absolute value

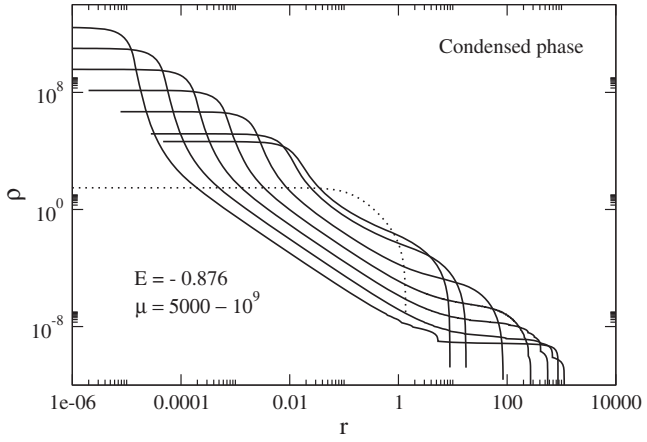

FIG. 38. Density profile of the condensed phase (solution C) for different values of μ in logarithmic scales (the central density increases with μ). For increasing μ, solution C contains a small degenerate nucleus with a relatively small mass but a more and more negative potential energy. As a result, the halo becomes hotter and hotter in order to conserve the total energy. This is why it forms a sort of plateau with constant density that extends at larger and larger distances. The resulting profile is very different from solution A (gaseous phase; dotted line) corresponding to the classical King model.

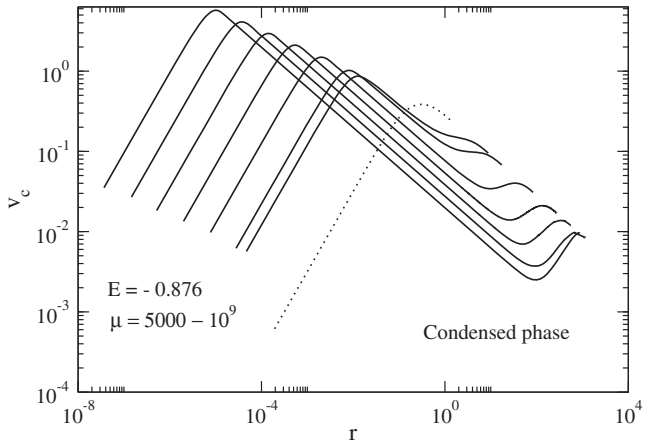

FIG. 39. Circular velocity profile of the condensed phase for different values of μ in logarithmic scales. It is very different from solution A (gaseous phase; dotted line) corresponding to the classical King model. This is because the halo is expelled at large distances as the nucleus becomes denser and denser, and more and more energetic.

of its potential energy increases.[16] The mass, radius, and temperature of the halo increase as μ increases. For $\mu \to +\infty$, the mass and the radius of the nucleus tend to zero but its potential energy tends to $-\infty$. The temperature of the halo tends to $+\infty$ in order to conserve the energy. The radius of the halo also tends to $+\infty$. Therefore, for

[16]The scaling of the mass, size, and potential energy of the nucleus as a function of μ were obtained analytically in Ref. [29] for box-confined self-gravitating fermions.

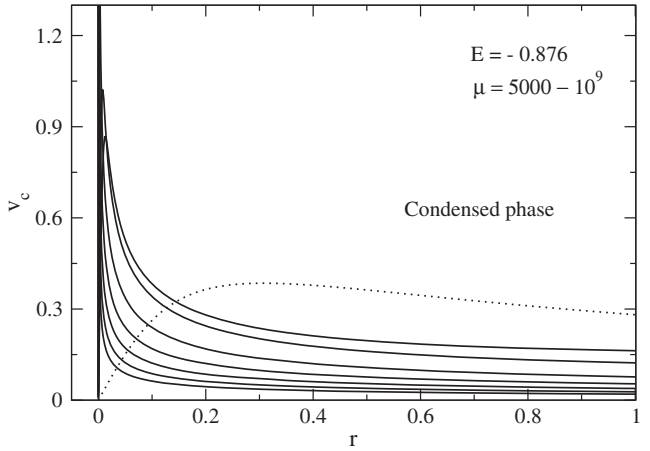

FIG. 40. Circular velocity profile of the condensed phase (solution C) for different values of μ in linear scales.

$\mu \to +\infty$, we recover the singular "binary + hot halo" structure with infinite entropy corresponding to the strict equilibrium state of classical self-gravitating systems in MCE (see footnote 3). For finite values of μ, quantum mechanics provides a regularization of this singular structure: the "tight binary" is replaced by a "fermion ball" whose size is fixed by quantum mechanics. The resulting structure has a finite entropy.

We now describe the form of the physical caloric curve when $\mu \to +\infty$. For $\mu > \mu_{\rm MCP}$ the physical caloric curve always looks like Fig. 13 (the spiral that develops for large values of μ does not play any role since it is made of unstable states). The upper branch (gaseous phase) does not change much with μ. For $\mu > \mu_{\rm MCP}$ it almost coincides with the classical King model ($\mu \to +\infty$). The collapse energy $E_c(\mu)$ is close to -1.54. The lower branch (condensed phase) depends sensibly on μ. For $\mu \to +\infty$, the explosion energy $E_*(\mu)$ tends to zero and the minimum energy $E_{\rm min}(\mu)$ tends to $-\infty$. The transition energy $E_t(\mu)$ also tends to zero. This implies that the gaseous phase corresponds to metastable states (LEM) while the condensed phase corresponds to fully stable states (GEM). For $\mu \to +\infty$ the condensed states are singular and have an infinite entropy. They are made of a "tight binary" (a degenerate core with a small mass but a huge potential energy) surrounded by a hot halo with $T \to +\infty$. As a result, the branch of condensed states coincides with the x axis at $\beta = 0$. Therefore, in the $\mu \to +\infty$ limit, the physical caloric curve is formed by the metastable gaseous branch of Fig. 1 up to MCE plus a singular stable condensed branch at $\beta = 0$ coinciding with the x axis (tight binary + hot halo). On the other hand, the saddle points are superposed to the spiral and to the branch of gaseous states although they have a very different structure presenting a germ.

B. The effect of decreasing E for fixed $\mu > \mu_{\rm MCP}$

We consider a value of μ larger than $\mu_{\rm MCP} = 1980$ for which a microcanonical phase transition (collapse) takes

place at the critical energy $E_c \sim -1.54$. Specifically, we choose $\mu = 10^4$ (large halo) corresponding to the caloric curve represented in Fig. 14. We start from the gaseous phase (solution A) and progressively decrease the energy. This is a natural evolution since the concentration parameter $k(t)$ increases with time as the system slowly evaporates until an instability takes place (see Appendix A). As a result, the system follows the series of equilibria from high energies to low energies. For $E_c < E < 0$ (corresponding to $0 \leq k \leq k_{\rm MCE}$), the system is nondegenerate. It can be described by the classical King model. When $E \to 0$ (corresponding to $k \to 0$), the system is equivalent to a polytrope of index $n = 5/2$. When E is close to E_c (corresponding to $k \sim k_{\rm MCE}$), the classical King profile can be approximated by the modified Hubble profile. This profile provides a good description of large dark matter halos (see Paper I). When $E < E_c$, the gaseous phase (solution A) disappears and the system undergoes a gravitational collapse towards the condensed phase (solution C). This corresponds to a saddle-node bifurcation. According to the discussion of Sec. V A, the gravitational collapse in MCE (gravothermal catastrophe) results in the formation of a compact degenerate object (fermion ball at $T = 0$) of much smaller mass and size than the initial cluster. This is accompanied by the expulsion of a hot and massive envelope at very large distances. Since the envelope is dispersed at large distances, only the degenerate object remains at the end. Therefore, when $E < E_c$, the system forms a compact object and ejects an envelope. This could be a mechanism leading to the formation of dwarf dark matter halos that are completely degenerate and whose dimensions are much smaller than the dimensions of large dark matter halos.[17]

This evolution is reminiscent of the red-giant phase where a star, having exhausted its nuclear fuel, collapses into a white dwarf and ejects its outer layers by forming a planetary nebula. This is also reminiscent of the supernovae explosion phenomenon leading to a degenerate compact object such as a neutron star or a black hole and to the expulsion of a massive envelope. We may wonder if a similar scenario can take place (or has already taken place!) at the galactic scale. We may speculate that large dark matter halos are described by stable classical King models with $k < k_{\rm MCE}$ but that some halos can reach the critical value $k = k_{\rm MCE}$ and collapse to give birth to degenerate dwarf dark matter halos of much smaller mass and size, with the expulsion of a massive envelope. We emphasize, however, that this phenomenon takes considerably much more time (of the order of the Hubble time) than the supernova phenomenon (a few seconds) since the gravothermal catastrophe is a rather slow process.

[17]This is not the only mechanism. Dwarf halos are thought to result from the Jeans instability of a spatially homogeneous primordial gas. Then, they merge to form larger structures during hierarchical clustering. However, it is not impossible that large halos having reached the point of gravothermal instability collapse again to form smaller structures. We can see in Fig. 38 that, for large values of μ, the size of the degenerate object that forms after collapse (full line) is smaller than the size of the initial halo (dotted line) by about 3 orders of magnitude (or more). This is consistent with the difference of size between dwarf and large dark matter halos (see Table I of Ref. [71]).

C. The effect of decreasing E for fixed $\mu < \mu_{\rm MCP}$

We consider a value of μ smaller than $\mu_{\rm MCP} = 1980$ for which there is no microcanonical phase transition (no collapse). Specifically, we choose $\mu = 100$ (small halo) corresponding to the caloric curve represented in Fig. 15. We start from $E = 0$ and progressively decrease the energy. At high energies, the system is nondegenerate. It can be described by the classical King model. When $E \to 0$, the solution is equivalent to a polytrope of index $n = 5/2$. As E decreases, the solutions become partially degenerate. They have a core-halo structure but the distinction between the core and the halo is not clear-cut (see Figs. 16 and 17). The core can be approximated by a polytrope of index $n = 3/2$ and the halo can be approximated by a polytrope of index $n = 5/2$. These solutions lie in the region of negative specific heats between $E_{\rm gas}$ and $E_{\rm cond}$. When $E \to E_{\rm min}$, the solutions are completely degenerate (ground state). They coincide with a polytrope of index $n = 3/2$. The size of the cluster decreases as the energy decreases.

D. The effect of increasing μ for fixed $T > T_C$

We now develop the same discussion in CE. We consider the series of equilibria of Fig. 19 corresponding to $\mu = 100$. We take a temperature $T = 0.971$ larger than the critical temperature $T_c = 0.613$ of gravitational collapse (isothermal collapse). At that temperature, the system can be found in three different states: a gaseous phase (solution A'), an embryonic phase (solution B'), and a condensed phase (solution C'). We study the evolution of the solutions A', B' and C' as μ increases.

For large values of μ, the branches A' and B' approach each other while the branch C' moves away. For $\mu \to +\infty$, the branches A' and B' superimpose while the branch C' is rejected to $E \to -\infty$ (see Fig. 30). In this limit, we recover the spiral corresponding to the classical King model (see Fig. 1).

The description of solutions A' (gaseous phase) and B' (embryonic phase) is similar to the description of solutions A and B in MCE (see Sec. V A). However, the description of solution C' (condensed phase) is different from that of solution C in MCE. Like solution C, it has a core-halo structure. It contains a small degenerate nucleus with high density (condensate) surrounded by a nondegenerate halo. However, unlike solution C, the nucleus contains almost all of the mass while the halo is very tenuous. Actually, the halo is almost absent from the density profile C' in Fig. 16. This is in sharp contrast with the density profile C in Fig. 8 in MCE that shows an extended halo. The fact that almost

all the mass is in the nucleus explains why $E_{C'}$ is very negative (see Fig. 30). The size of the nucleus decreases as μ increases while its mass and the absolute value of its potential energy increase (see footnote 16). For $\mu \to +\infty$, the radius of the nucleus tends to zero but its mass tends to M. Therefore, for $\mu \to +\infty$, we recover the "Dirac peak" with infinite free energy corresponding to the strict equilibrium state of classical self-gravitating systems in CE (see footnote 3). For finite values of μ, quantum mechanics provides a regularization of this singular structure: the "Dirac peak" is replaced by a "fermion ball" whose size is fixed by quantum mechanics. The resulting structure has a finite free energy.

We now describe the form of the physical caloric curve when $\mu \to +\infty$. For $\mu > \mu_{\rm CCP}$, the physical caloric curve always looks like Fig. 24 (the spiral that develops for large values of μ does not play any role since it is made of unstable states). The left branch (gaseous phase) does not change much with μ. For $\mu > \mu_{\rm CCP}$ it almost coincides with the classical King model ($\mu \to +\infty$). The collapse temperature $T_c(\mu)$ is close to 0.613. The right branch (condensed phase) depends sensibly on μ. For $\mu \to +\infty$, the explosion temperature $T_*(\mu)$ tends to $+\infty$. The transition temperature $T_t(\mu)$ also tends to $+\infty$. This implies that the gaseous phase corresponds to metastable states (LFEM) while the condensed phase corresponds to fully stable states (GFEM). For $\mu \to +\infty$, the condensed states are singular and have an infinite free energy. They are made of a "Dirac peak" containing all the mass. As a result, the branch of condensed states (vertical line) is rejected to $E \to -\infty$. Therefore, in the $\mu \to +\infty$ limit, the physical caloric curve is formed by the metastable gaseous branch of Fig. 1 up to CE plus a singular stable condensed branch at $E = -\infty$ (Dirac peak). On the other hand, the saddle points are superposed to the spiral and to the branch of gaseous states although they have a very different structure presenting a germ.

E. The effect of decreasing T for fixed $\mu > \mu_{\rm CCP}$

We consider a value of μ larger than $\mu_{\rm CCP} = 10.1$ for which a canonical phase transition (collapse) takes place at the critical temperature $T_c = 0.613$. We start from the gaseous phase and progressively decrease the temperature. This is a natural evolution since the concentration parameter $k(t)$ increases with time as the system slowly evaporates until an instability takes place (see Appendix A). As a result, the system follows the series of equilibria from high temperatures to low temperatures. For $T > T_c$ (corresponding to $0 \leq k \leq k_{\rm CE}$), the system is nondegenerate. It can be described by the classical King model. When $T \to +\infty$ (corresponding to $k \to 0$), the system is equivalent to a polytrope of index $n = 5/2$. When T is close to T_c (corresponding to $k \sim k_{\rm CE}$) the classical King profile can still be approximated by a polytrope $n = 5/2$. Such a profile does not account for the observations of large dark matter halos (see Paper I). This suggests that CE is not relevant to describe dark matter halos (see Appendix B). When $T < T_c$, the gaseous phase (solution A') disappears and the system undergoes a gravitational collapse towards the condensed phase (solution C'). This corresponds to a saddle-node bifurcation. According to the discussion of Sec. V D, the gravitational collapse results in the formation of a compact degenerate object (fermion ball at $T = 0$) of small size and high density that contains almost all the mass of the initial cluster. This object has only a very tenuous atmosphere with a small mass that is hardly visible. The mass of the nucleus increases as the temperature decreases and, at $T = 0$, all the mass is in the nucleus. Therefore, when $T < T_c$, the system forms a compact object containing almost all the mass. There is almost no atmosphere (solution C' in Fig. 16). This is very different from the gravitational collapse in MCE that leads to a degenerate object with a small mass and the expulsion of a massive atmosphere (see Fig. 38). Therefore, the collapse in CE cannot account for the formation of dwarf dark matter halos because their observed mass is much smaller than the mass of large dark matter halos. This is another argument that CE is not relevant to describe dark matter halos (see Appendix B).

F. The effect of decreasing T for fixed $\mu < \mu_{\rm CCP}$

We consider a value of μ smaller than $\mu_{\rm CCP} = 10.1$ for which there is no canonical phase transition (no collapse). We start from $T \to +\infty$ and progressively decrease the temperature. At high temperatures, the system is nondegenerate. It can be described by the classical King model. When $T \to +\infty$, the solution is equivalent to a polytrope of index $n = 5/2$. As T decreases, the solutions become partially degenerate. They have a core-halo structure but the distinction between the core and the halo is not clear-cut. The core can be approximated by a polytrope of index $n = 3/2$ and the halo can be approximated by a polytrope of index $n = 5/2$. When $T \to 0$, the solutions are completely degenerate. They correspond to a polytrope of index $n = 3/2$. The size of the cluster decreases as the temperature decreases.

VI. CAN LARGE DARK MATTER HALOS HARBOR A FERMION BALL?

Many observations have revealed that galaxies and dark matter halos contain a very massive object at their center. This compact object is usually interpreted as a black hole. Alternatively, some authors have suggested that this object could actually be a fermion ball made of the same matter as the rest of the halo. Indeed, some configurations of the self-gravitating Fermi gas at finite temperature have a nucleus-halo structure resembling a large dark matter halo with a small compact object at the center (see Secs. IV and V). This nucleus-halo structure is particularly clear in the

embryonic phase (solution B). These solutions are similar to the gaseous phase (solution A) except that they contain a small degenerate nucleus. The halo has the form of a King-truncated classical isothermal gas consistent with the observations of large dark matter halos (Burkert profile) and the nucleus has the form of a degenerate fermion ball. When μ is large, the fermion ball is very small so it does not affect the structure of the halo. The corresponding density profiles and rotation curves are represented in Figs. 35–37 (see also solution B in Figs. 41–43). The nucleus creates a secondary peak and a dip in the rotation curve at very small radii that may not be resolved observationally. This type of nucleus-halo configurations has been obtained by several authors [9,57,62,68,69]. Some of them [68] made the interesting suggestion that the fermion ball could mimic the effect of a central black hole. However, these authors [68] did not investigate the stability of such configurations. Our study (see also Refs. [9,29,62]) shows that these structures (solution B) are thermodynamically unstable (i.e. unreachable) because they are saddle points of entropy at fixed mass and energy. Therefore, large dark matter halos should not contain a degenerate nucleus (fermion ball). This is an important prediction of our study.[18] The fact that fermion balls are not observed at the center of galaxies (a central black hole is indeed observationally favored over a fermion ball [87,88]) is in agreement with our result.

We note that the solutions of the condensed phase (solution C) also have a core-halo structure with a degenerate nucleus and a nondegenerate envelope. These solutions are thermodynamically stable. However, in that case, the nucleus formed by gravitational collapse releases an enormous energy that heats the envelope and disperses it at very large distances. As a result, only the degenerate object remains at the end. These solutions do not resemble a large dark matter halo with a central nucleus because the atmosphere is too hot (compare solutions B and C in

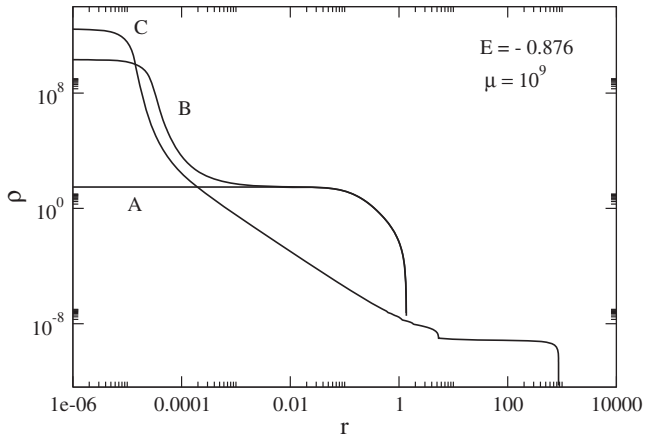

FIG. 41. Density profiles of the gaseous phase (solution A), embryonic phase (solution B) and condensed phase (solution C) for $\mu = 10^9$ and $E = -0.876$ corresponding to the caloric curve of Fig. 30. Solution A corresponds to the classical King model close to the critical point. This solution is stable and gives a good agreement with the observations of dark matter halos. Solution B is similar to solution A except that it contains a small fermion ball that could mimic a central black hole. However, this solution is thermodynamically unstable. Solution C is made of a fermion ball surrounded by a hot halo that is ejected at large distances. This solution is stable but it does not agree with the observations of dark matter halos.

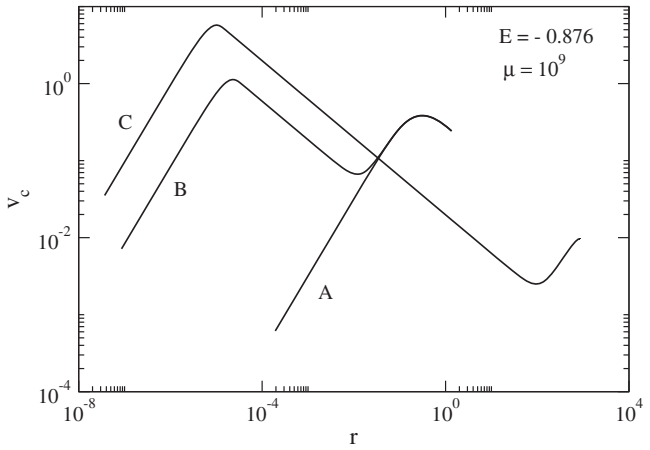

FIG. 42. Circular velocity profiles in logarithmic scale of the gaseous phase (solution A), embryonic phase (solution B) and condensed phase (solution C) for $\mu = 10^9$ and $E = -0.876$. Solution A is stable and agrees with the observations of dark matter halos. Solution B is similar to solution A except that it presents a secondary peak and a dip due to the presence of the fermion ball. This solution is thermodynamically unstable. Solution C is stable but it does not agree with the observations of dark matter halos.

[18]Some caution should be taken. We have shown that the solutions B are thermodynamically unstable. This means that they are unstable with respect to a "collisional" evolution. However, as discussed in Appendix A, they are Vlasov dynamically stable. This means that they are stable with respect to a "collisionless" evolution. On the other hand, even if we consider their thermodynamical instability, we note that these structures are saddle points of entropy. Therefore, they are unstable only for some particular perturbations. As a result, provided that they appear spontaneously from a collisionless relaxation (which is, however, very unlikely because these structures are also saddle points of Lynden-Bell's entropy, and hence a very improbable outcome of violent relaxation), they may persist for a long time, as long as the system does not spontaneously generate the dangerous perturbations that destabilize them. On the other hand, even if a destabilizing perturbation is produced, it may have a small growth rate. Therefore, it may be possible to observe a fermion ball at the center of a dark matter halo as a transient structure. Recalling that the fermion ball in solution B corresponds to a "germ" triggering a gravitational collapse (see Sec. IV B), their observation would be the signal of a phase transition to come. Finally, we should recall that our stability analysis assumes that the parameter A is fixed along the series of equilibria. It is not known whether other assumptions can change the results of the stability analysis and make the solutions B stable.

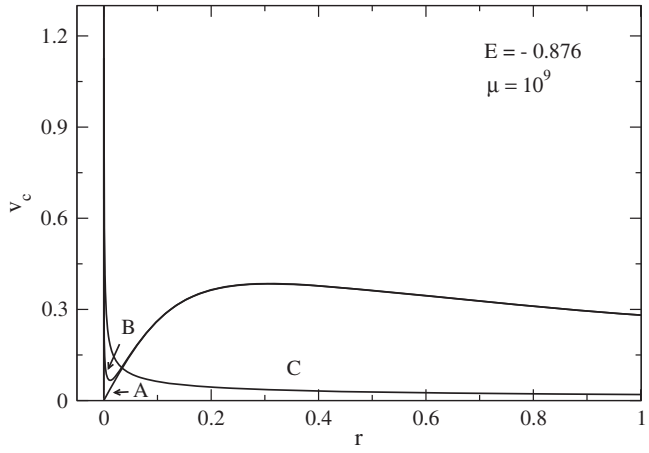

FIG. 43. Circular velocity profiles in linear scale of the gaseous phase (solution A), embryonic phase (solution B) and condensed phase (solution C) for $\mu = 10^9$ and $E = -0.876$. Solution A is stable and agrees with the observations of dark matter halos. Solution B is similar to solution A except that it presents a spike at the origin due to the presence of the fermion ball. This solution is thermodynamically unstable. Solution C is stable but it does not agree with the observations of dark matter halos.

Figs. 35–40 and in Figs. 41–43). However, the nucleus alone resembles a dwarf halo that is a completely degenerate object without atmosphere.

In conclusion, dark matter halos cannot harbor a fermion ball, unlike the proposition that has been made in the past [68], because the nucleus-halo structures that have been considered by these authors are unreachable: they correspond to saddle points of entropy at fixed mass and energy. As a result, dark matter halos should be either everywhere nondegenerate (solution A) or everywhere completely degenerate with an atmosphere dispersed at large distances (solution C). They cannot be made of a completely degenerate nucleus (fermion ball) surrounded by a nondegenerate halo similar to the halo of the gaseous phase because these intermediate structures (solution B) are thermodynamically unstable. Therefore, it should not be possible to observe a dark matter halo with a fermion ball.[19] This may explain why black holes at the center of galaxies are observationally favored over fermion balls [87,88].

Similar results apply in the case where dark matter is made of bosons instead of fermions. Slepian and Goodman [89] have calculated equilibrium states of a self-gravitating gas of self-interacting bosons at finite temperature. They obtained nucleus-halo configurations made of a classical isothermal halo and a nucleus equivalent to a Bose-Einstein condensate (BEC) at zero temperature. The BEC is the counterpart of the fermion ball. They determined the density profiles and the rotation curves of these configurations and obtained results very similar to those obtained in Figs. 35–37 (see also solution B in Figs. 41–43) for fermions.[20] They argued that these nucleus-halo structures are not consistent with observations because the rotation curves do not show the secondary peak and the dip corresponding to the presence of the nucleus. Actually, when the nucleus is very small, it is not clear whether the secondary peak can be resolved observationally. Therefore, their argument should be considered with caution. Anyway, it can be shown that these nucleus-halo structures are thermodynamically unstable [90], similarly to solutions B in the case of fermions. Therefore, they should not be observed in nature. Note, however, that noncondensed configurations of self-gravitating bosons at sufficiently high temperatures may describe large dark matter halos, totally condensed configurations of self-gravitating bosons (BEC) at low temperatures may describe dwarf halos, and partially condensed configurations may describe intermediate-size halos (the temperature may be effective as discussed at the end of Appendix F).

VII. CAN LARGE DARK MATTER HALOS HARBOR A BLACK HOLE?

We have seen in the previous section that the presence of a fermion ball at the center of large dark matter halos is unlikely because these nucleus-halo structures are unreachable: they are saddle points of entropy. The presence of a central black hole is more likely [87,88]. These black holes could be formed by the mechanism discussed by Balberg *et al.* [91] if dark matter is collisional [92]. In that case, large dark matter halos may undergo a gravothermal catastrophe when $E < E_c$. The increase of the density and temperature of the core during the collapse can trigger a dynamical (Vlasov) instability of general-relativistic origin leading to the formation of a black hole. During this process, only the core collapses. This can form a black hole of large mass without affecting the structure of the halo. Therefore, this process leads to large halos compatible with the Burkert profile for $r > 0$ but harboring a central black hole at $r = 0$.

In this scenario, the presence of black holes at the center of dark matter halos is conditioned by the possibility that dark matter halos may undergo a gravothermal catastrophe. Now, when quantum mechanics is taken into account, as in the fermionic King model, an important result of our study is the existence of a microcanonical critical point $\mu_{\rm MCP}$

[19]If we observe a dark matter halo, it should not contain a fermion ball. Inversely, if we observe a fermion ball, it should not be surrounded by a dark matter halo (the atmosphere has been expelled far away). It should not be possible to observe *simultaneously* a dark matter halo and a fermion ball.

[20]This confirms the claim made in Paper I that it is not possible at present to distinguish between fermionic and bosonic models of dark matter because they lead to very similar results. Therefore, the bosonic models cannot be rejected *a priori*.

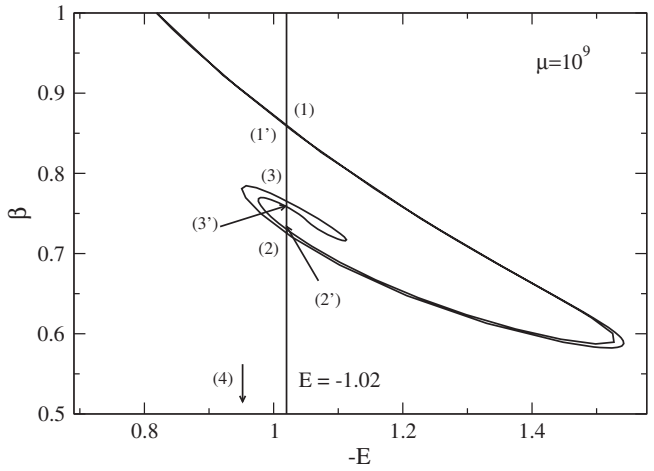

FIG. 44. Series of equilibria of the fermionic King model for $\mu = 10^9$. We show the different solutions corresponding to an energy $E = -1.02$.

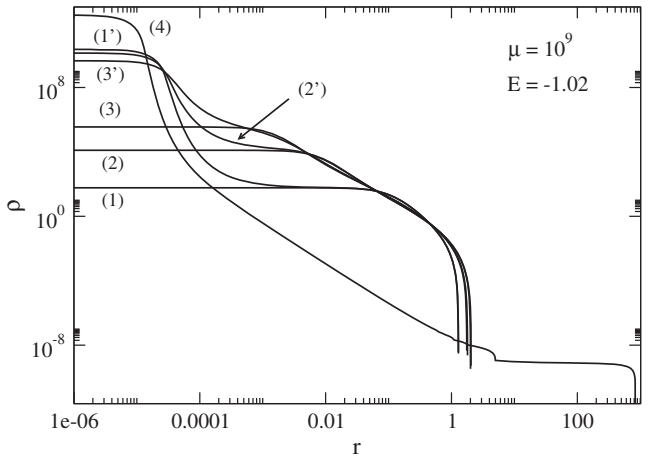

FIG. 45. Density profiles of the different solutions corresponding to a degeneracy parameter $\mu = 10^9$ and an energy $E = -1.02$.

below which the microcanonical phase transition (gravothermal catastrophe) is suppressed. Roughly speaking, this result implies that "large" dark matter halos ($\mu > \mu_{\rm MCP}$) that are nondegenerate can undergo a gravothermal catastrophe (although this is not compulsory[21]) and contain a central black hole while "small" dark matter halos ($\mu < \mu_{\rm MCP}$) that are quantum objects stabilized by the Pauli exclusion principle cannot contain a central black hole because they do not experience a gravothermal catastrophe. This result seems to qualitatively agree with the observations. Therefore, the presence (or absence) of black holes at the center of galaxies may be connected to the existence of a microcanonical critical point ($\mu_{\rm MCP} = 1980$) in the fermionic King model. In Appendix H, we provide a more quantitative criterion for the presence of a black hole at the center of dark matter halos based on these considerations.

VIII. COMPARISON WITH OTHER WORKS

In a recent paper, Ruffini *et al.* [93] revived the suggestion of Bilic *et al.* [68] that dark matter halos may contain a fermion ball at their center rather than a black hole. Although this suggestion is interesting, we would like to emphasize again that it is not obvious. To that purpose, as a complement to the discussion of Sec. VI (see Figs. 41–43), we offer another illustration of our results by taking a degeneracy parameter $\mu = 10^9$, appropriate to large dark matter halos, and selecting an energy $E = -1.02$ so that several (seven) solutions to the equations of hydrostatic equilibrium exist (see Figs. 44 and 45). The following description clarifies the structure of the series of equilibria of the fermionic King model and makes our previous arguments more precise.

Solution (1) is nondegenerate (nonquantum) and has a concentration parameter $k_1 < k_{\rm MCE}$ below the limit of instability. Solutions (2) and (3) are also nondegenerate but they have higher concentration parameters $k_{\rm MCE} < k_2 < k_3$ above the limit of instability. Degeneracy (quantum) effects start to come into play when the series of equilibria rotates anticlockwise. As is clear in Fig. 45, solutions (3'), (2'), (1') are similar to solutions (3), (2), (1) except that they contain a small degenerate nucleus (fermion ball) at their center. These "nucleus-halo" solutions are similar to those obtained by Ruffini *et al.* [93] (and previously in Refs. [9,57,62,68,69]). However, we stress that these solutions are thermodynamically unstable (and hence unreachable) because they are saddle points of entropy at fixed mass and energy. Only solutions (1) and (4) are stable. As shown in Paper I, solution (1) is relatively close to the modified Hubble profile, which is itself close to the empirical Burkert profile fitting observations. It is a pure classical gaseous solution without a fermion ball at its center. It provides a good description of large dark matter halos. On the other hand, solution (4) which lies on the lower branch of Fig. 30 is a pure condensed (quantum) solution with a hot envelope ejected at infinity (see Fig. 45). It may describe completely degenerate dwarf halos, but it cannot describe large halos with a fermion ball because it is very different from the Burkert profile.

Therefore, according to thermodynamics and equilibrium statistical mechanics, the existence of "nucleus-halo" solutions having the form of a fermion ball at $T = 0$ surrounded by a thermal halo is not granted since these structures are saddle points of entropy at fixed

[21]It is possible that a proportion of large dark matter halos have a concentration parameter $k < k_{\rm MCE}$ and have not undergone core collapse (these halos do not contain a black hole) while some halos have reached the critical threshold $k = k_{\rm MCE}$ and have undergone core collapse (these halos contain a black hole).

mass and energy. They are therefore less likely than pure halo solutions without a central compact object, resembling the Burkert profile, studied in Paper I. We note that the works of Refs. [68,93] were done in general relativity, while our study uses Newtonian gravity, but we do not think that this difference alters our conclusions.

Finally, we would like to mention that we do not completely reject the possibility of finding fermion balls at the center of dark matter halos. We just point out a difficulty in interpreting them as equilibrium structures since they are saddle points of entropy. However, equilibrium statistical mechanics says nothing about time scales. As suggested in footnotes 18 and 22, "nucleus-halo" configurations could be out-of-equilibrium structures persisting for very long times, of the order of the Hubble time. More work is needed to clarify these different issues.

IX. DIFFERENCES BETWEEN LARGE AND DWARF HALOS

The structure of dark matter halos crucially depends on their size through the value of the degeneracy parameter μ.

For large halos with $\mu > \mu_{\rm MCP} = 1980$, the series of equilibria is represented in Fig. 14. It displays an instability (gravothermal catastrophe) when $E < E_c$. When $\mu \gg \mu_{\rm MCP}$, two possibilities can occur: (i) the system collapses into a fermion ball and expels a halo at very large distances so that only the degenerate object remains at the end (see Fig. 38)[22]; (ii) a general-relativistic instability develops before the system reaches equilibrium, and the system forms a central black hole surrounded by a halo not affected by the collapse [91]. In that case, we get a halo compatible with the Burkert profile but containing a central black hole. This may explain the presence of black holes in large dark matter halos. When $\mu > \mu_{\rm MCP}$ is not very large, the system may be stabilized by quantum mechanics before the relativistic instability leading to a black hole takes place. In that case, one obtains a core-halo configuration with a fermion ball surrounded by a halo that is not too much dispersed (see solution C in Fig. 8). However, the structure of the halo is affected by the collapse of the core so that it is different from the Burkert profile.

For dwarf and intermediate-size halos with $\mu < \mu_{\rm MCP}$, the series of equilibria is represented in Fig. 15. There is no instability (no gravothermal catastrophe) because the collapse is prevented by quantum mechanics. In that case, there is no possibility to form black holes. This may explain why dwarf and intermediate-size halos do not contain black holes. These halos are partially or completely degenerate quantum objects. When $\mu < \mu_{\rm MCP}$, all the configurations of the fermionic King model are stable. The solutions in the region of negative specific heat have a core-halo structure with a partially degenerate nucleus surrounded by a nondegenerate atmosphere. However, in that case, the distinction between the nucleus and the halo is not clear-cut. In particular, the profile of these solutions (see Fig. 16) is very different from the nucleus-halo configurations that have been considered in the literature (see Fig. 8).

Obviously, several configurations of dark matter halos are possible within the fermionic King model making the study of this model very rich. The system can be nondegenerate (large halos), partially degenerate (intermediate-size halos), or completely degenerate (dwarf halos). We can obtain core-halo configurations with a wide diversity of nuclear concentration depending on μ (i.e. the size of the system) and E. This may account for the diversity of dark matter halos observed in the Universe. Large dark matter halos are nondegenerate classical objects. They may contain a black hole. Small halos are degenerate quantum objects. They should not contain a black hole. Our approach is the first attempt to determine the caloric curves of dark matter halos. This allows us to study the thermodynamical stability of the different configurations and to reject those that are unstable. In particular, we have shown that the nucleus-halo configurations considered in the past (as in Fig. 35) are thermodynamically unstable (saddle points of entropy). More work is needed to relate our theoretical results to the observations.

X. CONCLUSION

In this paper, we have studied the thermodynamical properties of the fermionic King model. The fermionic King model is interesting from the viewpoint of statistical mechanics for the following reasons. (i) It takes into account the evaporation of high-energy particles. As a result, the system has a finite mass without having to introduce an artificial box. (ii) It takes into account the Pauli exclusion principle for fermions.[23] As a result, the system is stabilized against gravitational collapse and there

[22]This is the equilibrium state of the fermionic King model for $E < E_c$. Note, however, that the collapse process can take a very long time in practice so that, on intermediate times, one should observe a contracting fermion ball surrounded by a halo similar to the halo before collapse (see Fig. 5 of Ref. [86] for a preliminary numerical simulation). We stress that this nucleus-halo structure is an *out-of-equilibrium* structure.

[23]The Pauli exclusion principle is justified by quantum mechanics. As explained in Paper I, if the evolution of the particles is collisionless, an exclusion principle similar to the Pauli exclusion principle arises because of dynamical constraints brought by the Vlasov equation. After a phase of violent relaxation, the system is expected to reach a quasistationary state described by the Lynden-Bell distribution function that is similar to the Fermi-Dirac distribution [62,81,82]. A fermionic King model can also be introduced in the context of the theory of violent relaxation in order to make the mass of the Lynden-Bell distribution function finite [63,80].

exists a nonsingular equilibrium state (with a finite entropy and a finite free energy) for all accessible energies $E_{\rm min} \leq E \leq 0$ and for all temperatures $T \geq 0$. (iii) It exhibits interesting phase transitions between gaseous states and condensed states similar to those described in Ref. [9] for a gas of self-gravitating fermions enclosed within a box. Of course, the form of the caloric curves and the values of the critical parameters differ quantitatively from the box model since the equilibrium states are different but the phenomenology of the phase transitions is the same.

We have studied the nature of phase transitions in the fermionic King model as a function of the degeneracy parameter μ which is a measure of the size of the system. For $\mu \to +\infty$, we recover the classical King model (Paper I). For finite values of μ, phase transitions can take place between a "gaseous" phase unaffected by quantum mechanics and a "condensed" phase dominated by quantum mechanics. The phase diagram exhibits two critical points, one in each ensemble. The microcanonical critical point corresponds to $\mu_{\rm MCP} = 1980$ and the canonical critical point corresponds to $\mu_{\rm CCP} = 10.1$. For $\mu > \mu_{\rm MCP}$, there exist microcanonical and canonical first-order phase transitions. For $\mu_{\rm CCP} < \mu < \mu_{\rm MCP}$, only canonical first-order phase transitions are present. For $\mu < \mu_{\rm CCP}$, there is no phase transition at all. There also exists a region of negative specific heats and a situation of ensemble inequivalence when $\mu > \mu_{\rm CCP}$. We have mentioned that metastable states have considerable lifetimes. As a result, the first-order phase transitions do not take place in practice. The physical phase transitions correspond to zeroth-order phase transitions associated with spinodal points and saddle-node bifurcations.

The fermionic King model also provides a realistic model of dark matter halos and, as such, is interesting from the viewpoint of astrophysics and cosmology. Large dark matter halos are nondegenerate objects stabilized by thermal pressure [70–74] so the classical King model can be used. We have shown in Paper I that the marginally stable King model in MCE provides a good description of large dark matter halos. Its density profile is flat in the core and decreases at large distances as r^{-3}, similarly to the Burkert profile [52] that fits a large number of galactic rotation curves.[24] We note that, for large dark matter halos, the cusp problem of the CDM model is solved by finite-temperature effects, without the need to invoke quantum mechanics. Therefore, WDM may account for the observations of large dark matter halos. By contrast, quantum mechanics must be taken into account in smaller dark matter halos. Dwarf dark matter halos are completely degenerate objects stabilized by quantum pressure (Pauli exclusion principle) [70–74] so they are equivalent to polytropes of index $n = 3/2$. In that case, the cusp problem is solved by quantum mechanics, not by thermal effects. Intermediate-size halos are partially degenerate (they are stabilized both by quantum and thermal pressure) [70–74] so they can be described by the fermionic King model at finite temperature.

In order to summarize our results, it is relevant to follow the series of equilibria from low values of the concentration parameter $k \to 0$ (high energies $E \to 0$ and high temperatures $T \to +\infty$) to high values of the concentration parameter $k \to +\infty$ (low energies $E \to E_{\rm min}$ and low temperatures $T \to 0$). This evolution is natural because the concentration parameter $k(t)$ of dark matter halos increases monotonically with time due to collisions and evaporation until an instability takes place (see Appendix A). Different evolutions are possible depending on the value of μ and according to whether we work in MCE or CE.

We first summarize our results in MCE.

(i) If $\mu > \mu_{\rm MCP}$ (large halos), the series of equilibria is represented in Fig. 7. For $E_c \leq E \leq 0$ (corresponding to $0 \leq k \leq k_{\rm MCE}$), the system is in the gaseous phase (upper branch). The solutions of this branch (solution A) are nondegenerate. They correspond to the classical King model. They may describe large dark matter halos for which quantum mechanics is negligible. The marginal King profile at $E = E_c$ (corresponding to $k = k_{\rm MCE}$) can be approximated by the modified Hubble profile. This is the last stable state on the gaseous branch. It accounts relatively well for the observation of large dark matter halos (see Paper I).[25] For $E < E_c$, the gaseous branch disappears and the system collapses. Gravitational collapse in MCE results in the formation of a completely degenerate object with a much smaller mass and radius than the original halo accompanied by the expulsion of a hot massive envelope (solution C). Since the envelope is expelled at large distances, only the completely degenerate object remains at the end. These objects may correspond to dwarf dark matter halos that are completely degenerate and that have a much smaller mass than large dark matter halos. Nucleus-halo solutions (solution B) are attractive because they are similar to large dark matter halos

[24]The r^{-3} decay at large distances is also consistent with the NFW profile [51]. However, unlike the NFW profile, the marginally stable King model has a flat core density (in agreement with the observations and with the Burkert profile) instead of a cuspy profile.

[25]Large dark matter halos that are observed at present are expected to have a concentration parameter close to $k_{\rm MCE}$. The concentration parameter cannot be much smaller than $k_{\rm MCE}$ because $k(t)$ increases with time and the halos are relatively old. The concentration parameter cannot be larger than $k_{\rm MCE}$ because above $k_{\rm MCE}$ the King profiles are unstable and the system collapses. These arguments may explain why large dark matter halos are relatively well described by the marginal King profile with $k = k_{\rm MCE}$.

(solution A) with a fermion ball at the center that could mimic a central black hole. However, we have shown that these structures are thermodynamically unstable. Therefore, when $\mu > \mu_{\rm MCP}$, only two types of equilibrium structures are stable: the nondegenerate solutions (solution A) corresponding to large dark matter halos and the completely degenerate solutions with a dispersed atmosphere (solution C) corresponding to dwarf dark matter halos. Nucleus-halo configurations (solution B) are unreachable. Note that instead of forming a completely degenerate dwarf halo (solution C), the gravitational collapse (gravothermal catastrophe) can trigger a dynamical instability of general-relativistic origin and lead to the formation of a black hole [91]. In that case, we obtain a nondegenerate large halo (solution A) harboring a central black hole.

(ii) If $\mu_{\rm CCP} < \mu < \mu_{\rm MCP}$ (intermediate-size halos), the series of equilibria is represented in Fig. 15. In that case, the evolution of the system along the series of equilibria is more progressive, without a sudden jump corresponding to a phase transition (collapse). Since there is no gravothermal catastrophe, there is no possibility to form black holes. At high energies, the solutions are nondegenerate. At intermediate energies, in the region of negative specific heats, the solutions are partially degenerate. They have a core-halo structure but the distinction between the degenerate core and the nondegenerate halo is not clear-cut. At low energies, the solutions are completely degenerate.

(iii) If $\mu < \mu_{\rm CCP}$ (dwarf halos), the evolution is similar to the previous case except that there is no region of negative specific heat. In that case, quantum effects are relatively strong along the whole series of equilibria.

We now summarize our results in CE.

(i) If $\mu > \mu_{\rm CCP}$, the series of equilibria is represented in Fig. 19. For $T \geq T_c$ (corresponding to $0 \leq k \leq k_{\rm CE}$), the system is in the gaseous phase (left branch). The solutions of this branch (solution A') are nondegenerate. They correspond to the classical King model. Because of ensemble inequivalence, the value of the concentration parameter corresponding to the marginal King profile in CE is smaller than in MCE (see Paper I). As a result, the marginal King profile at T_c (corresponding to $k = k_{\rm CE}$) is very different from the modified Hubble profile (corresponding to $k = k_{\rm MCE}$). It almost coincides with a polytrope $n = 5/2$ that is the exact solution of the King model for $T \to +\infty$. This profile does not correspond to the observations of large dark matter halos. This is an observational evidence that CE may not be appropriate to describe dark matter halos. For $T < T_c$, the gaseous branch disappears and the system collapses. Gravitational collapse in CE results in the formation of a completely degenerate object with a small radius but a large mass, of the same order as the mass of the original halo. This compact object is surrounded by a very tenuous envelope with a small mass that is hardly visible (solution C'). Therefore, the isothermal collapse leads to a small degenerate object of the same mass as the initial halo. Since dwarf dark matter halos have a much smaller mass than large dark matter halos, this result is not consistent with observations. This is another observational evidence that CE may not be appropriate to describe dark matter halos.

(ii) If $\mu < \mu_{\rm CCP}$, the evolution of the system along the series of equilibria is more progressive, without a sudden jump corresponding to a phase transition (collapse). In that case, quantum effects are relatively strong along the whole series of equilibria.

From these results, we conclude that MCE is more appropriate to describe dark matter halos than CE: (i) the marginally stable King profile in MCE is consistent with the observations of large dark matter halos while the marginally stable King profile in CE is not; (ii) the gravitational collapse in MCE leads to a small completely degenerate compact object with a much smaller mass than the initial halo (and the expulsion of a hot massive envelope) while the gravitational collapse in CE leads to a small completely degenerate compact object with the same mass as the initial halo (with almost no atmosphere). Therefore the gravitational collapse in MCE can account for the difference of mass between large and dwarf halos (a factor 1000 or more according to Table 1 of Ref. [71]) while the gravitational collapse in CE does not. That MCE provides a better description than CE is consistent with the fact that dark matter halos are rather isolated objects. Therefore a microcanonical description is more adapted than a canonical description which assumes that the system is dissipative and coupled to a thermal bath.

We note that the idea that dark matter halos contain a fermion ball mimicking a central black hole [68] is very attractive but, unfortunately, our study shows that these nucleus-halo structures (solution B) are unreachable because they are saddle points of entropy. Therefore, fermion balls should not be observed at the center of large dark matter halos (see, however, footnotes 18 and 22). It is more likely that dark matter halos contain a central black hole [91].

In future works, we will take general relativity into account. We will also relate the caloric curves that we have obtained to the observations of dark matter halos in order to show that the fermionic King model can account for the diversity of dark matter halos observed in the Universe. Finally, we will explore other models of dark matter such as the bosonic model. In our opinion, we cannot favor one

model over the other for the moment. We note, however, that de Vega and Sanchez [94] give arguments excluding the possibility that dark matter is bosonic.

APPENDIX A: DYNAMICAL VERSUS THERMODYNAMICAL STABILITY

In this appendix, we discuss subtle issues concerning the dynamical and thermodynamical stability of self-gravitating systems.

1. Thermodynamical stability

For $t \to +\infty$, a self-gravitating system of fermions is expected to reach a statistical equilibrium state described by the Fermi-Dirac distribution (I-1). This distribution function is the solution of the maximization problems (I-10) and (I-11) with the Fermi-Dirac entropy

$$S = -\int [f \ln f + (\eta_0 - f)\ln(\eta_0 - f)] d\mathbf{r}d\mathbf{v}. \tag{A1}$$

These maximization problems determine the most probable distribution of particles at statistical equilibrium, i.e. the macrostate that is represented by the largest number of microstates. In the classical (nondegenerate) limit, the Fermi-Dirac distribution (I-1) reduces to the Boltzmann distribution (I-2) and the Fermi-Dirac entropy (A1) reduces to the Boltzmann entropy

$$S = -\int \left[f \ln\left(\frac{f}{\eta_0}\right) - f \right] d\mathbf{r}d\mathbf{v}. \tag{A2}$$

If the system is isolated, the evolution of the distribution function is governed by the fermionic Landau equation

$$\frac{\partial f}{\partial t} + \mathbf{v}\cdot\frac{\partial f}{\partial \mathbf{r}} - \nabla\Phi\cdot\frac{\partial f}{\partial \mathbf{v}} = \frac{\partial}{\partial v^\mu}\int d\mathbf{v}_1 K^{\mu\nu}\left\{ f_1(1-f_1/\eta_0)\frac{\partial f}{\partial v^\nu} - f(1-f/\eta_0)\frac{\partial f_1}{\partial v_1^\nu}\right\}, \tag{A3}$$

$$K^{\mu\nu} = 2\pi G^2 m \ln N \frac{u^2\delta^{\mu\nu} - u^\mu u^\nu}{u^3}, \tag{A4}$$

where $f = f(\mathbf{r}, \mathbf{v}, t)$, $f_1 = f(\mathbf{r}, \mathbf{v}_1, t)$, and $\mathbf{u} = \mathbf{v}_1 - \mathbf{v}$. The collision term on the right-hand side of Eq. (A3) models the effect of two-body encounters between particles.[26] The fermionic Landau equation conserves mass and energy and monotonically increases the Fermi-Dirac entropy (H theorem). This corresponds to MCE. Alternatively, if the system is in contact with a thermal bath fixing the temperature, the evolution of the distribution function is governed by the fermionic Kramers equation

$$\frac{\partial f}{\partial t} + \mathbf{v}\cdot\frac{\partial f}{\partial \mathbf{r}} - \nabla\Phi\cdot\frac{\partial f}{\partial \mathbf{v}} = \frac{\partial}{\partial \mathbf{v}}\cdot\left\{ D\left[\frac{\partial f}{\partial \mathbf{v}} + \beta f(1-f/\eta_0)\mathbf{v}\right]\right\}. \tag{A5}$$

The term on the right-hand side of Eq. (A5) models the interaction with the thermal bath. The fermionic Kramers equation conserves mass and monotonically increases the Fermi-Dirac free energy (H theorem). This corresponds to CE. The classical Landau equation and the classical Kramers equation are recovered for $f \ll \eta_0$. A derivation of these kinetic equations is given in Refs. [80,95,96].

As recalled in the Introduction, there is no statistical equilibrium state for classical or quantum self-gravitating systems in an unbounded domain because the maximization problems (I-10) and (I-11) with the Boltzmann entropy or with the Fermi-Dirac entropy have no solution. When coupled to the Poisson equation, the Boltzmann distribution and the Fermi-Dirac distribution have infinite mass. The absence of a statistical equilibrium state simply reflects the fact that a system of particles has the tendency to evaporate. As a result, the kinetic equations (A3) and (A5) do not relax towards a steady state but display a permanent evolution driven by evaporation. In practice, evaporation is a slow process and it may be relevant to consider some form of confinement in order to describe the structure of the system on intermediate time scales.

A first possibility to avoid evaporation is to enclose the system within a box [1,2]. The maximization problems (I-10) and (I-11) have been studied for classical particles described by the Boltzmann entropy in Refs. [1,2,7,9,16–19] and for fermions described by the Fermi-Dirac entropy in Refs. [9,29–34]. For classical particles, there exist equilibrium states only above a critical energy E_c in MCE and only above a critical temperature T_c in CE. These equilibrium states are metastable but they are long-lived. Below E_c in MCE, the system undergoes a gravothermal catastrophe leading to a tight binary surrounded by a hot halo (at the collapse time, the singular density profile has infinite central density but zero central mass). Below T_c in CE, the system undergoes an isothermal collapse leading to a Dirac peak containing all the particles. If the particles are fermions, these singular structures (tight binary and Dirac peak) are regularized by quantum mechanics. In that case, the collapse stops when the system becomes degenerate because of the Pauli exclusion principle. As a result, there exist equilibrium states at all accessible energies and at all temperatures. This gives rise to phase transitions between a gaseous phase and a condensed phase.

[26] Depending on the nature of collisions, different kinetic equations can be considered. The fermionic Landau equation can be used to model systems with long-range interactions and the fermionic Boltzmann equation can be used to model systems with short-range interactions.

Instead of working within an artificial box, we can use the classical and fermionic King models. The study of Katz [21] and our study show that we get the same phenomenology as when we work in a box. One difference is the absence of states with positive energy since the system is self-bound. There is also, of course, a qualitative change in the form of the series of equilibria and in the values of the critical points. Apart from that, the results are very similar. In this analogy, the generalized entropies defined by Eqs. (I-9) and (8) for the classical King model and by Eqs. (I-9) and (7) for the fermionic King model play the same role as the Boltzmann entropy (A2) and the Fermi-Dirac entropy (A1) in the case of box-confined configurations. As a result, it is natural to interpret the maximization problems (I-10) and (I-11) as conditions of thermodynamical stability for tidally truncated isothermal distributions (classical or quantum). As explained in Paper I, in order to relate the turning points of energy and temperature to a change of microcanonical and canonical stability (Poincaré theorem), we must keep A fixed along the series of equilibria. Therefore, the parameter A is the counterpart of the box radius R for box-confined systems.

We note, however, that the analogy with thermodynamics remains heuristic (and maybe incorrect) because the King model is an out-of-equilibrium model. Indeed, the system keeps evolving by losing mass and energy as a result of evaporation. Therefore, it is not quite clear if one can use arguments of equilibrium thermodynamics to study the stability of the King model. Another possibility is to use kinetic theory.[27] The King distribution is a quasistationary solution of the Landau equation with coefficients that slowly change with time because of evaporation. During the collisional evolution, the system becomes more and more isothermal so the concentration parameter $k(t)$ increases monotonically with time. If we consider the nondegenerate limit (gaseous phase) and plot the Boltzmann entropy S_B calculated with the King distribution [Eqs. (I-9), (6) and (A2)] as a function of k, we obtain the curve reported in Fig. 46. We see that S_B increases monotonically for $k < k_* = 7.04$, then decreases. Since $k(t)$ increases with time, a decrease of $S_B(k)$ is not physically possible because it would violate the H theorem associated with the Landau equation. This implies that the King distribution is unstable for $k > k_*$. At that point, the system undergoes a gravothermal catastrophe and experiences core collapse. This instability takes it away from the King sequence. This argument was first put forward by Lynden-Bell and Wood [2]. Cohn [23] confirmed numerically that the actual path of evolution departs from the King sequence at some critical k_* corresponding to the maximum of $S_B(k)$. The value of k_* obtained by Cohn [23] is slightly different from ours. We obtain $K_* = 7.84$ ($k_* = 7.04$) by fixing A while

[27]We restrict our discussion to MCE for the reasons explained in Appendix B.

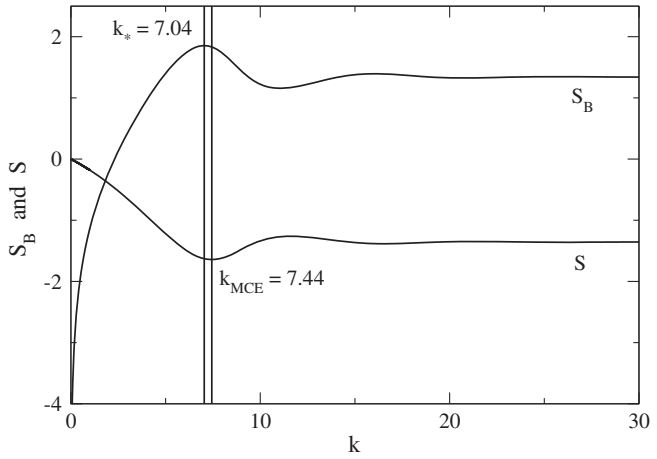

FIG. 46. Evolution of the Boltzmann entropy $S_B(k)$ calculated with the King distribution [Eqs. (I-9), (6) and (A2)] along the series of equilibria. It increases and reaches a maximum at $k_* = 7.04$ (corresponding to $K_* = 7.84$). By contrast, the entropy of the King model $S(k)$ [Eqs. (I-9), (6) and (8)] decreases and reaches a minimum at $k_{\rm MCE} = 7.44$ (corresponding to $K_{\rm MCE} = 8.13$). In the two cases, the value of A is fixed so the energy changes as k increases.

Cohn obtained $K_* = 9.3$ ($k_* = 8.82$) by scaling the King distribution to the mass and energy of the evolutionary model. We have also represented in Fig. 46 the evolution of the generalized entropy S calculated with the King distribution [Eqs. (I-9), (6) and (8)] as a function of k. As shown in Paper I, it reaches its extremal value at $k_{\rm MCE} = 7.44$. It is a little bit disturbing to see that this extremum value is actually a minimum and that $S(k)$ decreases for $k < k_{\rm MCE}$. There is no paradox, however, since the Landau equation satisfies an H theorem for S_B, not for S. Therefore, S may decrease with time. However, these considerations indicate that, for open systems, the Boltzmann entropy S_B and the generalized entropy S (both calculated with the King distribution) have a different physical meaning. The Boltzmann entropy S_B is appropriate to interpret the dynamical evolution of the system in relation to the H theorem (kinetic theory), and the generalized entropy S is appropriate to deduce stability limits from the series of equilibria of the King model by using the Poincaré theory.

We can make an additional comment. The value of the critical concentration $k_* = 8.82$ obtained by Cohn [23] is slightly larger than the value $k_{\rm MCE} = 7.44$ obtained from the Poincaré theory by fixing A. This suggests that the gravothermal catastrophe occurs slightly later than predicted by Katz [21] and in Paper I. This allows the slope α of the density profile to be substantially smaller than 3 (the slope corresponding to $k_* = 8.82$ is $\alpha = 2.52$). A larger value of the critical concentration slightly improves the agreement between the marginal King model and the Burkert profile. On the other hand, we remark that the critical concentration $k_* = 8.82$ obtained by Cohn [23] is relatively close to the value $k'_{\rm MCE} = 8.50$ obtained from the

Poincaré theory by fixing R (see Sec. VI of Paper I). It is not clear whether this is a coincidence or if it bears a deeper meaning than is apparent at first sight.

2. Dynamical stability

In the previous section, the system was assumed to have reached a statistical equilibrium state described by the fermionic King model as a result of collisions. In that case, the Fermi-Dirac distribution arises from the quantum properties of the particles (fermions). However, collisions generally take a very long time to establish a statistical equilibrium state (except possibly in the dense core of the system). For self-gravitating systems with a large number of particles, the collisional relaxation time is in general much larger than the age of the Universe because it scales with the number of particles as $(N/\ln N)t_D$, where t_D is the dynamical time [13]. As a result, most self-gravitating systems are collisionless and their evolution is governed by the Vlasov equation

$$\frac{\partial f}{\partial t}+\mathbf{v}\cdot\frac{\partial f}{\partial \mathbf{r}}-\nabla\Phi\cdot\frac{\partial f}{\partial \mathbf{v}}=0. \tag{A6}$$

It can be shown that any steady state of the Vlasov equation of the form $f=f(\epsilon)$ with $f'(\epsilon)<0$ is linearly [13], and even nonlinearly [97], dynamically stable. Therefore, all the King distributions are dynamically stable, whatever their degree of concentration k. The maximization problems (I-10) and (I-11) provide only sufficient, but not necessary, conditions of dynamical stability. That a stronger dynamical stability criterion exists for the Vlasov equation is due to the fact that this equation conserves an infinite number of integrals, beyond mass and energy—the so-called Casimir integrals [97,98].

However, stability analysis does not explain *how* a collisionless self-gravitating system reaches a steady state. Collisionless relaxation is actually a very nontrivial concept related to mechanisms known as violent relaxation, phase mixing, and nonlinear Landau damping [13]. This form of relaxation takes place on a very short time scale of the order of a few dynamical times t_D. It is therefore very relevant in astrophysics where the collisional relaxation time is very long. Assuming ergodicity, the quasistationary state (QSS) that results from violent relaxation can be predicted from the statistical theory of Lynden-Bell [62,81,82]. In that approach, the QSS reached by the system is the solution of the maximization problem (I-10) where S is the Lynden-Bell entropy defined by Eq. (A1) with a bar on f (it represents the coarse-grained distribution). The Lynden-Bell distribution, given by Eq. (I-1) with a bar on f, is similar to the Fermi-Dirac distribution but the reason has nothing to do with quantum mechanics. To avoid the infinite-mass problem arising in Lynden-Bell's theory, we can consider the fermionic King model defined by Eq. (1) with a bar on f [63,80]. The maximization problem (I-10) with the entropy defined by Eqs. (I-9) and (7) with a bar on f determines the most probable coarse-grained distribution $\bar{f}$ resulting from the intertwinement of the fine-grained distribution function f. While all the distribution functions of the form $\bar{f}=\bar{f}(\epsilon)$ with $\bar{f}'(\epsilon)<0$ are dynamically stable, some of them are more probable than others. This is the difference between Vlasov dynamical stability and Lynden-Bell thermodynamical stability. For example, in the dilute limit, all the King distributions (interpreted as tidally truncated Lynden-Bell distributions) are Vlasov dynamically stable but only the King distributions with $k<k_{\rm MCE}$ are Lynden-Bell thermodynamically stable, i.e. "most probable" (local maxima of entropy at fixed mass and energy). On the other hand, while the fine-grained distribution function $f(\mathbf{r},\mathbf{v},t)$ is the solution of the Vlasov equation (A6), the coarse-grained distribution function $\bar{f}(\mathbf{r},\mathbf{v},t)$ is not. It is the solution of a kinetic equation that has the form of the fermionic Landau equation (A3) with a bar on f [63,80]. This equation conserves mass and energy and satisfies an H theorem for the Lynden-Bell entropy. Therefore, the study of the collisionless relaxation is, in some sense, similar to the study of the collisional relaxation. Because of this analogy, the same arguments apply except that the distribution function f must be viewed as the *coarse-grained* distribution function $\bar{f}$. The main differences between collisionless and collisional relaxation are the following: (i) the time scale of collisionless relaxation is much shorter than the time scale of collisional relaxation; (ii) the equilibrium distribution of collisionless systems undergoing violent relaxation is similar to the Fermi-Dirac distribution even if the particles are classical while the equilibrium distribution of collisional systems is the Boltzmann distribution for classical particles and the Fermi-Dirac distribution for fermions; (iii) the evolution of collisionless systems stops when the system has reached a virialized state (on the coarse-grained scale) while collisional systems undergo a permanent evaporation.

APPENDIX B: MICROCANONICAL VERSUS CANONICAL ENSEMBLE

For the sake of completeness, we have considered both microcanonical and canonical ensembles in the thermodynamical analysis of the King model. However, we give below some arguments according to which MCE is more appropriate than CE to describe dark matter halos.

(i) Most self-gravitating systems such as galaxies and globular clusters are isolated rather than being coupled to a thermal bath [13]. This is the case for dark matter halos also. Therefore, the Boltzmann and the Landau equations (MCE) are more appropriate than the Kramers equation (CE) to describe the dynamics of dark matter halos.

(ii) The King model can be derived from the Landau equation whose diffusion coefficient $D(v)$ depends on the velocity of the particles and decreases as $1/v^3$

for $v \to +\infty$. This decay law is crucial in order to obtain the King model [14,63,80,81,99]. Since the diffusion coefficient appearing in the Kramers equation is constant, the King model cannot be rigorously derived from that equation.

(iii) The King profile at the limit of microcanonical stability $k_{\rm MCE} = 7.44$ can be approximated by the modified Hubble and Burkert profiles that fit a wide diversity of rotation curves of galaxies. By contrast, the King profile at the limit of canonical stability $k_{\rm CE} = 1.34$ is very different from the modified Hubble and Burkert profiles. In CE, only the King distributions that are close to a polytrope $n = 5/2$ are stable, and these distributions are very different from the observed structure of dark matter halos. Since $k_{\rm CE} < k_{\rm MCE}$ as a result of ensemble inequivalence, the King profiles with $k \simeq k_{\rm MCE}$ that are similar to the modified Hubble and Burkert profiles are stable in MCE but not in CE. Therefore, from the observation viewpoint, MCE gives better results than CE. This is because it contains a larger sequence of stable King models than CE as a result of ensemble inequivalence (i.e. because of the constraint resulting from the conservation of energy). As a matter of fact, all the observationally relevant King profiles are unstable in CE.

(iv) The consideration of MCE solves the apparent contradiction faced by Merafina and Ruffini [56]. These authors studied the dynamical stability of the classical King model and found, in the nonrelativistic regime, that it becomes unstable for $k > 1.3654$ (in our notations). They concluded therefore that "the configurations integrated by King are not in the stable branch". However, their stability criterion corresponds to the criterion of *canonical* stability $k_{\rm CE} = 1.34$ (the small difference between 1.3654 and 1.34 is probably a numerical effect). Since globular clusters are isolated, they should be treated in MCE where the limit of stability is $k_{\rm MCE} = 7.44$. In this proper ensemble, most of the configurations integrated by King are stable. Therefore, there is no contradiction. The same remark applies to dark matter halos.

(v) The gravitational collapse of a large dark matter halo of mass $M \sim 10^{12} M_\odot$ in MCE leads to a small compact degenerate object containing a much smaller mass $M \sim 10^6 M_\odot$ than the initial halo, accompanied by the expulsion of a hot and massive envelope (see Sec. V B). The compact object may correspond to a dwarf dark matter halo (see Table 1 of Ref. [71]). By contrast, the gravitational collapse of a large dark matter halo in CE leads to a small compact degenerate object containing almost all the mass of the initial halo, surrounded by a very tenuous atmosphere (see Sec. V E). The compact object cannot correspond to a dwarf dark matter halo because its mass is too large. Therefore, from the observation viewpoint, MCE gives better results than CE.

(vi) If the dark matter halos were coupled to a thermal bath (CE), they would all have the same temperature while observations reveal that their temperature (or their velocity dispersion) depends on their size (see Table 1 of Ref. [71]). By contrast, isolated systems (MCE) have different energies, and hence different temperatures.

(vii) That the temperature depends on the size of the halos may be in favor of Lynden-Bell's theory of violent relaxation [81] where T is an out-of-equilibrium temperature that has no reason to be the same for all clusters. In the Lynden-Bell theory, only MCE makes sense since this theory is based on the Vlasov equation that applies to an isolated collisionless system (fixed E).

(viii) Violent relaxation leads to core-halo structures with a density slope $\alpha = 4$ [100–103]. These configurations are consistent with a King model of index $k \sim 5$. They are stable in MCE but unstable in CE. This is another argument that MCE is more relevant than CE.

Remark: We would like to make clear that we consider here the *thermodynamical* stability of the fermionic King distribution. This implies that we are considering the stability of the system with respect to a collisional evolution or with respect to a violent relaxation on the coarse-grained scale (both described by the fermionic Boltzmann or Landau equation). We have seen that the fermionic King distributions are not always thermodynamically stable, and this puts interesting constraints on these distributions. On the other hand, we recall that the fermionic King distributions, and more generally all the distribution functions of the form $f = f(\epsilon)$ with $f'(\epsilon) < 0$, are nonlinearly *dynamically* stable with respect to the Vlasov equation describing a collisionless evolution [97]. The maximization problems (I-10) and (I-11) only provide sufficient, but not necessary, conditions of dynamical stability [98].

APPENDIX C: THE FUNCTIONS $\mathcal{R}$, F, G, AND H

In Paper I, we have introduced the functions

$$\frac{R}{r_h} = \frac{\zeta_1(k)}{\zeta_h(k)} \equiv \mathcal{R}(k), \tag{C1}$$

$$\frac{M_h}{\rho_0 r_h^3} = -4\pi \frac{\chi'[\zeta_h(k)]}{\zeta_h(k)} \equiv F(k), \tag{C2}$$

$$\frac{\sigma_0^2}{G\rho_0 r_h^2} = \frac{8\pi}{3} \frac{1}{\zeta_h^2(k)} \frac{I_2(k)}{I_1(k)} \equiv G(k), \tag{C3}$$

where r_h is the halo radius such that $\rho(r_h)/\rho_0 = 1/4$ [72]. These functions have been computed for the classical King

model. For the fermionic model, we introduce the additional function

$$\frac{\eta_0\sigma_0^3}{\rho_0}=\frac{\mu}{3\sqrt{3}}\frac{I_2(k)^{3/2}}{I_1(k)^{5/2}}\equiv H(k), \tag{C4}$$

which gives the ratio between the maximum value of the distribution function $\eta_0=gm^4/h^3$ fixed by the Pauli exclusion principle and the typical central phase-space density ρ_0/σ_0^3. To obtain the right-hand side of Eq. (C4), we have used Eqs. (I-28), (I-96) and (I-97). We also note that the exact central distribution function is $f_0=A\mathcal{F}_s(-k)$ so that

$$\frac{\eta_0}{f_0}=\frac{e^k+\mu}{e^k-1}. \tag{C5}$$

For the fermionic King model, we have the following asymptotic results. For $k\to 0$, we get $\mathcal{R}(0)=2.74$, $F(0)=1.89$, $G(0)=0.944$ (see Paper I), $H(k)\sim 15(1+\mu)/(56\pi\sqrt{7}k)\sim 3.22\times 10^{-2}(1+\mu)k^{-1}$, and $\eta_0/f_0\sim(1+\mu)/k$. For $k\to+\infty$, we get $\mathcal{R}(+\infty)=1.61$, $F(+\infty)=-4\pi\theta_h'/\xi_h=1.99$, $G(+\infty)=8\pi/(5\xi_h^2)=0.975$, $H(+\infty)=3/(20\pi\sqrt{5})=2.14\times 10^{-2}$, and $\eta_0/f_0\to 1$ where we have used $\xi_h=2.27$ and $\theta_h'=-0.360$ for a polytrope $n=3/2$.

For a given value of μ, Eq. (C5) can be used to determine the value of the concentration parameter k above which the system is degenerate. If we consider that the system is degenerate when $f_0>\eta_0/\nu$, where ν is a number that depends on our degree of precision (e.g. $\nu=10$), we find that the system is degenerate when $k>\ln[(\mu+\nu)/(\nu-1)]$. Inversely, for a given value of k we find that the system is degenerate when $\mu<(\nu-1)e^k-\nu$. As an illustration, taking $k=k_{\rm MCE}=7.44$, we find that the system is degenerate at that point when $\mu<15300$.

We can use the functions F, G, H to relate the theoretical results of the fermionic King model to the observations. This is beyond the scope of the present paper but this will be considered in a future work.

Remark: The functions defined by Eqs. (C1)–(C4) have been introduced by DdVSS [70–74] in relation to the usual Fermi-Dirac distribution. Our approach is different since our definitions apply to the fermionic King model with an energy cutoff. To avoid confusion, we recall that the functions $I_n(k)$ appearing in Eqs. (C1)–(C4) do *not* correspond to the Fermi integrals used in Refs. [70–74] but to the functions defined by Eq. (I-25).

APPENDIX D: FERMIONIC VERSUS BOSONIC DARK MATTER

In this appendix, we determine the mass of the particles that compose dark matter halos according to whether they correspond to fermions, bosons without self-interaction, or bosons with self-interaction. We use Newtonian gravity. The Newtonian approximation is valid when $2GM/Rc^2\ll 1$. This condition can be rewritten as $M/M_\odot\ll 0.339R/{\rm km}$ or as $M/M_\odot\ll 1.04\times 10^{13}R/{\rm pc}$. From this criterion it is easy to see that dark matter halos are nonrelativistic and that they can be treated by Newtonian gravity.

The smallest known dark matter halo is Willman 1 that has $r_h=33$ pc, $\rho_0=6.8M_\odot/{\rm pc}^3$, $M_h=0.39\times 10^6M_\odot$, and $\sigma_0=4$ km/s [71,72]. To determine the mass of the particles that compose dark matter halos, we consider that this most compact halo is completely degenerate (for fermions) or completely condensed (for bosons), i.e., that it corresponds to the ground state ($T=0$) of a self-gravitating Fermi or Bose gas. We compare the results with those obtained by considering that large dark matter halos such as the Medium Spiral (with $r_h=1.9\times 10^4$ pc, $\rho_0=7.6\times 10^{-3}M_\odot/{\rm pc}^3$, $M_h=1.01\times 10^{11}M_\odot$ and $\sigma_0=76.2$ km/s) are completely degenerate or completely condensed. This is incorrect but this estimate has been made in the past, so it is interesting to do the comparison.

A completely degenerate system of self-gravitating fermions at $T=0$ has the mass-radius relation $MR^3=1.49\times 10^{-3}h^6/(G^3m^8)$ [11]. This gives

$$\frac{m}{{\rm eV}/c^2}=2.27\times 10^4\left(\frac{\rm pc}{R}\right)^{3/8}\left(\frac{M_\odot}{M}\right)^{1/8}. \tag{D1}$$

Using the values of M and R corresponding to Willman 1, we obtain a fermion mass $m=1.23$ keV$/c^2$. This is the typical mass[28] obtained by DdVSS [70–74]. This particle could be a sterile neutrino [76,77]. In the past, some authors [54–59] have determined the fermion mass by considering that large dark matter halos are completely degenerate. Using the values of M and R corresponding to the Medium Spiral, this leads to a fermion mass $m=28.8$ eV$/c^2$. This is the typical mass obtained in Refs. [54–59]. However, if large dark matter halos were completely degenerate there would not be smaller halos such as Willman 1. Therefore, this prediction is not correct. Furthermore, the density profiles and the rotation curves of large dark matter halos do not correspond to those of a completely degenerate self-gravitating Fermi gas. In the fermionic scenario, large dark matter halos are nondegenerate tidally truncated isothermal systems described by the classical King model (see Paper I).

A completely condensed system of self-gravitating bosons (BEC) without self-interaction at $T=0$ has the

[28]This result assumes that (i) Willman 1 is completely degenerate, and that (ii) the observational values of r_h and M_h are accurate. More precise observational data may change the value of the particle mass m but its order of magnitude should remain the same. On the other hand, if the distribution function of the halos corresponds to the Lynden-Bell distribution function instead of the Fermi-Dirac distribution function, we must divide $\eta_0=2m^4/h^3$ by 2 since $\eta_0^{\rm LB}=\eta_0^{\rm Pauli}/2$ (see footnote 11 in Paper I). This implies that the particle mass m must be multiplied by $2^{1/4}$ giving $m=1.46$ keV$/c^2$.

mass-radius relation $MR = 9.95\hbar^2/(Gm^2)$ [104–106]. This gives

$$\frac{m}{\mathrm{eV}/c^2} = 9.22\times 10^{-17}\left(\frac{\mathrm{pc}}{R}\right)^{1/2}\left(\frac{M_\odot}{M}\right)^{1/2}. \quad \text{(D2)}$$

Using the values of M and R corresponding to Willman 1, we obtain a boson mass $m = 2.57\times 10^{-20}$ eV$/c^2$. This is a new prediction. In the past, some authors [107] have determined the boson mass by considering that large dark matter halos are completely condensed. Using the values of M and R corresponding to the Medium Spiral, this leads to a boson mass $m = 2.10\times 10^{-24}$ eV$/c^2$. This is the typical mass obtained in Ref. [107]. However, the Medium Spiral cannot be completely condensed otherwise there would not be smaller halos such as Willman 1. Therefore, this prediction is not correct. In the bosonic scenario, large dark matter halos have a solitonic core (BEC) surrounded by an envelope made of scalar radiation (see footnote 5 of Paper I and the end of Appendix F). It is the envelope that fixes their size.

A completely condensed system of self-gravitating bosons (BEC) with self-interaction at $T = 0$ in the Thomas-Fermi limit has a unique radius $R = \pi(a\hbar^2/Gm^3)^{1/2}$ (a is the scattering length) [108–112]. This gives

$$\left(\frac{\mathrm{fm}}{a}\right)^{1/3}\left(\frac{m}{\mathrm{eV}/c^2}\right) = 6.73\left(\frac{\mathrm{pc}}{R}\right)^{2/3}. \quad \text{(D3)}$$

Using the value of R corresponding to Willman 1, we obtain $(\mathrm{fm}/a)^{1/3}(mc^2/\mathrm{eV}) = 0.654$. This is a new prediction. In order to determine the mass of the bosons, we need another relation. This relation is provided by the constraint $\sigma/m < 1.25$ cm^2/g set by the Bullet Cluster [113], where $\sigma = 4\pi a^2$ is the self-interaction cross section. Assuming that the bound is reached (this gives an upper bound on the mass and on the scattering length of the bosons) we get $(a/\mathrm{fm})^2(\mathrm{eV}/mc^2) = 1.77\times 10^{-8}$. From these two constraints, we obtain $m = 1.69\times 10^{-2}$ eV$/c^2$ and $a = 1.73\times 10^{-5}$ fm. This boson mass is in agreement with the limit $m < 1.87$ eV$/c^2$ obtained from cosmological considerations [114]. In the past, some authors [110] have determined the ratio $m/a^{1/3}$ by considering that large dark matter halos are completely condensed. Using the value of R corresponding to the Medium Spiral, we obtain $(\mathrm{fm}/a)^{1/3}(mc^2/\mathrm{eV}) = 9.45\times 10^{-3}$. The constraint from the Bullet Cluster then yields $m = 1.05\times 10^{-4}$ eV$/c^2$ and $a = 1.36\times 10^{-6}$ fm. However, for the same reason as the one given for non-interacting bosons, this prediction is not correct.

The mass $m = 2.57\times 10^{-20}$ eV$/c^2$ obtained for bosons without self-interaction gives a lower bound on the mass of the bosonic dark matter particle. Inversely, the mass $m = 1.69\times 10^{-2}$ eV$/c^2$ obtained for self-interacting bosons in the Thomas-Fermi limit gives an upper bound on the mass of the bosonic dark matter particle. Therefore, we predict[29] that the mass of the bosonic particle is in the range 2.57×10^{-20} eV$/c^2 < m < 1.69\times 10^{-2}$ eV$/c^2$. The TF limit is valid for sufficiently large scattering lengths. An estimate of the critical scattering length can be obtained by substituting $m = 2.57\times 10^{-20}$ eV$/c^2$ in the relation $(\mathrm{fm}/a)^{1/3}(mc^2/\mathrm{eV}) = 0.654$. This gives $a_c = 6.07\times 10^{-59}$ fm. For $a < a_c$, the mass of the bosonic particle is $m = 2.57\times 10^{-20}$ eV$/c^2$ and for $a_c < a < 1.73\times 10^{-5}$ fm the mass of the bosonic particle is $2.57\times 10^{-20} < mc^2/\mathrm{eV} = 0.654(a/\mathrm{fm})^{1/3} < 1.69\times 10^{-2}$.

We note that, for a given dark matter particle mass m, the ground state of self-interacting bosons determines the radius of the most compact dwarf halos while the ground states of fermions and noninteracting bosons determine their mass-radius relation.

Finally, we can make the following remark. In the fermionic model, large dark matter halos are classical (see Appendix E) so we have the relation $\sigma_0^2 = k_B T/m$. Introducing relevant scales, this can be rewritten as

$$\frac{m}{\mathrm{eV}/c^2} = 7.74\times 10^{12}\left(\frac{\mathrm{m/s}}{\sigma_0}\right)^2\frac{T}{\mathrm{K}}. \quad \text{(D4)}$$

For the medium spiral, $\sigma_0 = 76.2$ km/s. If we argue that the temperature is in the Kelvin range, as is the case for the radiation background, and take $T \sim 1$ K, we obtain $m = 1.33$ keV$/c^2$. Thus, we find that the fermion mass is in the keV$/c^2$ range. This is a completely different argument than the one given previously (relying on the ground state of the self-gravitating Fermi gas) but we may find confidence in the fact that these two arguments lead to similar results.

APPENDIX E: QUANTUM VERSUS CLASSICAL HALOS

Once we know the mass of the dark matter particle (see Appendix D), we can determine if a given halo is quantum (Fermi degenerate or Bose condensed) or classical. We first consider the case of fermions. The parameter

$$H = \frac{2m^4\sigma_0^3}{\rho_0 h^3} \quad \text{(E1)}$$

measures the degree of degeneracy of the core of dark matter halos (see Appendix C). Using the results of Sec. III D, we find that a completely degenerate system of self-gravitating fermions at $T = 0$ has $H_0 = 0.0214$. On the other hand, one can show that a self-gravitating Fermi

[29] As in footnote 28, this prediction assumes that Willman 1 is completely condensed and that the observational values of r_h and M_h are reliable. Our prediction could be improved when more precise data are available.

gas is nondegenerate (classical) when $H > 1$ [90]. Introducing scaled variables, the parameter H can be written as

$$H = 1.03 \times 10^{-24} \left(\frac{m}{\mathrm{eV}/c^2}\right)^4 \left(\frac{\sigma_0}{\mathrm{m/s}}\right)^3 \left(\frac{M_\odot/\mathrm{pc}^3}{\rho_0}\right). \quad \text{(E2)}$$

According to the discussion of Appendix D, we take a fermion mass $m = 1.23\ \mathrm{keV}/c^2$. For Willman 1, we find $H = 0.0221 \simeq H_0$, a value expected for a completely degenerate system (this is how the mass $m = 1.23\mathrm{keV}/c^2$ has been obtained). For the Medium Spiral, we find $H = 1.35 \times 10^5 \gg 1$ indicating that this system is nondegenerate.[30] We can also compute H for a globular cluster with $r_h = 10$ pc, $\rho_0 = 8 \times 10^3 M_\odot/\mathrm{pc}^3$, $M_h = 6 \times 10^5 M_\odot$, $\sigma_0 = 7\mathrm{km/s}$, and $m_* = M_\odot = 1.12 \times 10^{66}\,\mathrm{eV}/c^2$ [13]. In that case, we get the huge number $H = 6.80 \times 10^{247} \gg 1$.

We now evaluate the parameter H in the case where dark matter is made of bosons. It is shown in Appendix F that the core of the halo is condensed (BEC) when $H < 4.86 \times 10^{-2}$ and noncondensed (thermal bosons) when $H > 4.86 \times 10^{-2}$. If we take a mass $m = 2.57 \times 10^{-20}\ \mathrm{eV}/c^2$ appropriate to noninteracting bosons (see Appendix D), we find that $H = 4.23 \times 10^{-93}$ for dwarf halos such as Willman 1 and $H = 2.62 \times 10^{-86}$ for large halos such as the Medium Spiral, indicating that their core is always condensed. If we take a mass $m = 1.69 \times 10^{-2}\ \mathrm{eV}/c^2$ appropriate to self-interacting bosons, we also find that both dwarf halos such as Willman 1 ($H = 7.91 \times 10^{-22}$) and large halos such as the Medium Spiral ($H = 4.89 \times 10^{-15}$) are quantum (Bose condensed) objects.

These results are potentially very important because they can help determining if dark matter is made of fermions or bosons. Indeed, in the fermion case ($m = 1.23\ \mathrm{keV}/c^2$), small dark matter halos are quantum objects while large dark matter halos are classical objects. By contrast, in the boson case ($m = 2.57 \times 10^{-20}\ \mathrm{eV}/c^2$ in the noninteracting case or $m = 1.69 \times 10^{-2}\ \mathrm{eV}/c^2$ in the self-interacting case), small and large dark matter halos are quantum objects. They have a core-halo structure made of a solitonic core surrounded by a halo of scalar radiation (see footnote 5 of Paper I and the end of Appendix F).

Since the surface density $\Sigma_0 = \rho_0 r_h$ is approximately the same for all the halos [72], it is relevant to express H in terms of this quantity. Using the results of Appendix C, we obtain

$$H = \frac{2m^4 G^{3/2} M_h^{5/4}}{\Sigma_0^{3/4} h^3} \frac{G(k)^{3/2}}{F(k)^{5/4}}. \quad \text{(E3)}$$

As shown in Paper I, the functions $F(k)$ and $G(k)$ do not sensibly change with k. Taking $F(k) \sim 1.8$ and $G(k) \sim 0.95$, and introducing relevant scales, we obtain

$$H = 1.29 \times 10^{-19} \left(\frac{m}{\mathrm{eV}/c^2}\right)^4 \left(\frac{M_h}{M_\odot}\right)^{5/4} \left(\frac{M_\odot/\mathrm{pc}^2}{\Sigma_0}\right)^{3/4}. \quad \text{(E4)}$$

Considering that $\Sigma_0 = 120 M_\odot/\mathrm{pc}^2$ is the same for all the halos, and assuming that dark matter is made of fermions with mass $m = 1.23\ \mathrm{keV}/c^2$, we find that the halos are degenerate ($H < 1$) for $M_h < 2.97 \times 10^6 M_\odot$ and classical ($H > 1$) for $M_h > 2.97 \times 10^6 M_\odot$. Therefore, the majority of the observed halos reported in Table 1 of Ref. [71] are classical. Still, the dwarf halos that correspond to the ground state of the self-gravitating Fermi gas are crucially important for determining the mass of the dark matter particle [71].

Assuming that dark matter is made of bosons of mass $m = 2.57 \times 10^{-20}\,\mathrm{eV}/c^2$ (noninteracting) or $m = 1.69 \times 10^{-2}\ \mathrm{eV}/c^2$ (self-interacting), we find that all the observed halos are quantum/Bose condensed ($H < 4.86 \times 10^{-2}$). The bosonic halos would become classical ($H > 4.86 \times 10^{-2}$) for $M_h > 1.11 \times 10^{79} M_\odot$ or $M_h > 9.53 \times 10^{20} M_\odot$, respectively.

Finally, assuming that dark matter is made of particles with mass $m \sim \mathrm{GeV}/c^2$, corresponding to the CDM model, we find that all the observed halos are classical ($H \gg 1$). These halos would become quantum for $M_h < 1.44 \times 10^{-3} M_\odot$. This bound is so small that quantum mechanics can be neglected in the CDM model. Therefore, if the CDM model were valid, we should observe halos of any size. The fact that we do not observe halos below the size of Willman 1 shows that there exists a minimum scale in the Universe (ground state) that is fixed by quantum mechanics (fermions or bosons).

APPENDIX F: THE TEMPERATURE OF THE HALOS

The results of the previous section can be expressed in terms of the temperature of the halos. We first consider the case of fermions. We have seen that the halos are classical if $H = 2m^4\sigma_0^3/\rho_0 h^3 > 1$. Since $\sigma_0^2 = k_B T/m$ for a classical isothermal equation of state, the classical limit corresponds to $T > T_F$ where

$$k_B T_F = \frac{2^{4/3}\pi^2\hbar^2\rho_0^{2/3}}{m^{5/3}} \quad \text{(F1)}$$

is the Fermi temperature. The halos are nondegenerate for $T > T_F$ and degenerate for $T < T_F$. The parameter H can

[30] We have to be careful that the observed central density $\rho_0 = 7.6 \times 10^{-3} M_\odot/\mathrm{pc}^3$ reported in Table 1 of Ref. [71] may be an apparent one. Large dark matter halos may contain a central nucleus (or a black hole) of very small size and huge density $\rho_0' \gg \rho_0$ that may not be resolved observationally (see Appendix H).

be rewritten as $H=(T/T_F)^{3/2}$. Introducing scaled variables, we obtain

$$\frac{T_F}{\mathrm{K}}=1.27\times 10^3\left(\frac{\rho_0}{M_\odot/\mathrm{pc}^3}\right)^{2/3}\left(\frac{\mathrm{eV}/c^2}{m}\right)^{5/3}. \quad \text{(F2)}$$

Using the results of Sec. VII.E of Paper I, the temperature of classical halos is given by $k_BT=G(k)mG\rho_0r_h^2=G(k)mG\Sigma_0r_h=[G(k)/F(k)]mGM_h/r_h=[G(k)/F(k)^{1/2}]\times mG\Sigma_0^{1/2}M_h^{1/2}$ with $F(k)\sim 1.8$ and $G(k)\sim 0.95$. Introducing scaled variables, we obtain

$$\frac{T}{\mathrm{K}}=5.28\times 10^{-10}\frac{m}{\mathrm{eV}/c^2}\frac{\rho_0}{M_\odot/\mathrm{pc}^3}\left(\frac{r_h}{\mathrm{pc}}\right)^2, \quad \text{(F3)}$$

$$\frac{T}{\mathrm{K}}=5.28\times 10^{-10}\frac{m}{\mathrm{eV}/c^2}\frac{\Sigma_0}{M_\odot/\mathrm{pc}^2}\frac{r_h}{\mathrm{pc}}, \quad \text{(F4)}$$

$$\frac{T}{\mathrm{K}}=2.93\times 10^{-10}\frac{m}{\mathrm{eV}/c^2}\frac{M_h}{M_\odot}\frac{\mathrm{pc}}{r_h}, \quad \text{(F5)}$$

$$\frac{T}{\mathrm{K}}=3.94\times 10^{-10}\frac{m}{\mathrm{eV}/c^2}\left(\frac{\Sigma_0}{M_\odot/\mathrm{pc}^2}\right)^{1/2}\left(\frac{M_h}{M_\odot}\right)^{1/2}. \quad \text{(F6)}$$

On the other hand, Eq. (D4) can be written as

$$\frac{T}{\mathrm{K}}=1.29\times 10^{-13}\frac{m}{\mathrm{eV}/c^2}\left(\frac{\sigma_0}{\mathrm{m/s}}\right)^2. \quad \text{(F7)}$$

These different equations can be directly obtained from Eq. (2.38) of Ref. [73]. We note that these relations are valid only for classical halos. In the quantum regime, we take them as a rough approximation of the halo temperature. This is sufficient for an order-of-magnitude estimate. Let us make a numerical application. We take a fermion mass $m=1.23\ \mathrm{keV}/c^2$. For dwarf halos such as Willman 1, we find that $T=4.81\times 10^{-3}$ K and $T_F=2.23\times 10^{-2}$ K so these halos are quantum. For large halos such as the Medium Spiral, we find that $T=1.78$ K and $T_F=3.48\times 10^{-4}$ K so these halos are classical. This is of course equivalent to the results of Appendix E.

We now turn to the case of bosons. The condensation temperature of the bosons, estimated at the center of the halo, is

$$T_c=\frac{2\pi\hbar^2\rho_0^{2/3}}{k_B\zeta^{2/3}m^{5/3}}, \quad \text{(F8)}$$

with $\zeta=2.61$. The bosons are condensed for $T<T_c$ and noncondensed for $T>T_c$. We note that the condensation temperature (F8) has the same scaling as the Fermi temperature (F1). They differ by a factor $T_F/T_c=2^{1/3}\pi\zeta^{2/3}=7.51$. Therefore

$$\frac{T_c}{\mathrm{K}}=169\left(\frac{\rho_0}{M_\odot/\mathrm{pc}^3}\right)^{2/3}\left(\frac{\mathrm{eV}/c^2}{m}\right)^{5/3}. \quad \text{(F9)}$$

Writing $\sigma_0^2=k_BT/m$, the parameter H defined by Eq. (E1) can be written as $H=4.86\times 10^{-2}(T/T_c)^{3/2}$. It measures the degree of condensation of dark matter halos. The bosons are condensed (quantum halos) when $H<4.86\times 10^{-2}$ and noncondensed (classical halos) when $H>4.86\times 10^{-2}$. Let us make a numerical application. We take a mass $m=2.57\times 10^{-20}\ \mathrm{eV}/c^2$ appropriate to noninteracting bosons. For dwarf halos such as Willman 1, we find $T=1.00\times 10^{-25}$ K and $T_c=2.72\times 10^{35}$ K. For large halos such as the Medium Spiral, we find $T=3.72\times 10^{-23}$ K and $T_c=2.92\times 10^{33}$ K. We now take a mass $m=1.69\times 10^{-2}\ \mathrm{eV}/c^2$ appropriate to self-interacting bosons. For dwarf halos such as Willman 1, we find $T=3.49\times 10^{-8}$ K and $T_c=5.45\times 10^5$ K. For large halos such as the Medium Spiral, we find $T=1.27\times 10^{-5}$ K and $T_c=5.87\times 10^3$ K. In all cases, $T\ll T_c$. The same conclusion is reached if we assume that the halos are in equilibrium with the radiation background at ~ 3 K. Therefore, if dark matter is made of bosons, all the halos are quantum (Bose condensed) objects. This is valid for both noninteracting and self-interacting bosons. Since $T\ll T_c$, we can consider in excellent approximation that all bosonic halos are at $T=0$.

This result leads, however, to an apparent contradiction. Indeed, if the halos are self-gravitating BECs at $T=0$ made of self-interacting bosons, they should all have the same radius $R=\pi(a\hbar^2/Gm^3)^{1/2}$, which is clearly not the case. If the halos are self-gravitating BECs at $T=0$ made of noninteracting bosons, their radius should decrease with their mass as $R=9.95\hbar^2/(GMm^2)$ which is in contradiction with the observations revealing that the radius of dark matter halos increases with their mass. A possibility to resolve this apparent contradiction is to assume that bosonic dark matter halos at $T=0$ have a core-halo structure with a solitonic core (BEC), which is a stationary solution of the Gross-Pitaevskii-Poisson equation, surrounded by a halo of scalar radiation in which the density decreases as r^{-3} similarly to the NFW [51] and Burkert [52] profiles. This core-halo structure may result from a process of gravitational cooling [115]. The extended halo of radiation behaves as an effective isothermal atmosphere with a temperature $T_{\mathrm{eff}}\neq 0$ that has to be taken into account in order to determine the size of the dark matter halos. Because of this atmosphere, dark matter halos may have a radius much larger than the radius of the soliton (BEC). Actually, the most compact dwarf dark matter halos such as Willman 1 are purely solitonic objects. They have just a solitonic core (BEC) without an atmosphere. Therefore, their size is equal to the size of the soliton. By contrast, large dark matter halos are extended objects with a core-halo structure. They have a solitonic core (BEC) surrounded by an extended atmosphere made of scalar radiation. It is the radiative atmosphere that fixes the size of large dark matter halos. The atmosphere can be

much larger than the size of the soliton (core). The presence of the radiative atmosphere solves the apparent paradox that BEC halos at $T=0$ should all have the same radius (in the self-interacting case) or that their radius should decrease with their mass (in the noninteracting case), in contradiction with the observations. In this way, there is no paradox when the bosonic dark matter halos are treated as a system at $T=0$.

APPENDIX G: MAXIMUM MASS OF RELATIVISTIC COMPACT OBJECTS

Once we know the mass of the dark matter particle (see Appendix D), we can determine the maximum mass and the minimum radius fixed by general relativity of a completely degenerate (for fermions) or completely condensed (for bosons) compact object at $T=0$. While we have argued that large dark matter halos should not contain such objects at their center (at least in the form of the solutions B in Figs. 8, 35 and 41, because these solutions are saddle points of entropy), it is nevertheless interesting to make the numerical application.

If dark matter is made of fermions, the maximum mass is $M_{\rm max}=0.376(\hbar c/G)^{3/2}/m^2$ and the minimum radius is $R_{\rm min}=9.36GM_{\rm max}/c^2$ [116]. Introducing scaled variables, we get

$$\frac{M_{\rm max}}{M_\odot}=6.13\times 10^{17}\left(\frac{\rm eV/c^2}{m}\right)^2,\quad \frac{R_{\rm min}}{\rm km}=13.8\frac{M_{\rm max}}{M_\odot}. \tag{G1}$$

For $m=1.23$ keV$/c^2$, we obtain $M_{\rm max}=4.05\times 10^{11}M_\odot$ and $R_{\rm min}=0.181$ pc.

If dark matter is made of noninteracting bosons, the maximum mass is $M_{\rm max}=0.633\hbar c/Gm$ and the minimum radius is $R_{\rm min}=9.53GM_{\rm max}/c^2$ [117]. Introducing scaled variables, we get

$$\frac{M_{\rm max}}{M_\odot}=8.48\times 10^{-11}\frac{\rm eV/c^2}{m},\quad \frac{R_{\rm min}}{\rm km}=14.1\frac{M_{\rm max}}{M_\odot}. \tag{G2}$$

For $m=2.57\times 10^{-20}$ eV$/c^2$, we obtain $M_{\rm max}=3.30\times 10^9M_\odot$ and $R_{\rm min}=1.51\times 10^{-3}$ pc.

If dark matter is made of self-interacting bosons, the maximum mass is $M_{\rm max}=0.307\hbar c^2\sqrt{a}/(Gm)^{3/2}$ and the minimum radius is $R_{\rm min}=6.25GM_{\rm max}/c^2$ [118]. Introducing scaled variables, we get

$$\frac{M_{\rm max}}{M_\odot}=1.12\left(\frac{a}{\rm fm}\right)^{1/2}\left(\frac{\rm GeV/c^2}{m}\right)^{3/2}, \tag{G3}$$

$$\frac{R_{\rm min}}{\rm km}=9.27\frac{M_{\rm max}}{M_\odot}. \tag{G4}$$

For $({\rm fm}/a)^{1/3}(mc^2/{\rm eV})=0.654$, we obtain $M_{\rm max}=6.70\times 10^{13}M_\odot$ and $R_{\rm min}=20.2$ pc. We note that this estimate depends on the mass m and scattering length a of the bosons only through the ratio m^3/a.

Remark: The large values $M_{\rm max}\sim 10^9-10^{13}M_\odot$ of the maximum mass of the compact objects (fermion balls or BECs) that we have obtained suggest that these compact objects, if they exist at the center of dark matter halos, are nonrelativistic ($M_*\ll M_{\rm max}$). By comparison, the typical mass of the black holes that are thought to be hosted at the center of the galaxies is $M_{\rm BH}\sim 10^4$–$10^7M_\odot$ (the mass of Sgr* is $\sim 4\times 10^6M_\odot$). General-relativistic configurations (fermion balls or BECs) approaching the maximum mass could be attained in the central compact cores observed in active galactic nuclei.

APPENDIX H: A CRITERION FOR THE POSSIBLE EXISTENCE OF A BLACK HOLE AT THE CENTER OF DARK MATTER HALOS

It is known that certain dark matter halos contain a central black hole. In Sec. VII, we have argued that "large" halos may contain a black hole because they can experience a gravothermal catastrophe while "small" halos should not contain a black hole because the gravothermal catastrophe is prevented by quantum mechanics. In this appendix, we determine a more precise criterion for the possible existence of a black hole at the center of dark matter halos.

To that purpose, we use the parameters of the box model [9] that are more convenient for numerical applications. In this model, the degeneracy parameter is $\mu_{\rm box}=\eta_0\sqrt{512\pi^4G^3MR^3}$. If we identify R with the halo radius r_h and M with the halo mass M_h, and introduce relevant scales, we obtain

$$\mu_{\rm box}=6.41\times 10^{-17}\left(\frac{m}{\rm eV/c^2}\right)^4\left(\frac{M_h}{M_\odot}\right)^{1/2}\left(\frac{r_h}{\rm pc}\right)^{3/2}. \tag{H1}$$

Our criterion for the possible existence of a black hole at the center of dark matter halos is that the system can undergo a gravothermal catastrophe. This is the case when $\mu_{\rm box}$ is above the microcanonical critical point $\mu_{\rm MCP}^{\rm box}=2670$ [9].[31] Now, $\mu_{\rm box}$ can be related to the parameter H. Using the results of Appendix C, we get

$$\mu_{\rm box}=\sqrt{512\pi^4}\frac{F(k)^{1/2}H(k)}{G(k)^{3/2}}. \tag{H2}$$

As shown in Paper I, the functions $F(k)$ and $G(k)$ do not sensibly change with k. Taking $F(k)\sim 1.8$ and $G(k)\sim 0.95$, we obtain $\mu_{\rm box}\simeq 324H$. Therefore, our criterion for the existence of a black hole at the center of a dark matter halo can be written as $H>8.24$. Taking $m=1.23$ keV$/c^2$, and using Eq. (E4), this corresponds to a halo mass

[31] Actually, μ must be substantially larger than $\mu_{\rm MCP}^{\rm box}$ so that the gravothermal catastrophe is sufficiently efficient to allow the system to enter the relativistic regime and trigger the dynamical instability to a black hole [91].

$M_h > 1.60 \times 10^7 M_\odot$. By comparison, the canonical critical point $\mu_{\rm CCP}^{\rm box} = 83$ [9] corresponds to $H = 0.256$ and to a halo mass $M_h = 9.96 \times 10^5 M_\odot$.

In conclusion, large dark matter halos of mass $M_h > 1.60 \times 10^7 M_\odot$ can experience a gravothermal catastrophe and may contain a central black hole. Small dark matter halos of mass $M_h < 1.60 \times 10^7 M_\odot$ should not contain a black hole because they cannot experience a gravothermal catastrophe.

As we have seen in Appendixes E and F, bosonic dark matter halos are quantum objects at $T = 0$. As a result, they cannot experience a gravothermal catastrophe and should not contain a black hole. They instead contain a central solitonic object (BEC) surrounded by a halo of scalar radiation. Therefore, the nature of the object that lies at the center of dark matter halos (black hole or BEC) may tell us the nature of dark matter (fermions or bosons).

Remark: Concerning solution B in Fig. 41, corresponding to a dark matter halo harboring a central fermion ball (possibly unstable), we can show that the fraction of mass contained in the nucleus scales as $M_* \propto M_h/\mu^{1/2}$ where M_h is the halo mass [29]. Since $\mu \sim H \sim M^{5/4}$ [from Eq. (E4)] we get the scaling $M_* \propto M_h^{3/8}$.

APPENDIX I: SCENARIOS OF FORMATION OF DARK MATTER HALOS

In this appendix, we discuss different scenarios of formation of dark matter halos depending on the nature of the dark matter particle.

We first assume that dark matter is made of classical particles (i.e. heavy particles of mass $m \sim {\rm GeV}/c^2$) as in the CDM model. Initially, dark matter can be considered as a spatially homogeneous gas at $T = 0$. The velocity of sound $c_s = 0$. This distribution is unstable and undergoes gravitational collapse (Jeans instability). Since the classical Jeans wave number $k_J = \sqrt{4\pi G\rho}/c_s \to +\infty$ for $c_s \to 0$, the gas is unstable at all wavelengths and, consequently, structures form at all scales. There is no ground state so we expect to observe dark matter halos of all sizes. Furthermore, small halos are cuspy because nothing prevents the divergence of the density resulting from gravitational collapse. Cusps are preserved during successive mergings (hierarchical clustering) so that large halos are also cuspy. As we know, these results do not agree with observations: halos are cored (cusp problem) and they are not observed below a certain scale (missing satellite problem). This suggests that quantum mechanics has to be taken into account.[32]

We now assume that dark matter is made of fermions. Initially, dark matter can be considered as a spatially homogeneous gas described by the relativistic Fermi distribution $f = \eta_0^{\rm Pauli}/(1 + e^{pc/k_BT})$ where $\eta_0^{\rm Pauli} = gm^4/h^3$ is the Pauli bound [119]. The maximum value of the distribution function is $f_0 \sim (1/2)\eta_0^{\rm Pauli} = (g/2)m^4/h^3$. At later times, the gas is nonrelativistic and collisionless, described by the Vlasov-Poisson system. A spatially homogeneous distribution is unstable and undergoes gravitational collapse (Jeans instability). The fermionic Jeans wave number $k_J = \sqrt{12\pi G}(8\pi/3)^{1/3} \times m^{4/3}\rho^{1/6}/h$, obtained from Eq. (15), is finite so that quantum mechanics prevents the formation of small-scale structures and fixes a ground state. This produces a sharp cutoff in the power spectrum. In the linear regime, some regions of overdensity form. When the density has sufficiently grown, these regions collapse under their own gravity at first in free fall. Then, as nonlinear gravitational effects become important at higher densities, these regions undergo damped oscillations (due to an exchange of kinetic and potential energy) and finally settle into a QSS on a coarse-grained scale. This corresponds to the process of violent relaxation first reported by Lynden-Bell [81] for stellar systems like elliptical galaxies.[33] This process is related to phase mixing and nonlinear Landau damping. It is applied here to dark matter. In this context, the QSSs represent dark matter halos. Because of violent relaxation, the halos are almost isothermal and have a core-halo structure. The density of the core is relatively large and can reach values at which quantum effects or Lynden-Bell's type of degeneracy are important.[34] On the other hand, the halo is relatively hot and behaves more or less as a classical isothermal gas. Actually, it cannot be exactly isothermal otherwise it would have an infinite mass. The finite extension of the halo may be due to incomplete violent relaxation [81]. The extension of the halo may also be limited by tidal effects. In that case, the complete configuration of the system can be described by the fermionic King model [63,80]. As we have demonstrated, the fermionic King model can show a wide diversity of configurations with different degrees of nuclear concentration. The system can be everywhere nondegenerate, everywhere completely degenerate, or have a core-halo structure with a degenerate core and a nondegenerate halo. Small halos, that are compact, are degenerate. Their flat core is due to quantum mechanics. Assuming that the smallest and most compact observed dark matter halo of mass $M_h = 0.39 \times 10^6 M_\odot$

[32]Another possibility is to consider WDM with $T \neq 0$. In that case, the Jeans wave number k_J and the maximum value of the distribution function f_0 are determined by thermal effects (i.e. by the velocity dispersion of the particles).

[33]The domain of validity of Lynden-Bell's theory is a complicated and still open question due to the lack of efficient mixing (ergodicity) in some cases. For recent works on this topic see, e.g., Refs. [120–122] and references therein.

[34]In the case of dark matter, the Lynden-Bell bound and the Pauli bound are of the same order, differing by a factor of 2, since $\eta_0^{\rm LB} = f_0 = \eta_0^{\rm Pauli}/2 = (g/2)m^4/h^3$.

and radius $r_h = 33$ pc (Willman 1) is completely degenerate ($T = 0$) leads to a fermion mass of the order of 1.23 keV/c^2 [70,71]. These particles may be sterile neutrinos [76,77]. Small halos can merge with each other to form larger halos. This is called hierarchical clustering. The merging of the halos also corresponds to a process of collisionless violent relaxation. Large halos, that are dilute, are nondegenerate. Their flat core is due to thermal effects.[35] Knowing the mass of the fermions, we can deduce from the observations that halos of mass $0.39 \times 10^6 M_\odot < M_h < 2.97 \times 10^6 M_\odot$ are quantum (degenerate) objects while halos of mass $M_h > 2.97 \times 10^6 M_\odot$ are classical (nondegenerate) objects [70,71]. In the classical limit, numerical simulations of violent relaxation generically lead to configurations presenting an isothermal core and a halo whose density decreases as $r^{-\alpha}$ with $\alpha = 4$ [100–103]. These configurations are relatively close to Hénon's isochrone profile. They can be explained by models of incomplete violent relaxation [123–125]. A density slope $\alpha = 4$ in the halo is also consistent with a King profile of concentration $k \sim 5$ (see Paper I). If the halos were truly collisionless, they would remain in a virialized configuration. However, if the core is dense enough, collisional effects can come into play and induce an evolution of the system on a long time scale (driven by the gradient of temperature—the velocity dispersion $\sigma^2(r)$—between the core and the halo) during which the concentration parameter $k(t)$ increases while the slope $\alpha(t)$ of the density profile decreases much like in globular clusters [23]. We now have to distinguish between small halos of mass $M_h < 1.60 \times 10^7 M_\odot$ (i.e. $\mu < \mu_{\rm MCP} = 1980$) and large halos of mass $M_h > 1.60 \times 10^7 M_\odot$ (i.e. $\mu > \mu_{\rm MCP}$). For small halos ($M_h < 1.60 \times 10^7 M_\odot$), the series of equilibria (see Fig. 15) does not present any instability so that $k(t)$ increases and $\alpha(t)$ decreases regularly due to collisions and evaporation. These halos are degenerate. They are stabilized against gravitational collapse by quantum mechanics. As a result, they do not experience the gravothermal catastrophe so they should not contain black holes. For large halos ($M_h > 1.60 \times 10^7 M_\odot$), the series of equilibria (see Fig. 14) presents an instability at $k_{\rm MCE} = 7.44$. Because of collisions and evaporation, the concentration parameter increases from $k \sim 5$ corresponding to a density slope $\alpha = 4$ (a typical outcome of violent relaxation) up to the critical value $k_{\rm MCE} = 7.44$ corresponding to a density slope $\alpha \sim 3$. Less steep halos ($\alpha < 3$) are unstable ($k > k_{\rm MCE}$). Large halos are expected to be close to the point of marginal stability (see solution A in Figs. 8, 32 and 41). At that point, the King profile can be approximated by the modified Hubble profile that is relatively close to the Burkert profile fitting observational halos. Some halos may be stable ($k < k_{\rm MCE}$) but some halos may undergo a gravothermal catastrophe ($k > k_{\rm MCE}$). In that case, they experience core collapse. The evolution is self-similar. The system develops an isothermal core surrounded by a halo with a density slope $\alpha = 2.2$ [23,91]. The core radius decreases with time while the central density and the central temperature increase. The halo does not change. The specific heat of the core is negative. Therefore, by loosing heat to the profit of the halo, the core grows hotter and enhances the gradient of temperature with the halo so the collapse continues. This is the origin of the gravothermal catastrophe [2]. For weakly collisional classical systems (globular clusters), core collapse leads to a finite-time singularity with a profile $\rho \propto r^{-2.2}$ at $t = t_{\rm coll}$. The singularity has infinite density but contains no mass. It corresponds to a tight binary surrounded by a hot halo [23]. However, for collisional dark matter halos, the situation is different. If the particles are fermions, and if the mass of the halo is not very large ($\mu > \mu_{\rm MCP}$ not very large), the gravothermal catastrophe stops when the core of the system becomes degenerate. This leads to a configuration with a small degenerate nucleus (condensed state) surrounded by an extended atmosphere that is relatively different from the structure of the halo before collapse (see solution C in Figs. 8 and 38). However, the formation of this equilibrium structure can be very long (of the order of the Hubble time) so that, on an intermediate time scale, the system is made of a contracting fermion ball surrounded by an atmosphere that is not too much affected by the collapse of the core. Alternatively, if the halo mass is large ($\mu > \mu_{\rm MCP}$ large), during the gravothermal catastrophe the system can develop a (Vlasov) dynamical instability of general-relativistic origin and form a central black hole without affecting the structure of the halo [91]. In this way, the system is similar to the halo before collapse (Burkert profile) except that it contains a central black hole.[36] Large halos should not contain a fermion ball because these nucleus-halos structures (solution B in Figs. 8, 35 and 41) are unreachable (saddle points of entropy).

[35]Here, the temperature is effective and it must be understood in the sense of Lynden-Bell.

[36]More precisely, the core collapse of large fermionic dark matter halos ($M_h > 1.60 \times 10^7 M_\odot$) is a two-stages process. In a first stage [91], the core collapses while the halo does not change. Only the density, the radius and the temperature of the core change. This creates strong gradients of temperature between the core and the halo. At sufficiently high temperatures (achievable if $\mu > \mu_{\rm MCP}$ is large) the system becomes relativistic and triggers a dynamical instability leading to a black hole with a large mass. Alternatively, if $\mu > \mu_{\rm MCP}$ is not very large, quantum mechanics can stop the increase of the central density and central temperature before the system enters the relativistic regime. In that case, core collapse stops. Then, in a second stage (never studied until now because it requires quantum simulations), the temperature uniformizes between the core and the halo. Therefore, the halo heats up and extends at large distances until an equilibrium state with a uniform temperature T is reached (solution C in Figs. 8 and 38).

We now assume that dark matter is made of bosons without self-interaction. Since the temperature of the Universe is very low, they form a BEC so they are described by the Schrödinger-Poisson system. These equations are equivalent to fluid equations with a quantum potential $Q = -\hbar^2\Delta\sqrt{\rho}/2m\sqrt{\rho}$ (Heisenberg). Initially, the distribution of dark matter is spatially homogeneous. This distribution is unstable and undergoes gravitational collapse (Jeans instability). The Jeans wave number $k_J = (16\pi G m^2\rho/\hbar^2)^{1/4}$ [111,126] is finite so that quantum mechanics prevents the formation of small-scale structures and fixes a ground state. In the linear regime, some regions of overdensity form. In the nonlinear regime, these overdensity regions oscillate and settle into a compact bosonic object through the radiation of a complex scalar field. This corresponds to the process of gravitational cooling first reported by Seidel and Suen [115] in the context of boson stars. It is extended here to dark matter. This process is similar to violent relaxation. The resulting structures correspond to dark matter halos. Because of gravitational cooling, the halos have a core-halo configuration. The core is equivalent to a self-gravitating BEC at $T = 0$ (soliton) stabilized against gravitational collapse by the Heisenberg uncertainty principle. The halo corresponds to quantum fluctuations and scalar radiation. It behaves similarly to a thermal halo. Assuming that the smallest and most compact observed dark matter halo (Willman 1) is completely condensed without a halo (no quantum fluctuation) implies that the boson mass is $m = 2.57\times 10^{-20}\ \mathrm{eV}/c^2$. Knowing the mass of the bosons, we can deduce from the observations that all the dark matter halos in the Universe are Bose condensed ($T \ll T_c$). They have a condensed core (soliton) and are surrounded by a halo of scalar waves that gives them their proper size. Although the true thermodynamic temperature $T = 0$, everything happens *as if* the halos have a core-halo structure with a core at $T = 0$ (soliton) and a halo with an effective temperature $T_{\rm eff} \neq 0$.

Self-interacting bosons are described by the Gross-Pitaevskii-Poisson system. These equations are equivalent to fluid equations with a quantum potential $Q = -\hbar^2\Delta\sqrt{\rho}/2m\sqrt{\rho}$ (Heisenberg) and a pressure $p = 2\pi a\hbar^2\rho^2/m^3$ due to the self-interaction. Self-interacting bosons can experience a Jeans instability. In the TF approximation, the Jeans wave number is given by $k_J = (Gm^3/a\hbar^2)^{1/2}$ [111] and its general expression (valid beyond the TF approximation) is given by Eq. (139) of Ref. [111]. This finite Jeans wave number prevents the formation of small-scale structures and fixes a ground state. The linear Jeans instability is followed by a nonlinear process of gravitational cooling, as in the case of noninteracting bosons. The resulting dark matter halo has a core-halo structure. The core is equivalent to a self-gravitating BEC at $T = 0$ (soliton) stabilized against gravitational collapse by the self-interaction of the particles. The halo corresponds to quantum fluctuations and scalar radiation. Assuming that the smallest and most compact observed dark matter halo (Willman 1) is completely condensed without a halo (no quantum fluctuation), we obtain the ratio $(\mathrm{fm}/a)^{1/3}(mc^2/\mathrm{eV}) = 0.654$ between the mass of the bosons and their scattering length (see Appendix D). Using the constraint of the Bullet Cluster, we get $m = 1.69\times 10^{-2}\ \mathrm{eV}/c^2$ and $a = 1.73\times 10^{-5}$ fm. Knowing the mass of the bosons, we can deduce from the observations that all the dark matter halos in the Universe are Bose condensed ($T \ll T_c$). They have a condensed core (soliton) and are surrounded by a halo of scalar waves that gives them their proper size.

In conclusion, dark matter halos made of fermions of mass $m = 1.23\ \mathrm{keV}/c^2$ are quantum object for $M_h < 2.97\times 10^6 M_\odot$ and classical objects for $M_h > 2.97\times 10^6 M_\odot$. Small halos are degenerate. Large halos are nondegenerate. They may contain a central black hole but not a central fermion ball (see Sec. VI). Dark matter halos made of bosons of mass $m = 2.57\times 10^{-20}\ \mathrm{eV}/c^2$ (noninteracting case) or $m = 1.69\times 10^{-2}\ \mathrm{eV}/c^2$ (self-interacting case) are quantum objects for all relevant sizes. They have a solitonic core surrounded by a halo of scalar radiation. Since fermionic and bosonic dark matter halos present different characteristics (the first may contain a black hole and the second a solitonic BEC), it should be possible to determine which of them better agrees with the observations. This may allow us to determine the nature of the dark matter particle. It is also important to perform cosmological simulations taking quantum mechanics into account. This was claimed by Feynman long ago: "I'm not happy with all the analysis that go with just the classical theory, because nature is not classical, dammit, and if you want to make a simulation of nature, you'd better make it quantum mechanical, and by golly it's a wonderful problem, because it does not look so easy." (See Ref. [127] and Appendix A of Ref. [71].) Recent simulations have been performed in Refs. [128–130] for noninteracting bosons. The case of fermions and self-interacting bosons should also be considered. We guess that future years will see the development of exciting quantum cosmological simulations of fermions and bosons.

[1] V. A. Antonov, Vest. Leningr. Gos. Univ. **7**, 135 (1962).
[2] D. Lynden-Bell and R. Wood, Mon. Not. R. Astron. Soc. **138**, 495 (1968).
[3] A. S. Eddington, *The Internal Constitution of the Stars* (Cambridge University Press, Cambridge, England, 1926).
[4] W. Thirring, Z. Phys. **235**, 339 (1970).
[5] D. Lynden-Bell and R. M. Lynden-Bell, Mon. Not. R. Astron. Soc. **181**, 405 (1977).
[6] A. Campa, T. Dauxois, and S. Ruffo, Phys. Rep. **480**, 57 (2009).
[7] T. Padmanabhan, Phys. Rep. **188**, 285 (1990).
[8] J. Katz, Found. Phys. **33**, 223 (2003).
[9] P. H. Chavanis, Int. J. Mod. Phys. B **20**, 3113 (2006).
[10] C. Sire and P. H. Chavanis, Phys. Rev. E **66**, 046133 (2002).
[11] S. Chandrasekhar, *An Introduction to the Theory of Stellar Structure* (Dover, New York, 1942).
[12] P. H. Chavanis, Astron. Astrophys. **556**, A93 (2013).
[13] J. Binney and S. Tremaine, *Galactic Dynamics* (Princeton University, Princeton, NJ, 1987).
[14] I. R. King, Astron. J. **70**, 376 (1965).
[15] R. Emden, *Gaskugeln* (Teubner Verlag, Leipzig, 1907).
[16] J. Katz, Mon. Not. R. Astron. Soc. **183**, 765 (1978).
[17] P. H. Chavanis, Astron. Astrophys. **381**, 340 (2002).
[18] P. H. Chavanis, Astron. Astrophys. **401**, 15 (2003).
[19] P. H. Chavanis, Astron. Astrophys. **432**, 117 (2005).
[20] M. Kiessling, J. Stat. Phys. **55**, 203 (1989).
[21] J. Katz, Mon. Not. R. Astron. Soc. **190**, 497 (1980).
[22] P. H. Chavanis, M. Lemou, and F. Méhats, Phys. Rev. D **91**, 063531 (2015) (Paper I).
[23] H. Cohn, Astrophys. J. **242**, 765 (1980).
[24] C. Sire and P. H. Chavanis, Phys. Rev. E **69**, 066109 (2004).
[25] G. Horwitz and J. Katz, Astrophys. J. **211**, 226 (1977).
[26] G. Horwitz and J. Katz, Astrophys. J. **222**, 941 (1978).
[27] H. J. de Vega and N. Sanchez, Nucl. Phys. **B625**, 409 (2002).
[28] H. J. de Vega and N. Sanchez, Nucl. Phys. **B625**, 460 (2002).
[29] P. H. Chavanis, Phys. Rev. E **65**, 056123 (2002).
[30] P. H. Chavanis, in *Dark Matter in Astro- and Particle Physics*, edited by H. V. Klapdor-Kleingrothaus and R. D. Viollier (Springer, New York, 2002).
[31] P. H. Chavanis and I. Ispolatov, Phys. Rev. E **66**, 036109 (2002).
[32] P. H. Chavanis and M. Rieutord, Astron. Astrophys. **412**, 1 (2003).
[33] P. H. Chavanis, Phys. Rev. E **69**, 066126 (2004).
[34] P. H. Chavanis, Eur. Phys. J. B **87**, 9 (2014).
[35] E. Follana and V. Laliena, Phys. Rev. E **61**, 6270 (2000).
[36] C. M. Trott and A. Melatos, Astrophys. J. **618**, 38 (2005).
[37] C. Destri and H. J. de Vega, Nucl. Phys. **B763**, 309 (2007).
[38] L. Casetti and C. Nardini, Phys. Rev. E **85**, 061105 (2012).
[39] E. B. Aronson and C. J. Hansen, Astrophys. J. **177**, 145 (1972).
[40] B. Stahl, M. K. H. Kiessling, and K. Schindler, Planet. Space Sci. **43**, 271 (1995).
[41] M. Champion, A. Alastuey, T. Dauxois, and S. Ruffo, J. Phys. A **47**, 225001 (2014).
[42] V. P. Youngkins and B. Miller, Phys. Rev. E **56**, R4963 (1997).
[43] B. Miller and V. P. Youngkins, Phys. Rev. Lett. **81**, 4794 (1998).
[44] V. P. Youngkins and B. Miller, Phys. Rev. E **62**, 4583 (2000).
[45] P. J. Klinko and B. Miller, Phys. Rev. E **62**, 5783 (2000).
[46] P. J. Klinko, B. Miller, and I. Prokhorenkov, Phys. Rev. E **63**, 066131 (2001).
[47] P. J. Klinko and B. Miller, Phys. Rev. E **65**, 056127 (2002).
[48] P. J. Klinko and B. Miller, Phys. Rev. Lett. **92**, 021102 (2004).
[49] M. Hénon, in *Proceedings of IAU Symposium No. 69*, edited by A. Hayli (Reidel, Dordrecht, 1975), p. 133.
[50] M. Persic, P. Salucci, and F. Stel, Mon. Not. R. Astron. Soc. **281**, 27 (1996).
[51] J. F. Navarro, C. S. Frenk, and S. D. M. White, Astrophys. J. **462**, 563 (1996).
[52] A. Burkert, Astrophys. J. **447**, L25 (1995).
[53] G. Kauffmann, S. D. M. White, and B. Guiderdoni, Mon. Not. R. Astron. Soc. **264**, 201 (1993).
[54] J. G. Gao and R. Ruffini, Phys. Lett. **97B**, 388 (1980).
[55] R. Ruffini and L. Stella, Astron. Astrophys. **119**, 35 (1983).
[56] M. Merafina and R. Ruffini, Astron. Astrophys. **221**, 4 (1989).
[57] J. G. Gao, M. Merafina, and R. Ruffini, Astron. Astrophys. **235**, 1 (1990).
[58] M. Merafina and R. Ruffini, Astron. Astrophys. **227**, 415 (1990).
[59] G. Ingrosso, M. Merafina, R. Ruffini, and F. Strafella, Astron. Astrophys. **258**, 223 (1992).
[60] A. Kull, R. A. Treumann, and H. Böhringer, Astrophys. J. **466**, L1 (1996).
[61] N. Bilic and R. D. Viollier, Phys. Lett. B **408**, 75 (1997).
[62] P. H. Chavanis and J. Sommeria, Mon. Not. R. Astron. Soc. **296**, 569 (1998).
[63] P. H. Chavanis, Mon. Not. R. Astron. Soc. **300**, 981 (1998).
[64] D. Tsiklauri and R. D. Viollier, Astrophys. J. **500**, 591 (1998).
[65] N. Bilic and R. D. Viollier, Eur. Phys. J. C **11**, 173 (1999).
[66] N. Bilic and R. D. Viollier, Gen. Relativ. Gravit. **31**, 1105 (1999).
[67] N. Bilic, R. J. Lindebaum, G. B. Tupper, and R. D. Viollier, Phys. Lett. B **515**, 105 (2001).
[68] N. Bilic, F. Munyaneza, G. B. Tupper, and R. D. Viollier, Prog. Part. Nucl. Phys. **48**, 291 (2002).
[69] N. Bilic, G. B. Tupper, and R. D. Viollier, Lect. Notes Phys. **616**, 24 (2003).
[70] C. Destri, H. J. de Vega, and N. G. Sanchez, New Astron. **22**, 39 (2013).
[71] C. Destri, H. J. de Vega, and N. G. Sanchez, Astropart. Phys. **46**, 14 (2013).
[72] H. J. de Vega, P. Salucci, and N. G. Sanchez, Mon. Not. R. Astron. Soc. **442**, 2717 (2014).
[73] H. J. de Vega and N. G. Sanchez, arXiv:1310.6355.
[74] H. J. de Vega and N. G. Sanchez, arXiv:1401.0726.

[75] V. Domcke and A. Urbano, J. Cosmol. Astropart. Phys. 01 (2015) 002.
[76] A. Boyarsky, O. Ruchayskiy, and M. Shaposhnikov, Annu. Rev. Nucl. Part. Sci. **59**, 191 (2009).
[77] M. R. Lovell, C. S. Frenk, V. R. Eke, A. Jenkins, L. Gao, and T. Theuns, Mon. Not. R. Astron. Soc. **439**, 300 (2014).
[78] A. Boyarsky, O. Ruchayskiy, D. Iakubovskyi, and J. Franse, Phys. Rev. Lett. **113**, 251301 (2014).
[79] E. Bulbul, M. Markevitch, A. Foster, R. K. Smith, M. Loewenstein, and S. W. Randall, Astrophys. J. **789**, 13 (2014).
[80] P. H. Chavanis, in *Multiscale Problems in Science and Technology*, edited by N. Antonić, C. J. van Duijn, W. Jäger, and A. Mikelić (Springer, New York, 2002).
[81] D. Lynden-Bell, Mon. Not. R. Astron. Soc. **136**, 101 (1967).
[82] P. H. Chavanis, J. Sommeria, and R. Robert, Astrophys. J. **471**, 385 (1996).
[83] B. Moore, T. Quinn, F. Governato, J. Stadel, and G. Lake, Mon. Not. R. Astron. Soc. **310**, 1147 (1999).
[84] P. Hertel and W. Thirring, Commun. Math. Phys. **24**, 22 (1971).
[85] P. Hertel and W. Thirring, in *Quanten und Felder*, edited by H. P. Dürr (Vieweg, Braunschweig, 1971).
[86] P. H. Chavanis, M. Ribot, C. Rosier, and C. Sire, Banach Center publications **66**, 103 (2004).
[87] R. Schödel *et al.*, Nature (London) **419**, 694 (2002).
[88] M. J. Reid, Int. J. Mod. Phys. D **18**, 889 (2009).
[89] Z. Slepian and J. Goodman, Mon. Not. R. Astron. Soc. **427**, 839 (2012).
[90] P. H. Chavanis (to be published).
[91] S. Balberg, S. L. Shapiro, and S. Inagaki, Astrophys. J. **568**, 475 (2002).
[92] D. N. Spergel and P. J. Steinhardt, Phys. Rev. Lett. **84**, 3760 (2000).
[93] R. Ruffini, C. Raúl Argüelles, and J. A. Rueda, Mon. Not. R. Astron. Soc. **451**, 622 (2015).
[94] H. J. de Vega and N. G. Sanchez, arXiv:1401.1214.
[95] P. H. Chavanis, Physica (Amsterdam) **332A**, 89 (2004).
[96] P. H. Chavanis, Eur. Phys. J. B **62**, 179 (2008).
[97] M. Lemou, F. Méhats, and P. Raphaël, Commun. Math. Phys. **302**, 161 (2011).
[98] A. Campa and P. H. Chavanis, J. Stat. Mech. (2010), P06001
[99] M. Lemou and P. H. Chavanis, Physica (Amsterdam) **389A**, 1021 (2010).
[100] M. Hénon, Ann. Astrophys. **27**, 83 (1964).
[101] T. S. van Albada, Mon. Not. R. Astron. Soc. **201**, 939 (1982).
[102] F. Roy and J. Perez, Mon. Not. R. Astron. Soc. **348**, 62 (2004).
[103] M. Joyce, B. Marcos, and F. Sylos Labini, Mon. Not. R. Astron. Soc. **397**, 775 (2009).
[104] R. Ruffini and S. Bonazzola, Phys. Rev. **187**, 1767 (1969).
[105] M. Membrado, A. F. Pacheco, and J. Sanudo, Phys. Rev. A **39**, 4207 (1989).
[106] P. H. Chavanis and L. Delfini, Phys. Rev. D **84**, 043532 (2011).
[107] M. R. Baldeschi, G. B. Gelmini, and R. Ruffini, Phys. Lett. **122B**, 221 (1983).
[108] J. Goodman, New Astron. **5**, 103 (2000).
[109] A. Arbey, J. Lesgourgues, and P. Salati, Phys. Rev. D **68**, 023511 (2003).
[110] C. G. Böhmer and T. Harko, J. Cosmol. Astropart. Phys. 06 (2007) 025.
[111] P. H. Chavanis, Phys. Rev. D **84**, 043531 (2011).
[112] P. H. Chavanis, in *Quantum Aspects of Black Holes*, edited by X. Calmet (Springer, New York, 2015).
[113] S. W. Randall, M. Markevitch, D. Clowe, A. H. Gonzalez, and M. Bradac, Astrophys. J. **679**, 1173 (2008).
[114] T. Fukuyama, M. Morikawa, and T. Tatekawa, J. Cosmol. Astropart. Phys. 06 (2008) 033.
[115] E. Seidel and W.-M Suen, Phys. Rev. Lett. **72**, 2516 (1994).
[116] J. R. Oppenheimer and G. M. Volkoff, Phys. Rev. **55**, 374 (1939).
[117] D. J. Kaup, Phys. Rev. **172**, 1331 (1968).
[118] P. H. Chavanis and T. Harko, Phys. Rev. D **86**, 064011 (2012).
[119] S. Tremaine and J. E. Gunn, Phys. Rev. Lett. **42**, 407 (1979).
[120] I. Arad and D. Lynden-Bell, Mon. Not. R. Astron. Soc. **361**, 385 (2005).
[121] F. Staniscia, P. H. Chavanis, and G. de Ninno, Phys. Rev. E **83**, 051111 (2011).
[122] F. P. C. Benetti, A. C. Ribeiro-Teixeira, R. Pakter, and Y. Levin, Phys. Rev. Lett. **113**, 100602 (2014).
[123] G. Bertin and M. Stiavelli, Astron. Astrophys. **137**, 26 (1984).
[124] M. Stiavelli and G. Bertin, Mon. Not. R. Astron. Soc. **229**, 61 (1987).
[125] J. Hjorth and J. Madsen, Mon. Not. R. Astron. Soc. **253**, 703 (1991).
[126] W. Hu, R. Barkana, and A. Gruzinov, Phys. Rev. Lett. **85**, 1158 (2000).
[127] R. P. Feynman, Int. J. Theor. Phys. **21**, 467 (1982).
[128] T. P. Woo and T. Chiueh, Astrophys. J. **697**, 850 (2009).
[129] H. Y. Schive, T. Chiueh, and T. Broadhurst, Nat. Phys. **10**, 496 (2014).
[130] H. Y. Schive, M.-H. Liao, T.-P. Woo, S.-K. Wong, T. Chiueh, T. Broadhurst, and W-Y. Pauchy Hwang, Phys. Rev. Lett. **113**, 261302 (2014).